BRNO UNIVERSITY OF TECHNOLOGY

VYSOKÉ UČENÍ TECHNICKÉ V BRNĚ

FACULTY OF ELECTRICAL ENGINEERING AND COMMUNICATION

FAKULTA ELEKTROTECHNIKY
A KOMUNIKAČNÍCH TECHNOLOGIÍ

DEPARTMENT OF RADIO ELECTRONICS

ÚSTAV RADIOELEKTRONIKY

SIW-BASED CIRCULARLY POLARIZED ANTENNA ARRAYS

KRUHOVĚ POLARIZOVANÉ ANTÉNNÍ ŘADY NA BÁZI SIW

DOCTORAL THESIS
DIZERTAČNÍ PRÁCE

AUTHOR
AUTOR PRÁCE

Ing. Jan Špůrek

SUPERVISOR
ŠKOLITEL

prof. Dr. Ing. Zbyněk Raida

BRNO 2021

ABSTRACT

This dissertation thesis presents a new concept of SIW-based circularly polarized antenna arrays. The main property of the concept is modularity where the base building block can be utilized to create more complex antenna arrays and at the same time it serves also as the template to design the more complex structure. The antenna array was simulated and experimentally verified for the frequencies of 17 and 60 GHz. Based on the obtained results, design methodology was derived, and key design areas were identified.

Next, the thesis introduces a technique of increasing axial ratio bandwidth of circularly polarized antenna arrays by utilizing parasitic patches, which are placed above the radiating elements at defined distance. The antenna array from the first section of the thesis was used in the simulations and experimental verification for the frequencies of 17 and 60 GHz, where this array was extended with the parasitic structure, adding another level of modularity into the concept.

KEYWORDS

Antenna array, patch antenna, circular polarization, parasitic structures, substrate integrated waveguide, axial ratio, modularity

ABSTRAKT

Tato disertační práce prezentuje nový koncept kruhově polarizovaných anténních řad na bázi vlnovodu integrovaného do substrátu. Hlavní devízou konceptu je modularita, kdy je základní stavební blok řady použitelný pro tvorbu komplexnějších řad a tento blok zároveň slouží jako šablona pro návrh komplexnější struktury. Anténní řada byla simulována a experimentálně ověřena pro frekvence 17 a 60 GHz. Na základě dosažených výsledků byla odvozena metodologie pro návrh a identifikovány klíčové oblasti návrhu.

Následně práce představuje techniku zvýšení šířky pásma osového poměru kruhově polarizovaných anténních řad pomoci parazitních flíčků, které jsou umístěny nad zářiče v definované vzdálenosti. Anténní řada z první části práce byla použita v simulacích a experimentálním ověření pro frekvence 17 a 60 GHz, kdy byla tato řada rozšířena o parazitní strukturu, přidávajíc další vrstvu modularity do konceptu.

KLÍČOVÁ SLOVA

Anténní řada, flíčková anténa, kruhová polarizace, parazitní struktury, vlnovod integrovaný do substrátu, osový poměr, modularita

BIBLIOGRAFICKÁ CITACE

SPUREK, J., SIW-based circularly polarized antenna arrays. Brno: Brno University of Technology, Faculty of Electrical Engineering and Communication, Department of Radio Electronics, 2021. Supervised by prof. Zbynek Raida.

DECLARATION

I declare that I have written the Doctoral Thesis titled “SIW-based circularly polarized antenna arrays” independently, under the guidance of the advisor and using exclusively the technical references and other sources of information cited in the thesis and listed in the comprehensive bibliography at the end of the thesis.

As the author I furthermore declare that, with respect to the creation of this Doctoral Thesis, I have not infringed any copyright or violated anyone’s personal and/or ownership rights. In this context, I am fully aware of the consequences of breaking Regulation § 11 of the Copyright Act No. 121/2000 Coll. of the Czech Republic, as amended, and of any breach of rights related to intellectual property or introduced within amendments to relevant Acts such as the Intellectual Property Act or the Criminal Code, Act No. 40/2009 Coll., Section 2, Head VI, Part 4.

Brno, the 25th of August 2021 …….

Author’s signature

ACKNOWLEDGEMENT

I would like to express my gratitude to my supervisor prof. Zbyněk Raida for his valuable guidance and the opportunities given to me. I thank doc. Jaroslav Láčík for his professional help with measurements and advise. Special thanks belong to NXP Semiconductors s.r.o company for the support in my research and making it possible to realize it together with my employment. Many thanks to all my colleagues that helped me to maintain the right direction and created friendly atmosphere and most importantly to my wife Šárka and family for their support, patience and tolerance throughout my research. This could not have been realized without you. Thank you.

Brno ……. ……
Jan Špůrek

CONTENTS

Contents 5

1 INTRODUCTION 7

2 STATE OF THE ART 8

2.1 Substrate integrated waveguides 8
2.1.1 Electromagnetic modes in the substrate integrated waveguides 8
2.2 Circularly polarized patch antennas 9
2.2.1 Feeding options of a patch antenna 9
2.2.2 Extending axial ratio bandwidth of the patch antennas 9
2.3 References 10

3 OBJECTIVES 13

4 ANTENNA ARRAY DESIGN AT 17 GHZ 15

4.1 Introduction 15
4.2 Design of the array 15
4.3 Simulations and measurements 19
4.4 Design methodics 22
4.5 Conclusion 23
4.6 References 24

5 CONVERSION TO 60 GHZ 25

5.1 Introduction 25
5.2 WR15 to SIW transition 25
5.3 Conversion of the array to 60 GHz 27
5.4 Simulated Results 28
5.5 Sensitivity analysis 30
5.5.1 Position of the patches in relation to the coupling slots 33
5.5.2 Dimensions of the coupling slots 35
5.5.3 Dimensions of the coupling slots between the layers 37
5.5.4 Position of the coupling slots between the layers 39
5.5.5 Position of the shorting pin of the power divider 41
5.5.6 Width of the waveguides 43
5.5.7 Dimensions of the patches 45
5.5.8 Summary 47
5.6 Measured results 47
5.7 Results of the array with the larger via diameter 49
5.7.1 Comparison between the array with smaller and larger via diameter 50
5.7.2 Measured results of the array with the larger via diameter 54

5.8 Conclusion 58
6 EXTENDING AXIAL RATIO BANDWIDTH OF THE ARRAY BY PARASITIC PATCHES 60
6.1 Principle 60
6.2 extenstion of the array by Parasitic patches 60
6.2.1 Simulations and measurements 62
6.3 Adaptation of the array to 60 GHz 68
6.3.1 Simulations and measurements 68
6.4 Conclusion 70
7 SUMMARY 71
REFERENCES 72
LIST OF FIGURES 76
LIST OF TABLES 80
CURRICULIM VITAE 81
LIST OF AUTHOR'S PUBLICATIONS 82

1 INTRODUCTION

The first substrate integrated waveguide (SIW), proposed by Dominic Deslandes in 2001 demonstrated that a structure of shorting pins arranged to a set of two mutually parallel rows in a dielectric substrate shows similar properties as a conventional rectangular waveguide. Since then, SIWs became very broadly used in the microwave designs.

The main advantage of the SIWs in comparison to the conventional waveguides is low weight since a microwave substrate, covered by thin metal layers on top and bottom is used, instead of thick metal walls. In effect, also material costs of such a structure are reduced. To manufacture a SIW, no special approach is needed, existing and refined printed circuit board technology is reused, making the SIWs widely accessible to various institutions and audience. The SIW technology also allows to easily create various shapes and network interconnects that would be rather difficult, if not impossible, to realize with the conventional waveguides. The most important examples are the transitions between the microstrip line and grounded coplanar waveguide (GCPW). Those transitions allowed natural integration of the waveguide structures to microwave electronics, resulting in increased efficiency and space savings.

Among the disadvantages we can include higher losses in comparison to conventional waveguides and radiation leakage through the side walls, which are made of the shorting pins. However, the advantages of the SIWs by far outweigh their disadvantages in most of the applications.

One of the areas, where the SIWs became very popular, is antenna and antenna array design. It is very convenient that the antenna elements can be integrated to the SIW, like it is usual for classical waveguides. An obvious limitation is, that only top and bottom wall can be utilized for this purpose. This way, the radiating elements are part of the transmission line, therefore an integrated and space saving solution is obtained. With all the above mentioned advantages, the SIWs are ideal for integration of the antenna structures to the systems.

Not only simple, but also stacked multilayer antenna structures can be based on a SIW. This further increases their level of utilization in the area. An example can be a patch antenna on the top layer, excited by a coupling slot on the bottom layer to whom the energy is delivered by a SIW. This particular set up excels in modularity and customizability. Simply by varying the shape of the patch and its position, linearly or circularly polarized antennas can be obtained without the need to redesign the whole structure. A stack up of two layers can be used for design of arbitrarily large antenna arrays, using smaller blocks as building modules.

As the current trend is to increase the operation frequency of systems up to the band of millimeter waves, such a setup is very suitable for use in the research and it is precisely the objective of this thesis.

2 STATE OF THE ART

Brief introduction into the field of substrate integrated waveguides and circularly polarized patch antennas is given in this chapter. The focus is drawn to the electromagnetic modes that can be created inside the substrate integrated waveguides. Next, operational principles of a circularly polarized patch antenna are described.

2.1 SUBSTRATE INTEGRATED WAVEGUIDES

Until 2001, conventional waveguides were used in microwave designs. To approximate a conventional waveguide by two sets of parallelly placed rows of shorting pins in a metalized microwave substrate was for the first time proposed in [1]. Since the SIWs had been introduced, interest of the researches in this technology grew rapidly. Good reference materials can be found in [2].

The basic operation of a SIW is very analogous to operation of a classical rectangular waveguide. If the SIW is excited by an EM wave, whose frequency is higher than the SIW's cutoff frequency, then the wave propagates through the SIW almost without attenuation [1]. This cutoff frequency is given by the width of the SIW (distance between the rows of shorting pins) and the dielectric constant of the used microwave substrate. To obtain a so called equivalent SIW (to a classical rectangular waveguide), also the diameter of the shorting pins and their spacing need to be considered in the calculations [2].

Many microwave structures have been designed, using the SIW technology. Microstrip line to SIW or GCPW to SIW transitions are used to connect the SIW to traditionally used transmission lines and connectors [1, 3]. In principle, the SIWs are not subject to any standardized sets (WR waveguides), therefore various types of unique power dividers and couplers can be designed [4, 5, 6]. Microwave filters are also devices, where the advantages of SIWs bring considerable improvements in customization [7, 8, 9]. Finally, antennas and antenna arrays based on SIW were presented [10, 11, 12, 13]. Though, modular designs have not been discussed in the known literature. The SIWs therefore offer a complex set needed to integrate the microwave part of the system to the printed circuit board.

In the known literature, the current maximum operation frequency on which the SIW structures have been designed on conventional microwave substrates is 94 GHz [14, 15, 16].

2.1.1 Electromagnetic modes in the substrate integrated waveguides

Comparing to a classical rectangular waveguide, the number of mode types that can propagate through a SIW, is considerably reduced. Because the side walls are composed of shorting pins, therefore there are not solid, TM modes cannot propagate through the structure without significant attenuation [17]. Since the height of a SIW is usually much lower than its width, the cutoff frequencies of TE_{0x} modes are much higher than the cutoff frequencies of TE_{x0} modes. Therefore, the SIWs practically

operate with TE_{x0} modes only. Since the most microwave waveguide designs operate under the condition of the exclusive existence of TE_{10} mode (single mode band), this property is not limiting and can be viewed rather as an advantage.

Since the only limitations are the cutoff frequencies of TE_{10} and TE_{20} modes and the bandwidth required by the particular system, the SIWs offer great customizability in terms of their width. This allows to tune the guided wavelength in continuous way and precisely adapt it to the needs of the design.

2.2 CIRCULARLY POLARIZED PATCH ANTENNAS

The principles on which the patch antennas operate, are very well explained in [18]. A typical patch has the shape of a rectangle, however other shapes are also applicable. The first resonant frequency (mode) of a patch antenna is a frequency whose half-wavelength corresponds with the length of the patch. Under this condition, the field distribution within the patch creates a regular radiation pattern with the main lobe maximum directed perpendicularly to the antenna structure. Such an antenna radiates a linearly polarized wave. A patch antenna can also operate with the circular polarization under the condition of exciting two orthogonal modes within the patch with mutual phase shift of 90 degrees [18]. Currently, circularly polarized patch antennas are in the known literature described up to the frequency of 60 GHz [19, 20].

2.2.1 Feeding options of a patch antenna

A patch antenna can be fed by various techniques. The most common is microstrip line and coaxial probe [18]. The feeding point is located with respect to the impedance of the antenna so it would be matched with the characteristic impedance of the transmission line used for feeding. Exciting the patch by a coupling slot has been described in [21]. Such a configuration combines the advantages of both previously mentioned solutions – the patch is not disrupted by the transmission line and therefore its properties are not degraded (feeding by coaxial probe) while preserving the ease of constructing antenna arrays with no significant increase of the structure's profile. In such case, a SIW can be used as the transmission media, creating a multilayer structure [22].

2.2.2 Extending axial ratio bandwidth of the patch antennas

The conditions for generation of a circularly polarized wave with a patch antenna are typically met only for a narrow interval of wavelengths. Since the increasing data rate is closely related to the required bandwidth of the system, wider bandwidths are also demanded in case of the antennas. In effect, techniques how to increase the axial ratio bandwidth have been proposed [23, 24, 25, 26]. However, for some applications, the bandwidth is still insufficient.

2.3 REFERENCES

[1] DESLANDES, D. a K. WU. Integrated microstrip and rectangular waveguide in planar form. IEEE Microwave and Wireless Components Letters. 2001, 11(2), 68-70. DOI: 10.1109/7260.914305. ISSN 1531-1309.

[2] DESLANDES, Dominic a Ke WU. Design Consideration and Performance Analysis of Substrate Integrated Waveguide Components. In: *32nd European Microwave Conference, 2002*. IEEE, 2002, 2002, pp. 1-4. DOI: 10.1109/EUMA.2002.339426.

[3] CHEN, Xiao-Ping a Ke WU. Low-loss ultra-wideband transition between conductor-backed coplanar waveguide and substrate integrated waveguide. In: 2009 IEEE MTT-S International Microwave Symposium Digest. IEEE, 2009, 2009, pp. 349-352. DOI: 10.1109/MWSYM.2009.5165705. ISBN 978-1-4244-2803-8.

[4] KARIMABADI, Sara Sadat a Amir Reza ATTARI. Broadband substrate integrated waveguide four-way power divider. In: 6th International Symposium on Telecommunications (IST). IEEE, 2012, 2012, pp. 80-83. DOI: 10.1109/ISTEL.2012.6482959. ISBN 978-1-4673-2073-3.

[5] MOHAMMADI, Pejman a Simsek DEMIR. Two layers substrate integrated waveguide power divider. In: 2011 XXXth URSI General Assembly and Scientific Symposium. IEEE, 2011, 2011, pp. 1-4. DOI: 10.1109/URSIGASS.2011.6050563. ISBN 978-1-4244-5117-3.

[6] ZHARGCHENG HAO, WEI HONG, HAO LI, HUA ZHANG a KE WU. Multiway broadband substrate integrated waveguide (SIW) power divider. In: 2005 IEEE Antennas and Propagation Society International Symposium. IEEE, 2005, pp. 639-642 . DOI: 10.1109/APS.2005.1551401. ISBN 0-7803-8883-6.

[7] WANG, Liyuan, Chuanfang ZHANG, Mengjia LUO, Chunchun MA a Cheng JIN. W-band substrate integrated waveguide filter with cross-coupling. In: 2015 Asia-Pacific Microwave Conference (APMC). IEEE, 2015, 2015, pp. 1-3. DOI: 10.1109/APMC.2015.7413089. ISBN 978-1-4799-8765-8.

[8] NASRI, Abdelkhalek, Hassen ZAIRI a Ali GHARSALLAH. A compact bandpass substrate integrated waveguide filter. In: 2014 International Conference on Electrical Sciences and Technologies in Maghreb (CISTEM). IEEE, 2014, 2014, pp. 1-4. DOI: 10.1109/CISTEM.2014.7076931. ISBN 978-1-4799-7300-2.

[9] BHATTACHARJEE, A.K., A.K. MUKHOPADHYAY, J. KUNDU, B. MONDAL a S. MOITRA. Substrate integrated waveguide (SIW) filter using stepped-inductive posts for KU-Band applications. In: Third International Conference on Computational Intelligence and Information Technology (CIIT 2013). Institution of Engineering and Technology, 2013, 2013, pp. 398-401. DOI: 10.1049/cp.2013.2619. ISBN 978-1-84919-859-2.

[10] BEN CHAIEB, Tahar, Abdelkhalek NASRI a Hassen ZAIRI. Low loss substrate integrated waveguide slot antenna. In: 2017 International Conference on Advanced Systems and Electric Technologies (IC_ASET). IEEE, 2017, 2017, pp. 25-29. DOI: 10.1109/ASET.2017.7983661. ISBN 978-1-5090-6634-6.

[11] TAN, Ke-jun a Xiu-zhen LUAN. Millimeter wave circularly polarized substrate integrated waveguide antenna. In: 2008 International Conference on Microwave and Millimeter Wave Technology. IEEE, 2008, 2008, pp. 1058-1061. DOI: 10.1109/ICMMT.2008.4540604. ISBN 978-1-4244-1879-4.

[12] ZHIJUN CHEN, WEI HONG, ZHENQI KUAI, JIXIN CHEN a KE WU. Circularly polarized slot array antenna based on substrate integrated waveguide. In: 2008 International Conference on Microwave and Millimeter Wave Technology. IEEE, 2008, 2008, pp. 1066-1069. DOI: 10.1109/ICMMT.2008.4540606. ISBN 978-1-4244-1879-4.

[13] LEMBERG, K. V., O. A. NAZAROV, V. S. PANKO a Y. P. SALOMATOV. X-band substrate integrated waveguide (SIW) slot antenna array. In: 2013 International Siberian Conference on Control and Communications (SIBCON). IEEE, 2013, 2013, pp. 1-2. DOI: 10.1109/SIBCON.2013.6693589. ISBN 978-1-4799-1062-5.

[14] HAO WANG, Y. ZHENG, L. QIAN, J. XI, S. JI. Low Side-Lobe Substrate Integrated Cavity Antenna Array Using Unequal Microstrip-Ridge Gap Waveguide Feeding Network at 94 GHz. In: Applied Computational Electromagnetics Society Symposium (ACES), 2017. IEEE, 2017. ISBN: 978-0-9960-0785-6

[15] LIU, Hao, Anyong QING, Ziqiang XU a Zhao YANG. Low-Cost and High-Gain W-Band Circularly Polarized SIW Slot Antenna. In: 2019 IEEE International Symposium on Antennas and Propagation and USNC-URSI Radio Science Meeting. IEEE, 2019, 2019, s. 661-662. ISBN 978-1-7281-0692-2. doi:10.1109/APUSNCURSINRSM.2019.8888551

[16] WU, Yi-Wen, Zhang-Cheng HAO a Zhuo-Wei MIAO. A Planar W -Band Large-Scale High-Gain Substrate-Integrated Waveguide Slot Array. IEEE Transactions on Antennas and Propagation. 2020, 68(8), 6429-6434. ISSN 0018-926X. doi:10.1109/TAP.2020.2969999

[17] KE WU, D. DESIANDES a Y. CASSIVI. The substrate integrated circuits - a new concept for high-frequency electronics and optoelectronics. In: 6th International Conference on Telecommunications in Modern Satellite, Cable and Broadcasting Service, 2003. TELSIKS 2003. IEEE, 2003, P-III-P-X. DOI: 10.1109/TELSKS.2003.1246173. ISBN 0-7803-7963-2.

[18] BALANIS, Constantine A. Antenna theory: analysis and design. 3rd ed. Hoboken, NJ: John Wiley, c2005. ISBN 9780471667827.

[19] RAPHAEL, Reshma a T. SUDHA. Single-fed circularly polarized patch antenna for 60 GHz wireless applications. In: 2016 International Conference

on Emerging Technological Trends (ICETT). IEEE, 2016, 2016, pp. 1-6. DOI: 10.1109/ICETT.2016.7873695. ISBN 978-1-5090-3751-3.

[20] JANG, Tae Hwan, Young Hun HAN, Joonhyung KIM a Chul Soon PARK. 60 GHz Wideband Low-Profile Circularly Polarized Patch Antenna With an Asymmetric Inset. IEEE Antennas and Wireless Propagation Letters. 2020, 19(1), 44-48. ISSN 1536-1225. doi:10.1109/LAWP.2019.2952405

[21] BHATTACHARYYA, A., Y.M.M. ANTAR a A. ITTIPIBOON. Aperture-coupled patch antenna-theoretical and experimental investigations. In: Antennas and Propagation Society Symposium 1991 Digest . IEEE, 1991, pp. 1090-1093. DOI: 10.1109/APS.1991.175036. ISBN 0-7803-0144-7.

[22] ROSSELLO, Joaquim, Fermin MIRA, Ana COLLADO a Apostolos GEORGIADIS. Substrate integrated waveguide aperture coupled patch antenna array for 24 GHz wireless backhaul and radar applications. In: 2014 IEEE Conference on Antenna Measurements & Applications (CAMA). IEEE, 2014, 2014, pp. 1-2. DOI: 10.1109/CAMA.2014.7003408. ISBN 978-1-4799-3678-6.

[23] ALAM, Syah, Indra SURJATI a Yuli Kurnia NINGSIH. Patch modification and slot arrangement of microstrip antenna for improving the axial ratio. In: 2017 International Conference on Broadband Communication, Wireless Sensors and Powering (BCWSP). IEEE, 2017, 2017, pp. 1-5. DOI: 10.1109/BCWSP.2017.8272553. ISBN 978-1-5386-2833-1.

[24] Yue Li, Zhi Ning Chen, Xianming Qing, Zhijun Zhang, Junfeng Xu and Zhenghe Feng, “Axial ratio bandwidth enhancement of 60-GHz substrate integrated waveguide-fed circularly polarized LTCC antenna array,” IEEE Trans. Antennas Propag., vol. 60, no. 10, pp. 4619-4626, 2012.

[25] WU, Qiong-Sen, Xiao ZHANG a Lei ZHU. A Wideband Circularly Polarized Patch Antenna With Enhanced Axial Ratio Bandwidth via Co-Design of Feeding Network. IEEE Transactions on Antennas and Propagation. 2018, 66(10), 4996-5003. ISSN 0018-926X. doi:10.1109/TAP.2018.2851616

[26] LIU, Neng-Wu, Lei ZHU, Zhong-Xun LIU, Guang FU a Ying LIU. Design Approach of a Single Circularly Polarized Patch Antenna With Enhanced AR-Bandwidth Under Triple-Mode Resonance. IEEE Transactions on Antennas and Propagation. 2020, 68(8), 5827-5834. ISSN 0018-926X. doi:10.1109/TAP.2020.2995303

3 OBJECTIVES

The previous, state of the art section of this thesis described the properties of two technologies – substrate integrated waveguides and patch antennas. The attention was mostly focused on versatility and customizability of both solutions, resulting in a good potential of utilizing these structures for construction of antenna array systems in the millimeter wavelength band. Based on this analysis, the main objectives of this dissertation thesis are formulated in this section. The objectives can be divided into two main research areas.

Objective 1: Design a circularly polarized 2x2 antenna array of patch antennas fed by substrate integrated waveguide.

The design of the array will be realized ascendingly at two frequency setpoints: 17 GHz and 60 GHz. The results will be compared, and sensitivity analysis will be performed in order to assess feasibility of the solution at the 60 GHz frequency setpoint with respect to the accuracy of the existing manufacturing methods and available materials. Power division network based on substrate integrated waveguides will use suitable elements to ensure proper phase distribution of the signal within the array. Cutoff frequencies and corresponding dimensions of the substrate integrated waveguides will be analyzed in order to optimize parameters of the array. The array should serve as a base building block to create larger arrays therefore, the design should show modular properties. A suitable transition to the substrate integrated waveguide will be analyzed for each frequency setpoint. Focus will be also drawn to maximization of the level of integration resulting in minimization of needed layers of the microwave substrate and used area. Existing improvement techniques of extending the axial ratio bandwidth will be incorporated in the array design. Guidelines and methodology will be the result of the first objective.

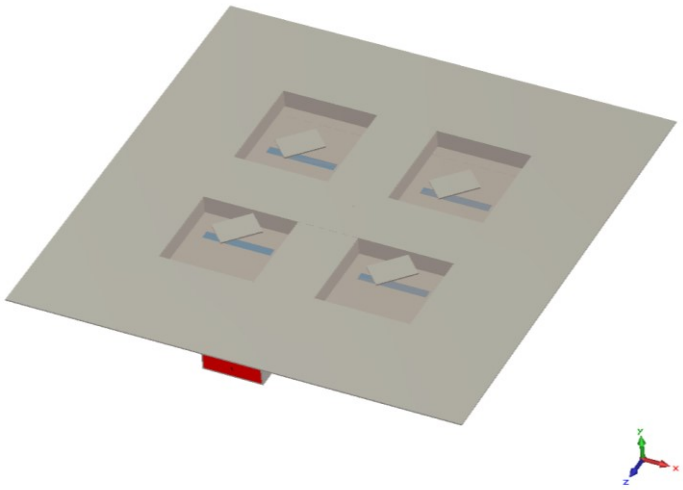

Fig. 3.1 Proposed antenna array

Objective 2: The research of possibilities of increasing the axial ratio bandwidth of circularly polarized patch antennas

Exploitation of parasitic patches, placed above the original antenna array structure, to increase the axial ratio bandwidth of the array, will be introduced as a new technique to considerably improve the characteristics. Verification will be done by simulations and measurements. Parametric sweep will be performed in order to identify the key parameters, which influence the properties of the system. Description of the new technique and methodology will be the result of the second objective.

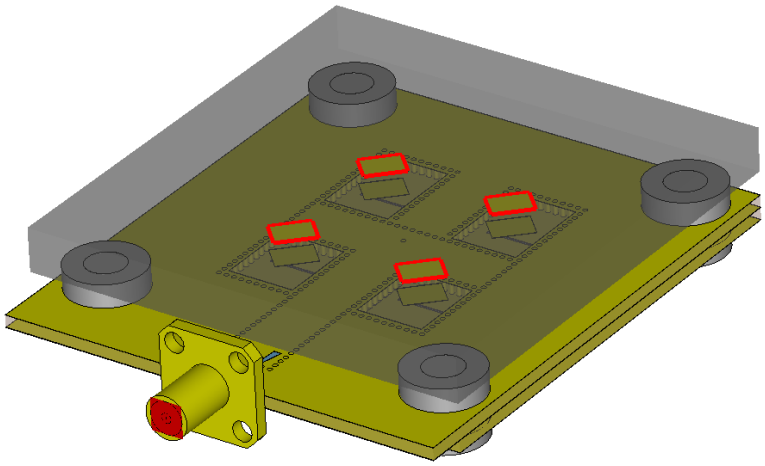

Fig. 3.2 Proposed antenna array with parasitic patches

4 ANTENNA ARRAY DESIGN AT 17 GHZ

4.1 INTRODUCTION

The array is required to have the following properties:

- Center frequency of 17 GHz.
- Modularity – the array should serve as a base building block to create larger arrays.
- Circular polarization.
- Patch radiating elements.
- Maximum utilization of the substrate area.

4.2 DESIGN OF THE ARRAY

The array consists of two layers of Cuclad 217LX with relative permittivity $\varepsilon_r = 2.17$ and height $h = 1.524$ mm.

Power flow within the structure is shown in Fig. 4.1. In the top layer a grounded coplanar waveguide to substrate integrated waveguide transition is exploited to provide means of connecting an SMA connector, which is necessary to conduct the measurements [2]. Further on there is a power divider, which splits the power with the same amplitude and phase into two arms using a shortening pin. At the shortened end of each arm a coupling slot (*A*) is used as a transition into the bottom layer [3].

The coupling slot (*A*) also plays role of another power divider which divides the power with the same amplitude but the opposite phase to a set of two substrate integrated waveguides in the bottom layer whose purpose is to distribute the power to the radiating elements. The phase inversion is here necessary to obtain a radiation pattern with the maximum located in the direction perpendicular to the structure. At both shortened ends of each substrate integrated waveguide there is a coupling slot (*B*), which excites the radiating element in the top layer. Considering the fact that the coupling slot (*A*) cannot be located in the middle of the substrate integrated waveguide in the top layer, the structure is not axially symmetrical in the horizontal direction. Otherwise, the coupling slot (*A*) would have to be moved and an additional and unwanted phase shift would be introduced into the structure due to different distances to the coupling slots (*B*) resulting in divergence of the main lobe from the direction perpendicular to the structure.

The rectangular-shaped patches in the top layer are the radiating elements of the array. The patches were rotated by 45° in order to obtain circularly polarized wave. Around each patch a via fence was added to reduce coupling between the patches, resulting in wider axial ratio bandwidth [5]. Vias, which form the inner part of the fence around the bottom patches, serve also as walls of the substrate integrated waveguide power divider. Finally, metallization around the array was added to improve symmetry of the radiation pattern and axial ratio bandwidth.

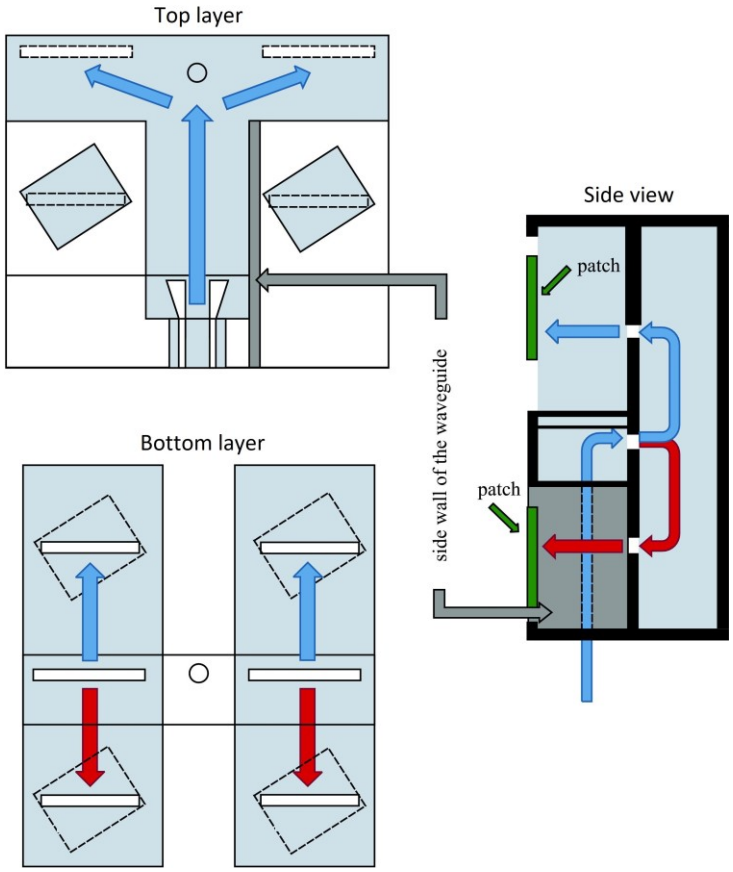

Fig. 4.1 Power flow within the array structure

Width of the substrate integrated waveguide in the top layer has been reduced to minimize the distance between the patches in the horizontal direction. Therefore, the cutoff frequency of this waveguide is close to 17 GHz which is the center frequency of the array. Width of the substrate integrated waveguide in the bottom layer has been increased to reduce guided wavelength and minimize the distance between the patches in the vertical direction. As a result, area of the array has been minimized.

The ratio between the sides of the rectangular patches has been optimized to maximize axial ratio bandwidth.

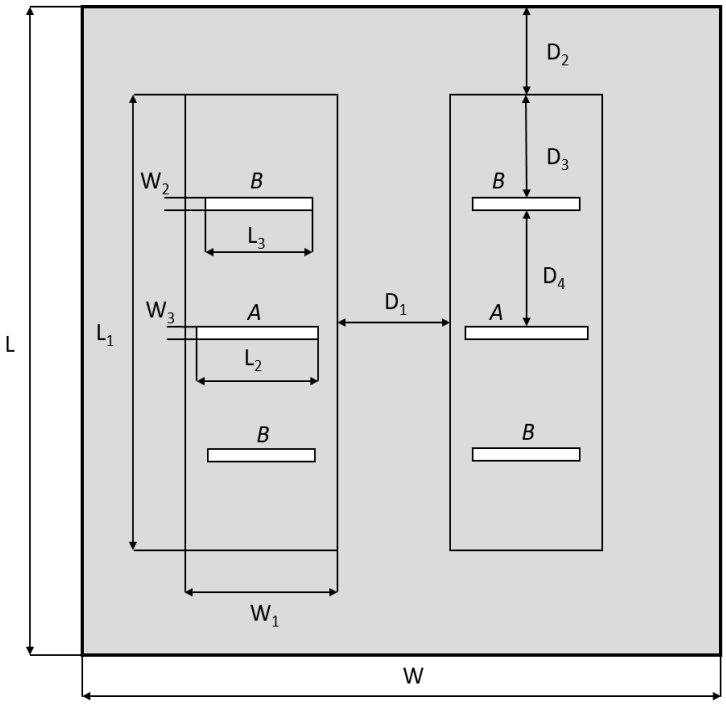

Fig. 4.2 Layout of the bottom layer

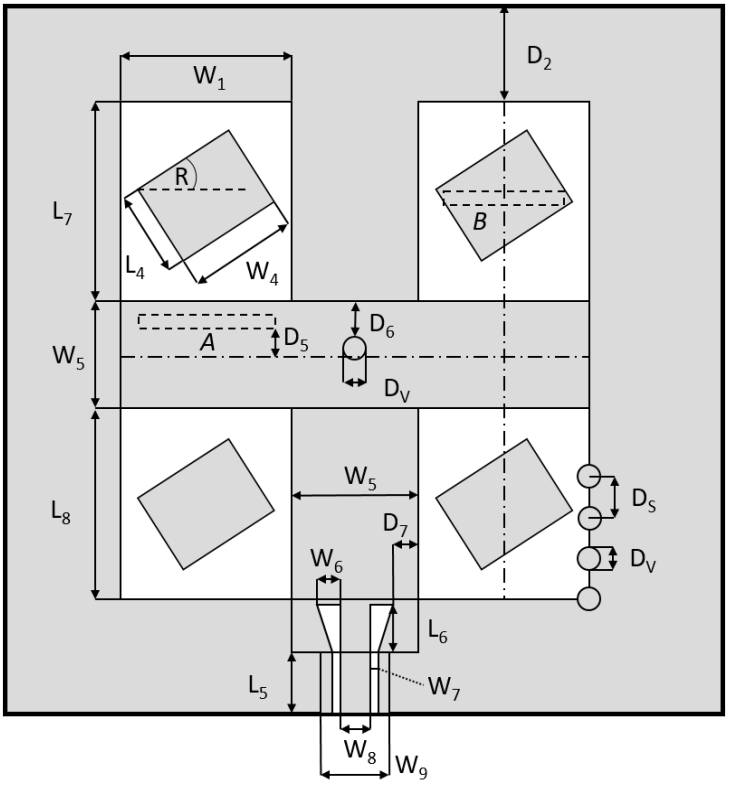

Fig. 4.3 Layout of the top layer

The dimensions of the array are summarized in Table I. Refer to Fig 4.2 and Fig 4.3 to see how each parameter corresponds to the design of the array. Unless denoted otherwise in the figures, all dimensions related to the SIWs are referenced to the centers of the vias.

Table I Dimensions of the array for the center frequency of 17 GHz

parameter	***dimension (mm)***	***parameter***	***dimension (mm)***
L	65.00	W_6	1.00
L_1	32.40	W_7	0.30
L_2	7.50	W_8	3.00
L_3	6.50	W_9	5.00
L_4	3.92	D_1	7.20
L_5	5.00	D_2	12.80
L_6	3.50	D_3	7.25
L_7	13.60	D_4	8.35
L_8	11.60	D_5	0.70
W	57.27	D_6	2.50
W_1	10.00	D_7	0.90
W_2	0.30	D_v	0.60
W_3	0.60	D_S	1.01
W_4	5.08	R	45.00°
W_5	7.20		

The final structure is suitable to be used as a base building block for larger arrays as the feeding network is designed to be easily connectable by SIW interconnects that have the same configuration as within the base building block. Such an array will then have a fractal-like configuration since the same pattern is applied for each iteration and the design elements within the base building block serve as the construction template. The time required to design this kind of an array is therefore greatly reduced. A 4x4 array shown in Fig. 4.4 can serve as an example.

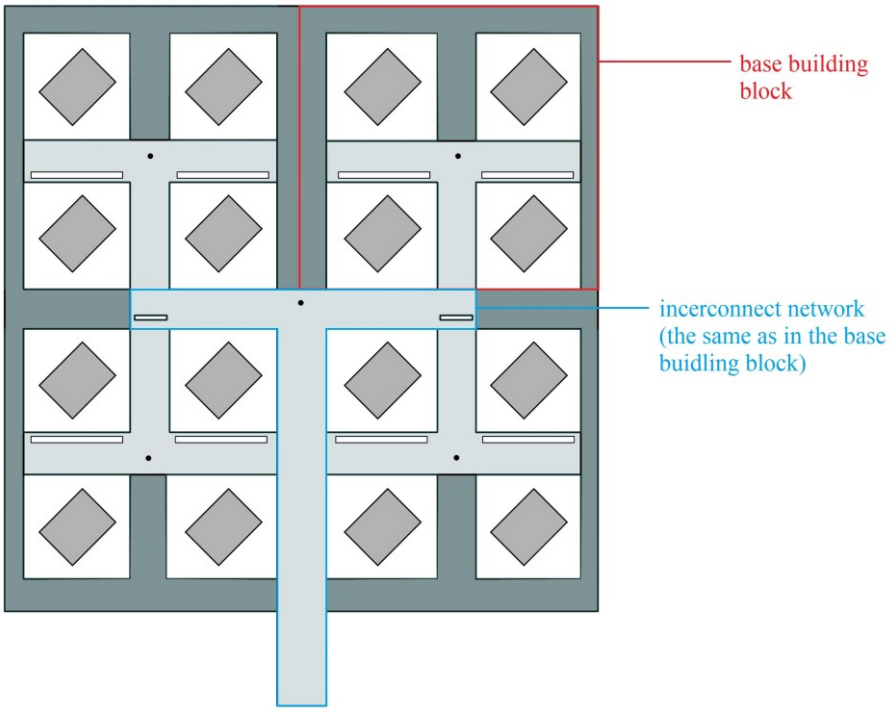

Fig. 4.4 Example of a 4x4 array assembled from four 2x2 base building blocks

4.3 SIMULATIONS AND MEASUREMENTS

In the initial step, solid side walls of the waveguides, perfect electric conductivity of all metallic surfaces and lossless dielectrics have been considered to reduce simulation time. At the advanced stage of the design, ideal properties of the materials were changed to realistic models and solid side walls of the waveguides were replaced by vias. Optimization has been performed to obtain an equivalent substrate integrated waveguide.

In addition, by omitting the rotation of the radiation elements, the array can easily be modified to radiate a linearly polarized wave.

Photograph of the fabricated array is shown in Fig. 4.5.

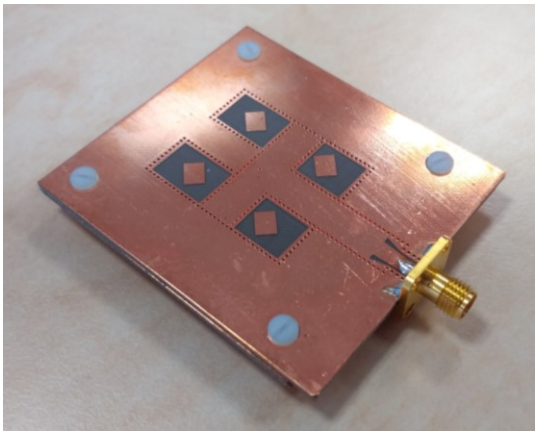

Fig. 4.5 Manufactured array

Impedance characteristics of the array are shown in Fig. 4.6. Resonance frequencies of the simulated array appear at 16.82 and 17.23 GHz. The fabricated array shows resonance at 16.77 and 17.27 GHz. The absolute value of the reflection coefficient of the fabricated array is higher due to finite precision of the manufacturing process and imperfect SMA connector mounting, which has been done by hand. The connection therefore does not reach the ideal quality assumed in the simulation model.

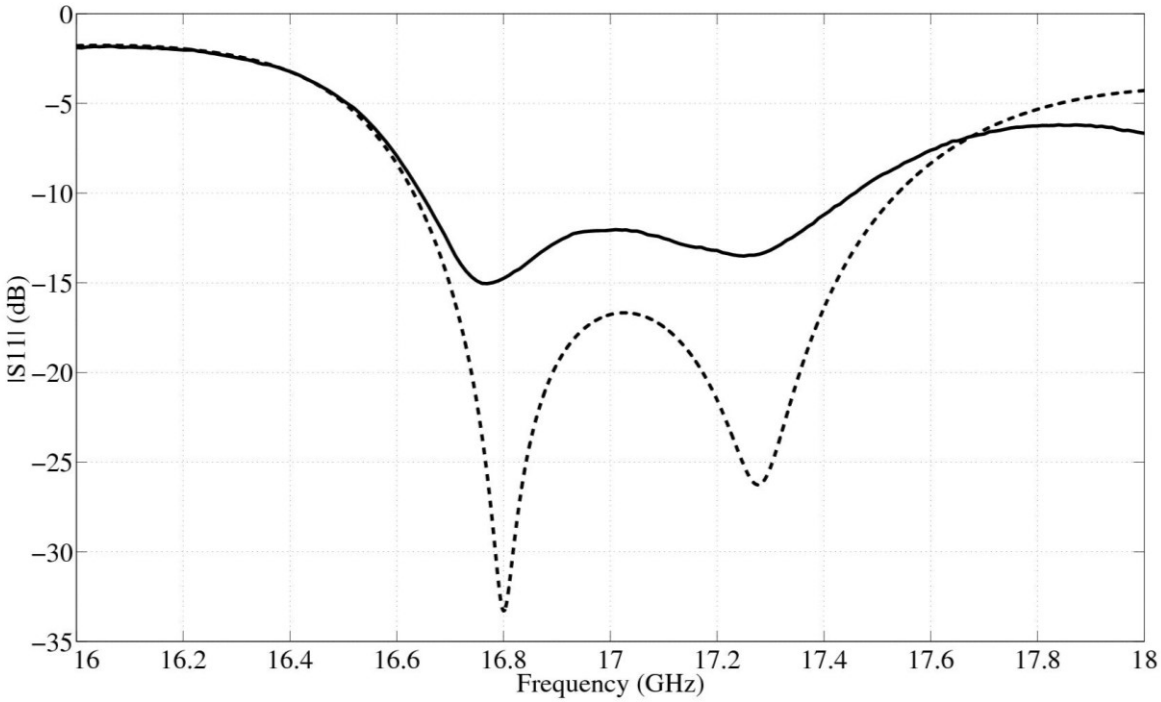

Fig. 4.6 Frequency response of the magnitude of reflection coefficient at the input of the antenna array: measured (solid), simulated (dotted).

Impedance bandwidth of the simulated array (the condition $|S_{11}| < -10$ dB) is from 16.64 GHz to 17.55 GHz (5.1 % relatively). The low frequency limit of the measured array appears at 16.65 GHz, and the upper one is at 17.46 GHz.

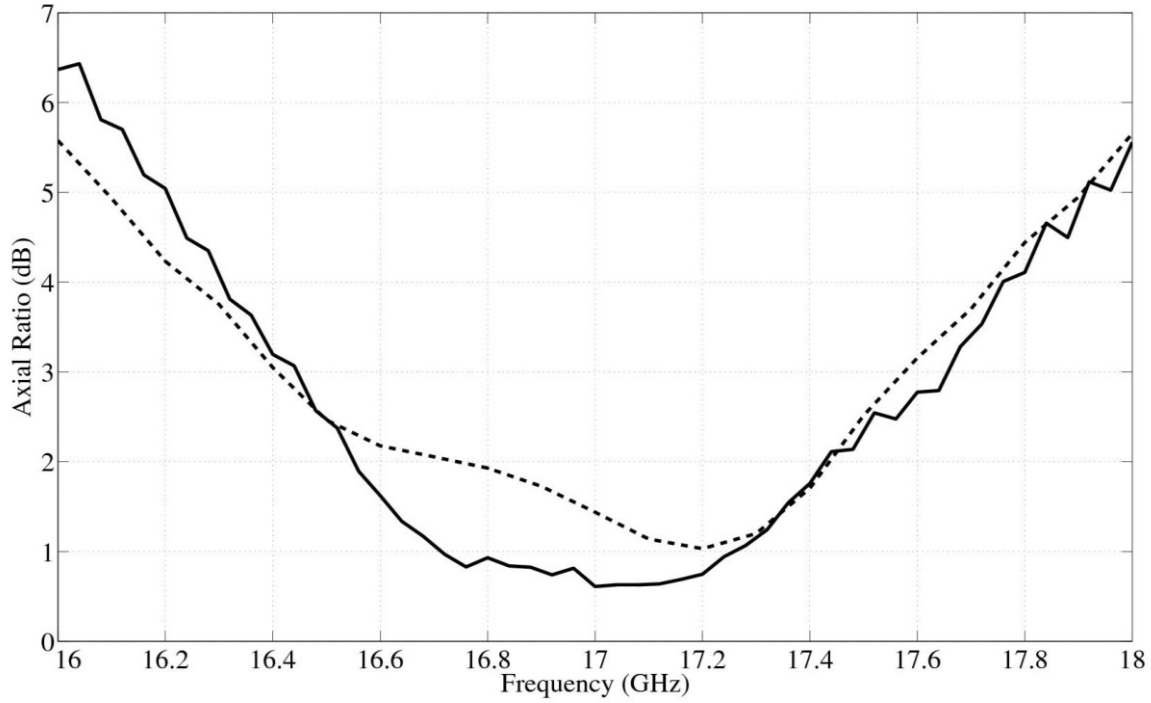

Fig. 4.7 Frequency response of the axial ratio in the main lobe direction of the antenna array: measured (solid), simulated (dotted).

Polarization properties of the designed antenna are characterized by axial ratio (see Fig. 4.7). The circular polarization bandwidth (the condition $|AR| < 3$ dB) of the simulated array is from 16.4 GHz to 17.58 GHz. The low frequency limit of the measured antenna appears at 16.45 GHz, and the upper one is at 17.65 GHz.

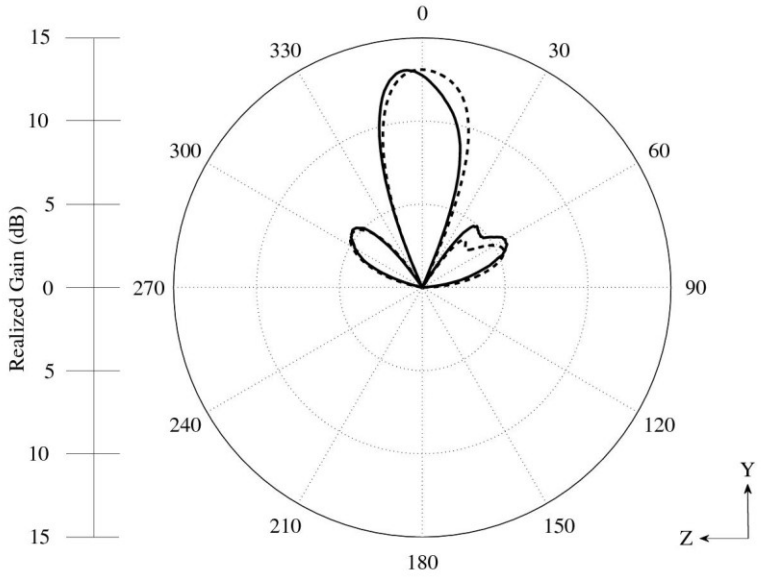

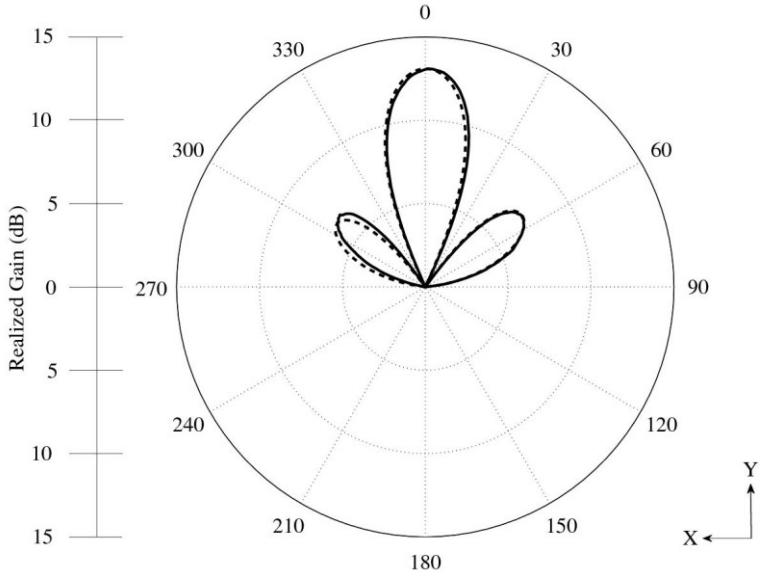

Fig. 4.8 Radiation patterns of the array in YZ and XY plane: measured (solid), simulated (dotted).

Radiation patterns of the antenna are shown in Fig. 4.8. The main lobe is oriented perpendicularly to the surface of the substrate. The beam width (3 dB decrease of gain with respect to main lobe direction) is 27.1° in the *xy* plane and 30.1° in the *yz* plane. Minor pattern distortion of the manufactured array is caused by the fact that some of the vias were not ideally manufactured. Ratio between diameter and height of the vias was beyond safe limits of the used technology for the chosen material therefore manufacturing without defects was not guaranteed.

4.4 DESIGN METHODICS

The design process can be summarized into the following list:

1. Define the desired center frequency of the array structure and choose a suitable material for the substrate.
2. Design and optimize classical rectangular waveguides to be used for signal delivery in the first iteration of the model.
3. Design and optimize the power division and phase shifting elements to achieve the desired transformations of the input signal.
4. Calculate and optimize the positions of the coupling slots that feed the radiating elements.
5. Identify and design a suitable method of feeding the array structure with respect to the defined center frequency.
6. Optimize the dimensions of the radiating element (rectangular patch) and the ratio of its dimensions to achieve the desired polarization properties at the defined center frequency.
7. By using a simplified model, consisting of only a simple rectangular waveguide, the radiating element and the feeding coupling slot, optimize the dimensions of

the coupling slot and its relative position to the radiating element to achieve optimal performance with the radiating element.

8. By assembling the designed components, create the base building block consisting of four radiating elements and by using optimization methods, fine tune its properties to provide maximum performance at the defined center frequency.
9. Design and optimize equivalent substrate integrated waveguides to replace the classical rectangular waveguides.
10. Confirm properties of the array with substrate integrated waveguides. If needed, further optimize the structure.

4.5 CONCLUSION

In the chapter, design of a modular circularly polarized patch antenna array for the center frequency of 17 GHz is described.

The design brings the following improvements:

- The feeding network geometry has been designed in such way that the array can be considered as a base building block to create larger arrays. The array therefore shows modular properties. A 2x2 matrix of the building blocks (see Fig. 4.4) forms a 4x4 array. The only task for the designer is to connect the blocks by an interconnect network that utilizes the same pattern as the base block. The base building block then also serves as the template to realize the larger array – the design is self-documented. Structural regularity is a natural property of such an array and the time needed to design it is greatly reduced because the critical part is ready to use. Resulting array structures resemble fractals and the number of radiating elements can be theoretically extended infinitely while maintaining the constant number of layers and the level of complexity. Open literature does not deal with structures that incorporate this kind of modularity.

- In open literature, similar arrays consist of three layers [5]. This design reduces the number of layers to two by increasing the level of integration, utilizing the walls of the substrate integrated waveguides (SIWs) as part of the via fence. This way, all the available area gets utilized, reducing space and material requirements.

- Disproportion of reflective surfaces around the radiating elements cause distortion of the radiation pattern and narrows down the axial ratio bandwidth [4]. Metallization around the array structure has been added to compensate for those effects.

The achieved results were presented in the following publications:

[1] J.Spurek, Z. Raida, “Circularly polarized modular patch antenna array fed by substrate integrated waveguide,“ Microwave and Optical Technology Letters, 2018, vol. 60, no. 6, pp. 1398-1403. ISSN: 1098-2760.

4.6 REFERENCES

[2] Y. Cai, Z. Qian, W. Cao, Y. Zhang, J. Jin, L. Yang, and N. Jing, “Compact wideband SIW horn antenna fed by elevated-CPW structure,” IEEE Trans. Antennas Propag., vol. 63, no. 10, pp. 4551-4557, 2015.

[3] D. M. Pozar, Microwave Engineering, 4th ed. Hoboken, NJ: J. Wiley & Sons, 2012.

[4] J. Spurek, J. Velim, M. Cupal, Z. Raida, J. Prasek, and J. Hubalek, “Slot loop antennas printed on 3D textile substrate,” in Proc. MIKON, Krakow, Poland, 2016.

[5] Yue Li, Zhi Ning Chen, Xianming Qing, Zhijun Zhang, Junfeng Xu and Zhenghe Feng, “Axial ratio bandwidth enhancement of 60-GHz substrate integrated waveguide-fed circularly polarized LTCC antenna array,” IEEE Trans. Antennas Propag., vol. 60, no. 10, pp. 4619-4626, 2012.

5 CONVERSION TO 60 GHZ

5.1 INTRODUCTION

The requirements for the array are the same as listed in chapter 4.1, except for the center frequency, which is in this case 60 GHz.

5.2 WR15 TO SIW TRANSITION

As for 60 GHz, feeding the array by an SMA connector is not feasible, a new feeding structure had to be designed. A waveguide to SIW transition was chosen. The transition from a classical WR15 waveguide is first realized by 8 vertical steps to gradually assume the height of the SIW and then a linear horizontal taper is used to match the SIW's width (see Fig. 5.1). Outer dimensions of the transition were chosen with respect to the standardized waveguide equipment in order to attach it to measurement instruments.

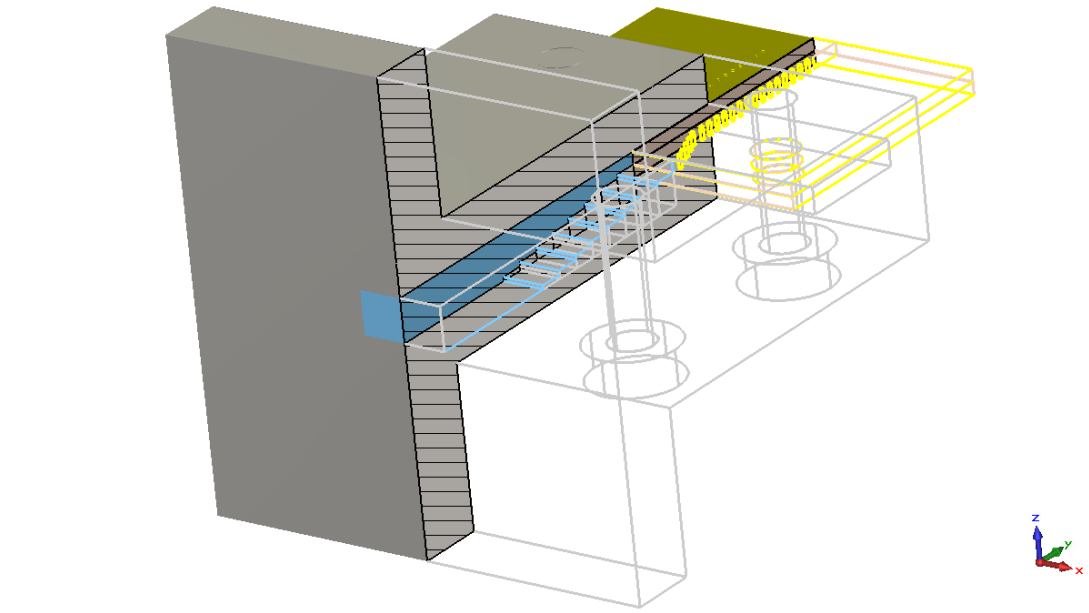

Fig. 5.1 WR15 to SIW transition

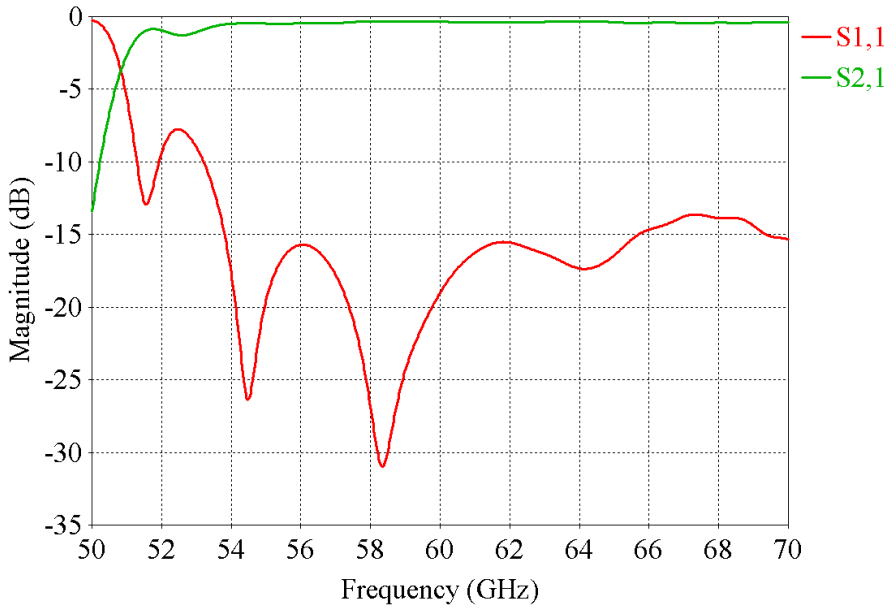

Fig. 5.2 Simulated frequency response of the reflection coefficient (S11) and the transmission coefficient (S21) of the designed WR15-SIW transition.

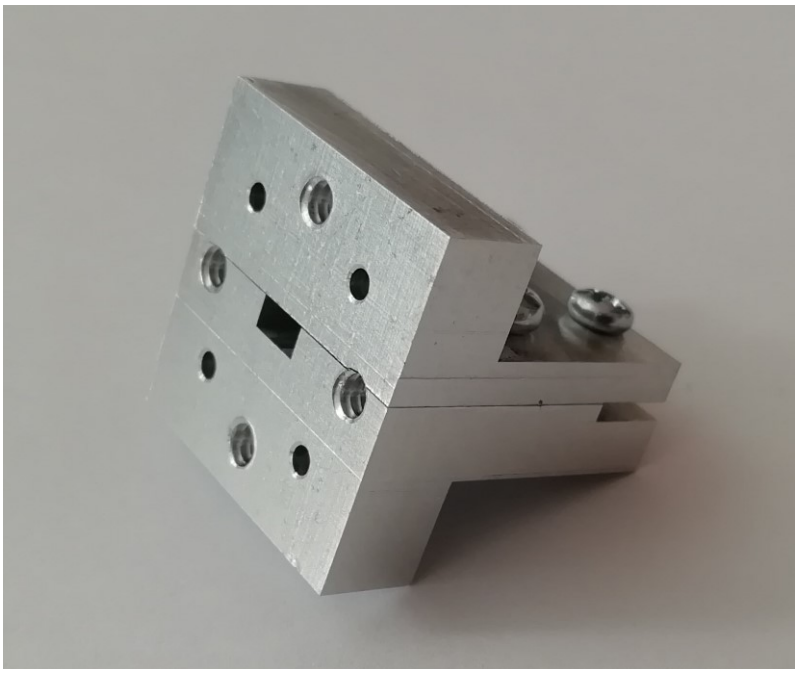

Fig. 5.3 Manufactured WR15 to SIW transition (1).

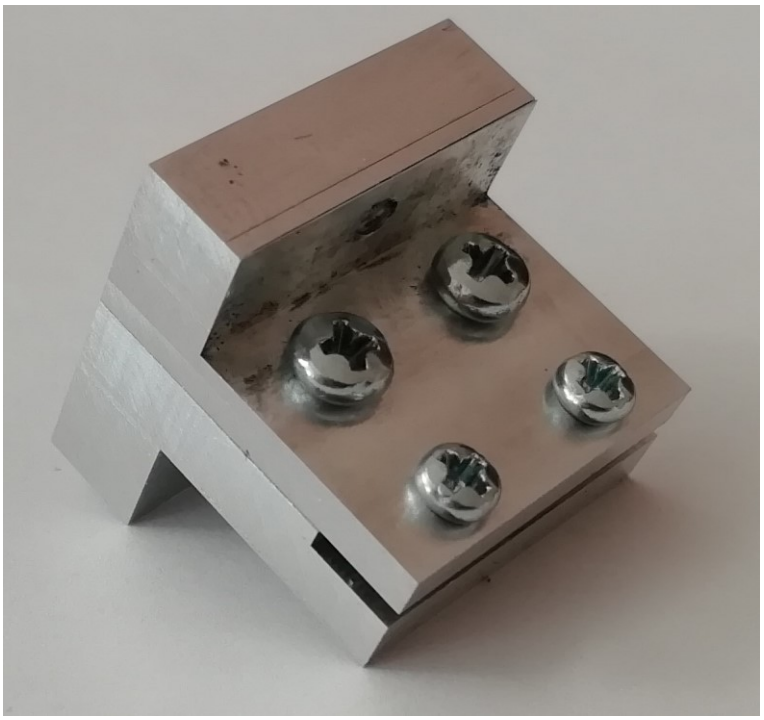

Fig. 5.4 Manufactured WR15 to SIW transition (2).

5.3 CONVERSION OF THE ARRAY TO 60 GHZ

The converted antenna array is built on the same microwave substrate (Cuclad 217LX), however the height was reduced to h = 0.508 mm. In the first step, all the components were scaled down with respect to the shortened wavelengths. After that, the model was optimized by the same workflow as for 17 GHz to obtain properties as similar as possible. First, using the solid side wall model, later the fully realistic model.

The final model for 60 GHz setpoint was created by addition of the WR15 to SIW transition to the converted antenna array structure's SIW input (see Fig. 5.5).

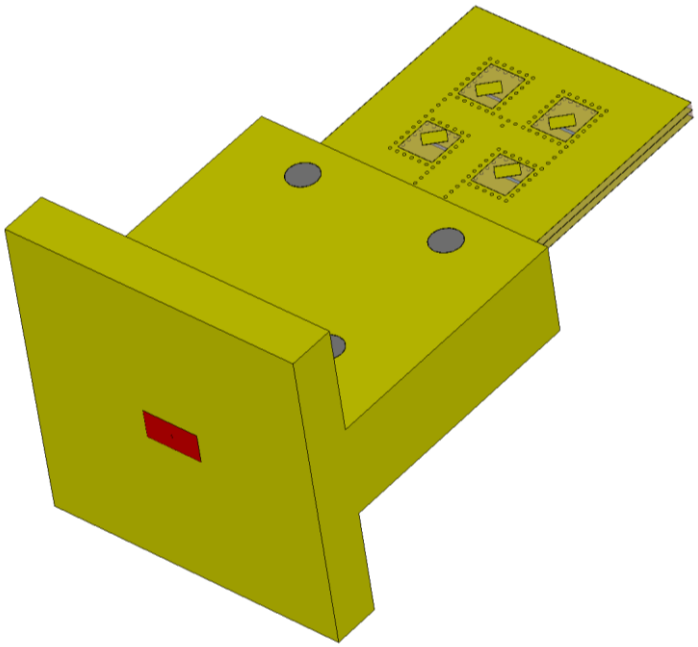

Fig. 5.5 Final model for 60 GHz

5.4 SIMULATED RESULTS

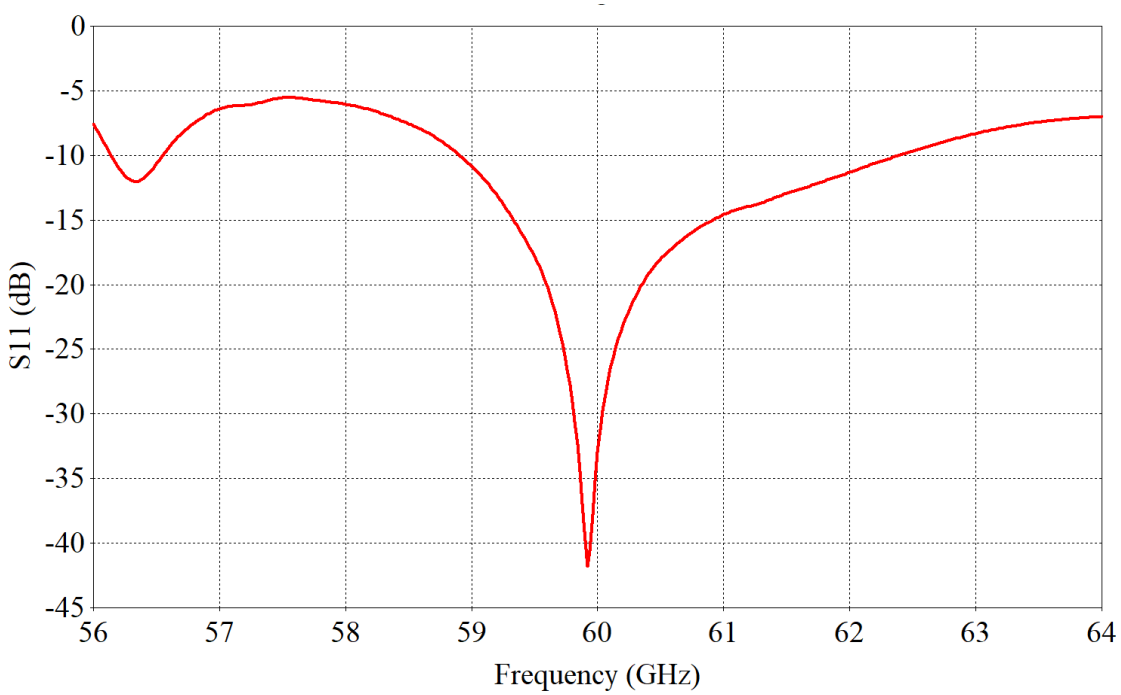

Fig. 5.6 Frequency response of the reflection coefficient of the simulated array at 60 GHz.

Impedance characteristics of the simulated array are shown in Fig. 5.6. Impedance bandwidth of the converted array is from 58.9 – 62.4 GHz (5.8% relatively).

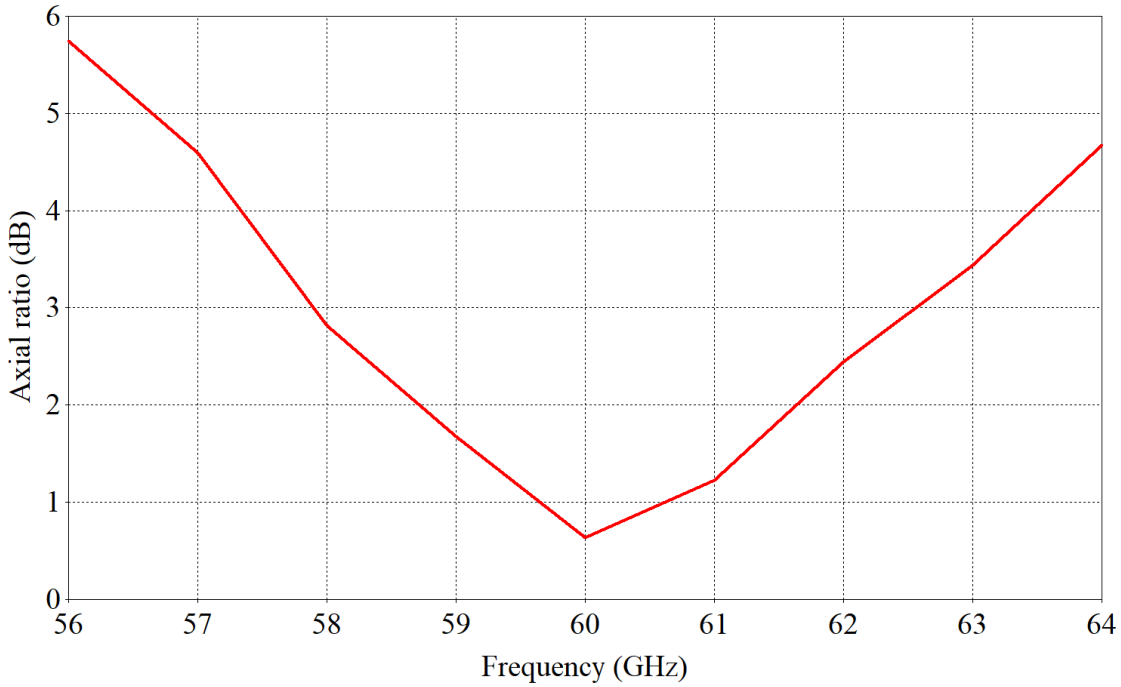

Fig. 5.7 Frequency response of axial ratio of the simulated array at 60 GHz

Polarization properties of the simulated array are characterized by axial ratio (see Fig. 5.7). The circular polarization bandwidth of the simulated array is from 57.9 GHz to 62.6 GHz (7.8 % relatively).

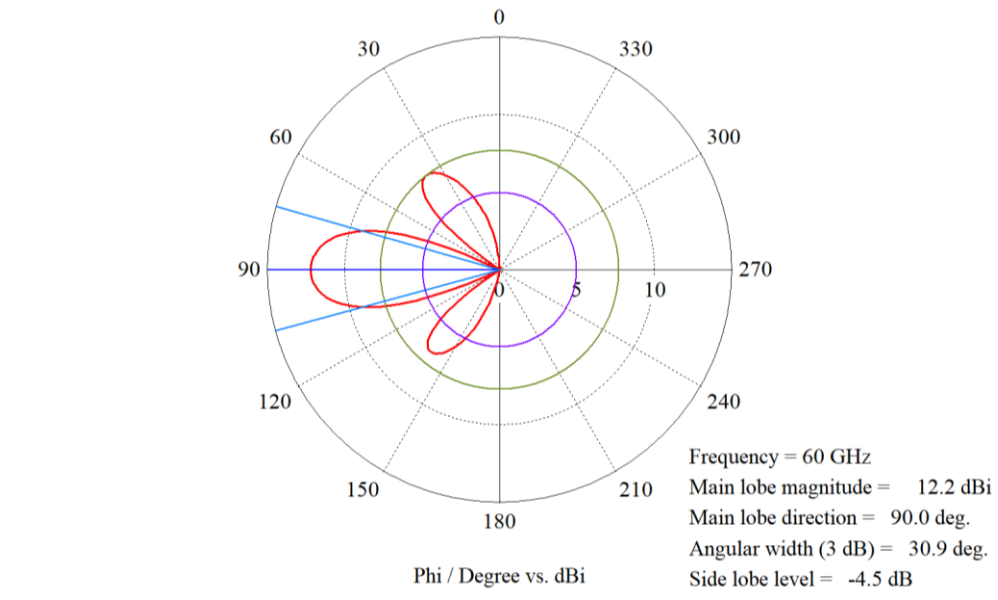

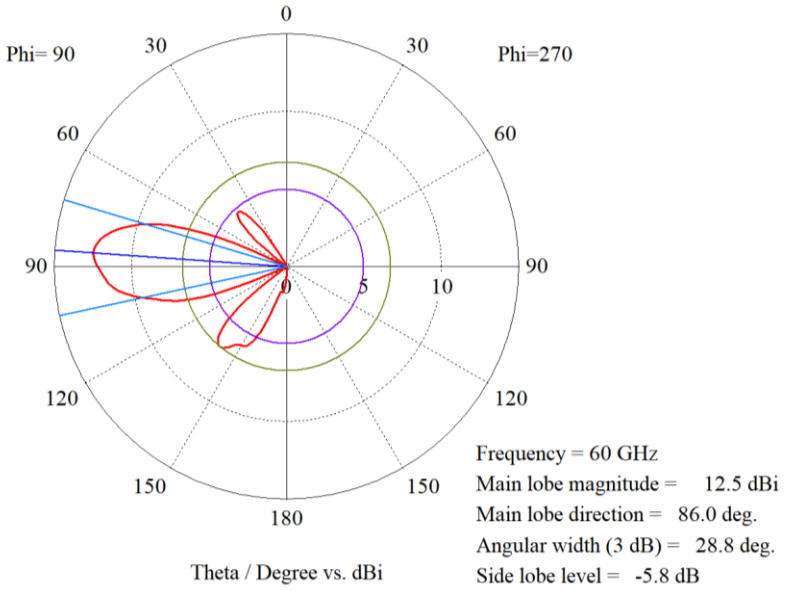

Fig. 5.8 Radiation patterns of the simulated array in YZ (down) and XY (up) plane (LHCP, realized gain).

Radiation patterns of the simulated antenna array in YZ and XY planes are shown in Fig. 5.8. The beam width is 30.9° in the *xy* plane and 28.8° in the *yz* plane.

In summary, the array converted to the center frequency of 60 GHz shows comparable properties in terms of relative bandwidths and radiation properties as the original array designed at the center frequency of 17 GHz.

5.5 SENSITIVITY ANALYSIS

In order to assess tolerance of the proposed structure to manufacturing variations, a sensitivity analysis was performed. It is expected that the manufacturing technique can provide precision of 0.1 mm around the mean value. The following parameters were subjected to the analysis (illustrated in Fig 5.9):

A Position of the patches in relation to the coupling slots.
B Dimensions of the coupling slots
C Dimensions of the coupling slots between the layers.
D Position of the coupling slots between the layers
E Position of the shorting pin in the power divider
F1, F2 Width of the waveguides
G Dimensions of the patches

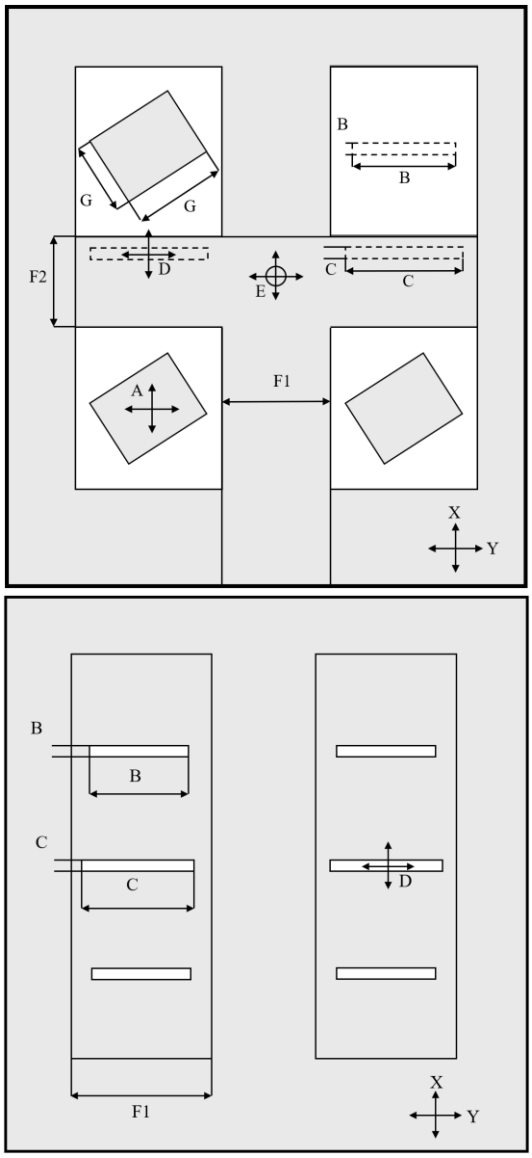

Fig. 5.9 Illustration of the swept dimensions – top and bottom layer.

In order to minimize the simulation time, a simplified numerical model was used for the analysis (the shorting pins of the substrate integrated waveguides were replaced by solid walls, forming a conventional rectangular waveguide). This allowed to significantly cut the number of mesh cells, reducing the time of each run by 90%, approximately.

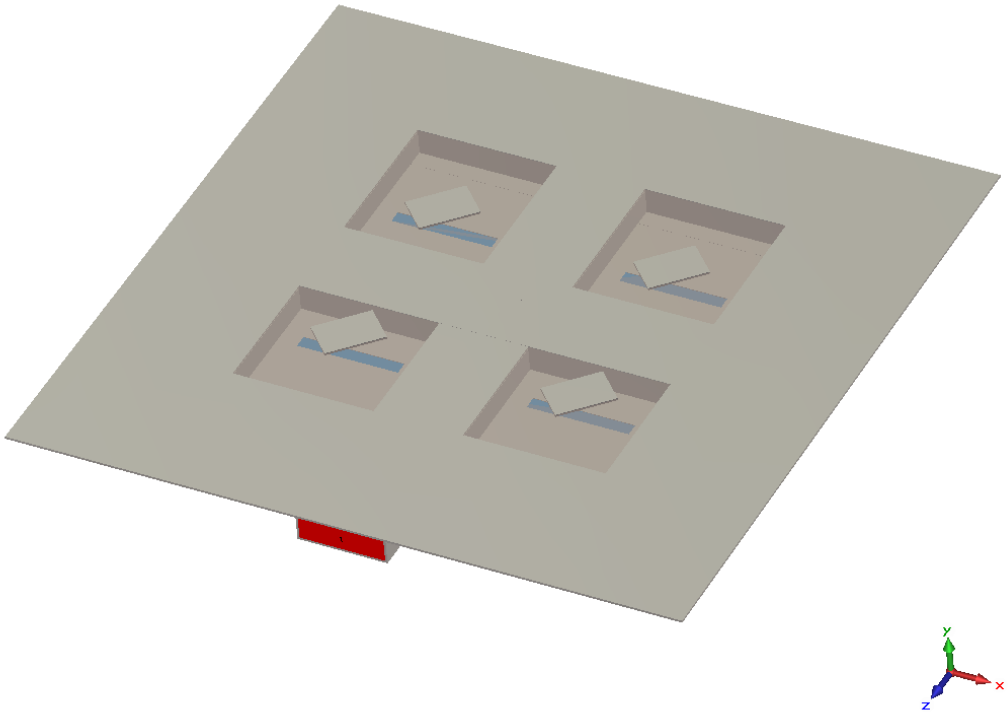

Fig. 5.10 Simplified model of the array with solid side walls.

To minimize the area of the legend, simulations are denoted as runs 1 to 9 in the charts. Runs correspond to variations of the parameters *A–E*, *F1*, *F2*, *G* in **X** and **Y** axes as shown in Table II.

Table II Mapping of the simulation runs to the parameter changes.

	varying parameters A-E, G	***varying parameters F1, F2***
run 1	*x* – 0.1 mm; *y* – 0.1 mm	*F1* – 0.1 mm; *F2* – 0.1 mm
run 2	*x* – 0.1 mm; *y*	*F1* – 0.1 mm; *F2*
run 3	*x* – 0.1 mm; *y* + 0.1 mm	*F1* – 0.1 mm; *F2* + 0.1 mm
run 4	*x*; *y* – 0.1 mm	*F1*; *F2* – 0.1 mm
run 5	*x*; *y* (optimum)	*F1*; *F2* (optimum)
run 6	*x*; *y* + 0.1 mm	*F1*; *F2* + 0.1 mm
run 7	*x* + 0.1 mm; *y* – 0.1 mm	*F1* + 0.1 mm; *F2* – 0.1 mm
run 8	*x* + 0.1 mm; *y*	*F1* + 0.1 mm; *F2*
run 9	*x* + 0.1 mm; *y* + 0.1 mm	*F1* + 0.1 mm; *F2* + 0.1 mm

5.5.1 Position of the patches in relation to the coupling slots

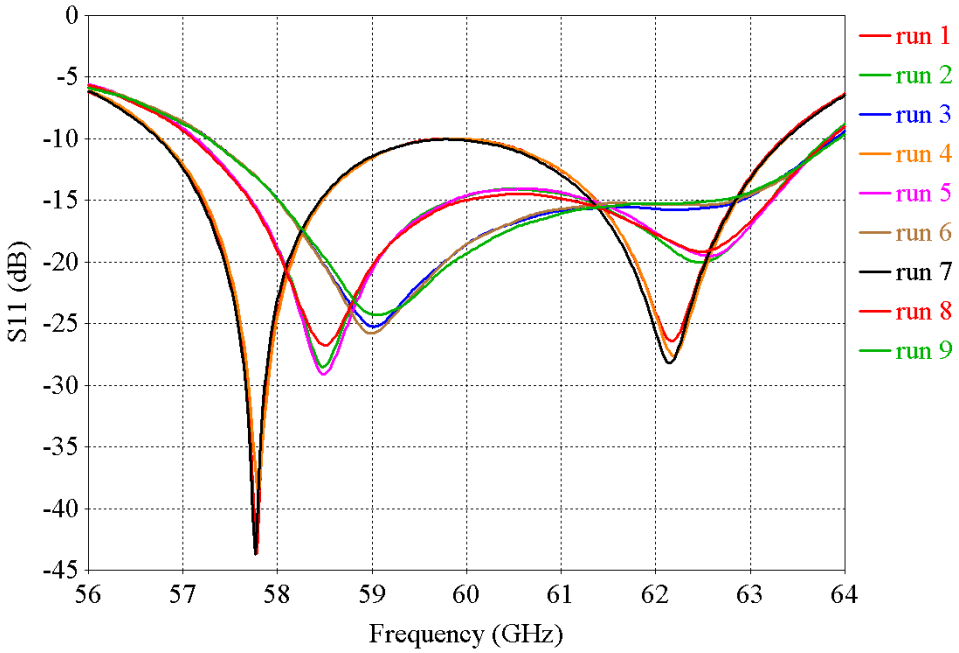

Fig. 5.11 Frequency responses of the reflection coefficient for 0.1 mm variance around the center value

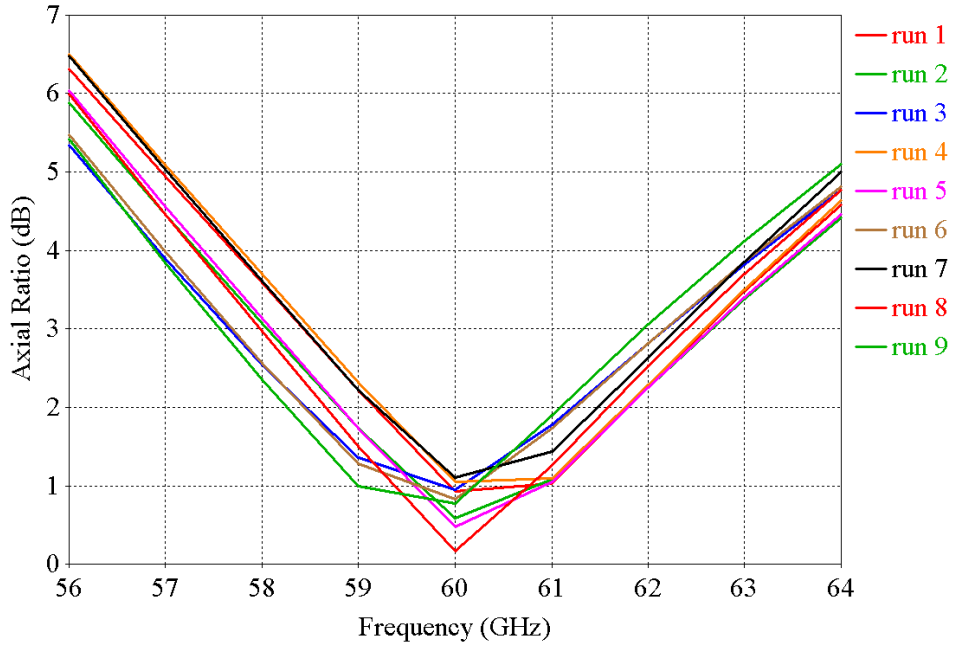

Fig. 5.12 Frequency responses of the axial ratio for 0.1 mm variance around the center value

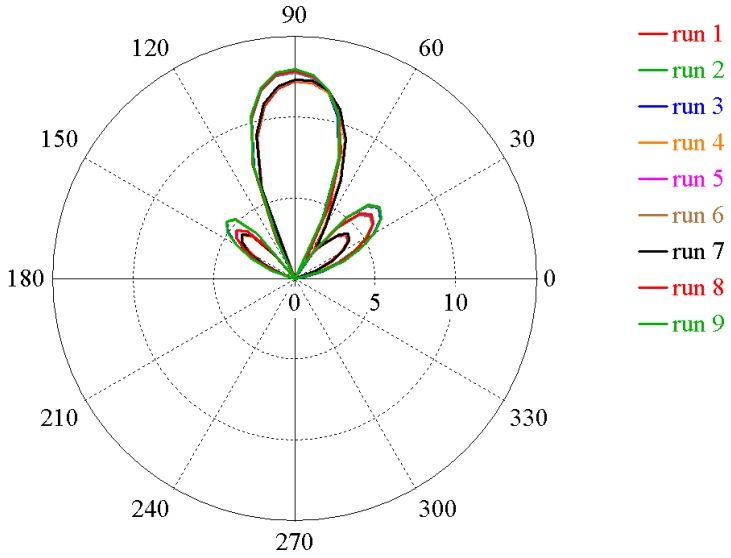

Fig. 5.13 Radiation patterns in XY plane for 0.1 mm variance around the center value

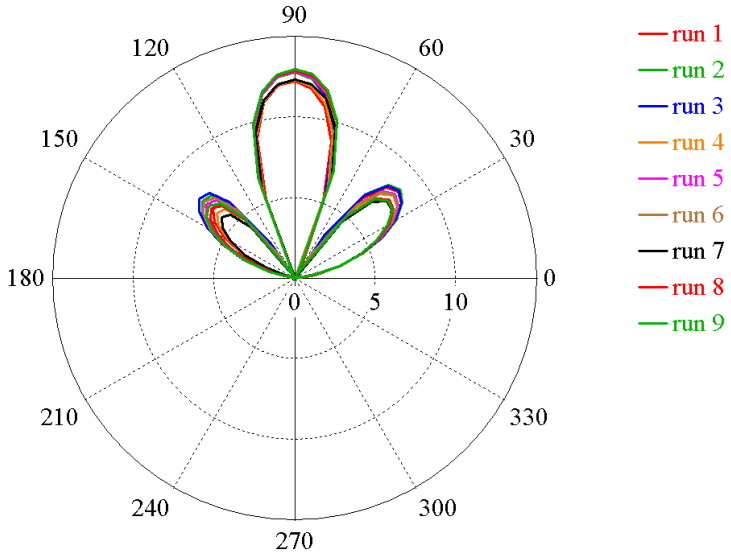

Fig. 5.14 Radiation patterns in YZ plane for 0.1 mm variance around the center value

As can be seen in Fig. 5.11 – 5.14, variance of the patch positions in relation to the coupling slots influences all the properties of the array. Misplacing the patches leads to larger magnitude of the reflection coefficient, though it is still under -10 dB in the frequency range of interest. Radiation patterns show degradation in terms of decreased gain in the main lobe direction and increased side lobe level. In addition, the direction of the main lobe in the XY plane deviates from its optimum since varying the patch positions causes changes in the phasing properties of the array. The structure shows the least influence on the axial ratio. The changes are considered as acceptable.

5.5.2 Dimensions of the coupling slots

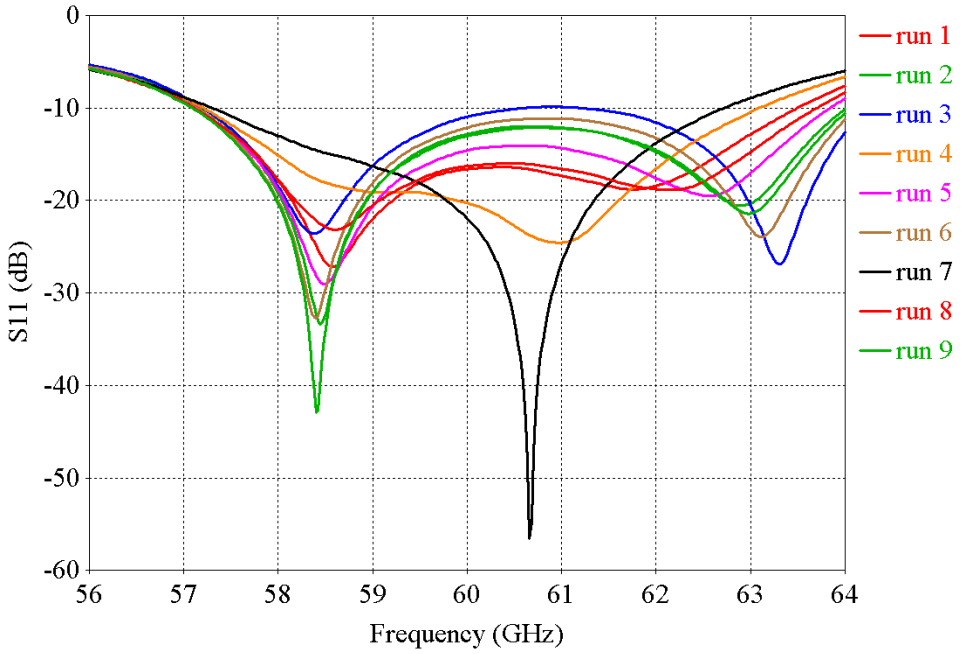

Fig. 5.15 Frequency responses of the reflection coefficient for 0.1 mm variance around the center value

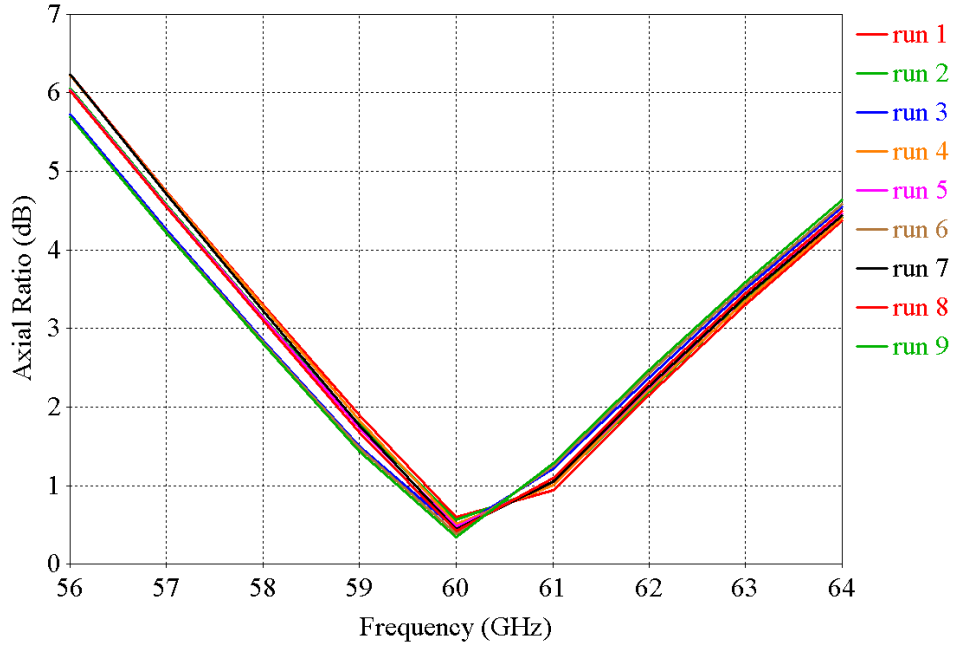

Fig. 5.16 Frequency responses of the axial ratio for 0.1 mm variance around the center value

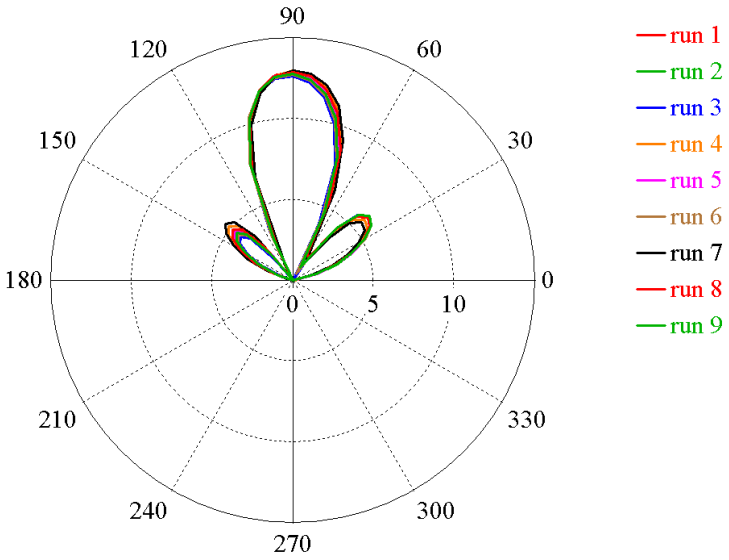

Fig. 5.17 Radiation patterns in XY plane for 0.1 mm variance around the center value

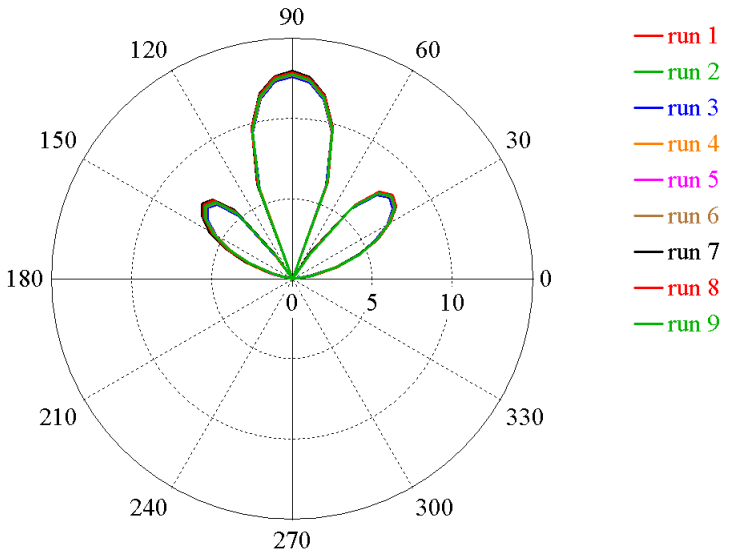

Fig. 5.18 Radiation patterns in YZ plane for 0.1 mm variance around the center value

As can be seen in Fig. 5.15 – 5.18, by varying the dimensions of the coupling slots, mainly the reflection coefficient is influenced whose magnitude has risen however, still remains under -10 dB. The changes are considered as acceptable.

5.5.3 Dimensions of the coupling slots between the layers

This analysis takes into consideration also the situation of misaligned substrate layers since the effect will be the same as if the dimensions of the coupling slot were changed.

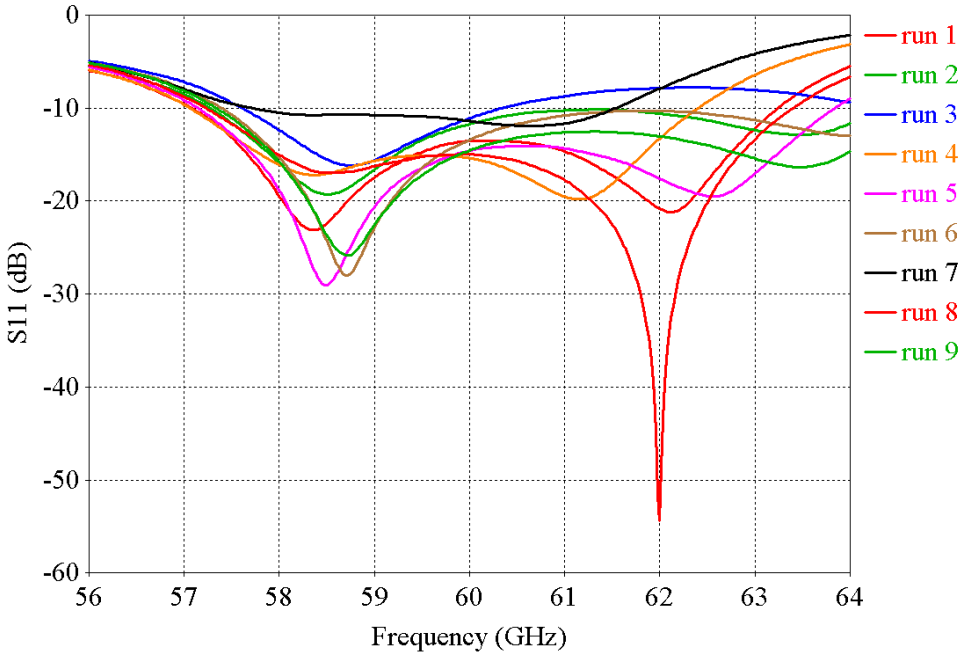

Fig. 5.19 Frequency responses of the reflection coefficient for 0.1 mm variance around the center value

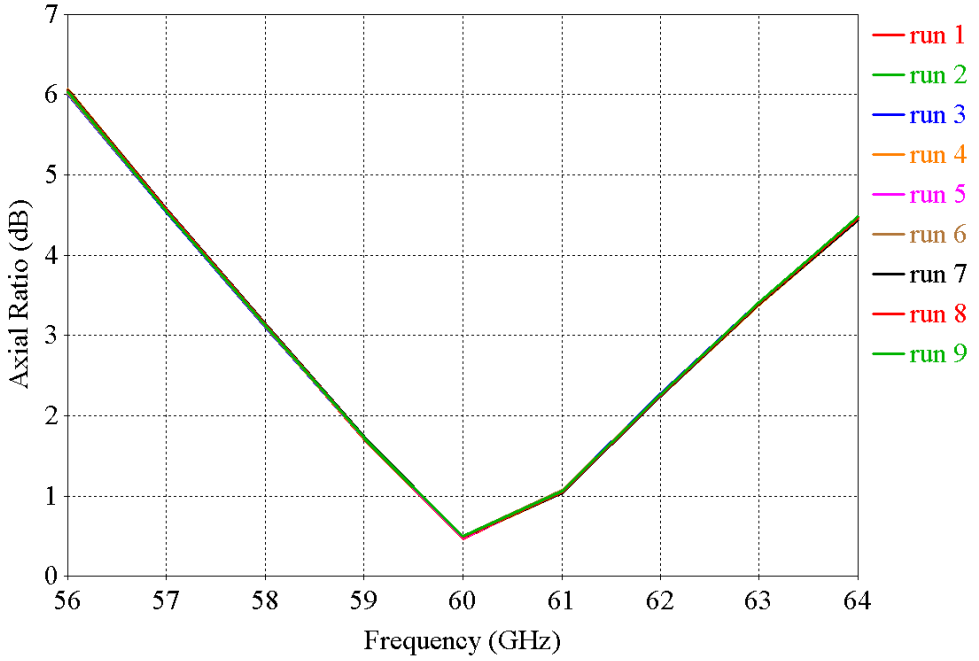

Fig. 5.20 Frequency responses of the axial ratio for 0.1 mm variance around the center value

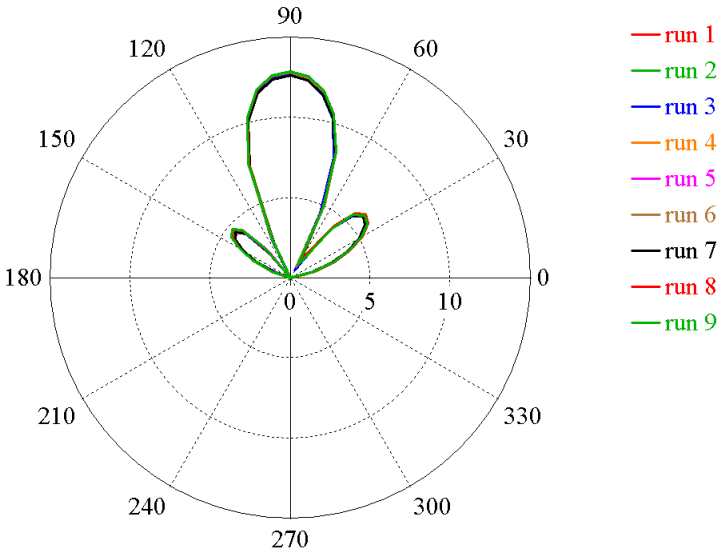

Fig. 5.21 Radiation patterns in XY plane for 0.1 mm variance around the center value

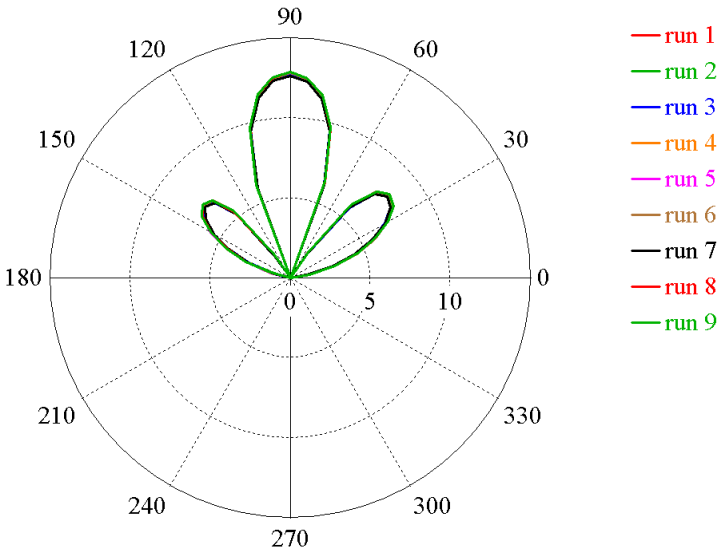

Fig. 5.22 Radiation patterns in YZ plane for 0.1 mm variance around the center value

As can be seen in Fig. 5.19 – 5.22, by varying the dimensions of the slot between the layers, mainly the reflection coefficient is influenced whose magnitude has risen. In this case the changes are unacceptable since the bandwidth is significantly reduced, identifying precision of the dimensions as critical for the design.

5.5.4 Position of the coupling slots between the layers

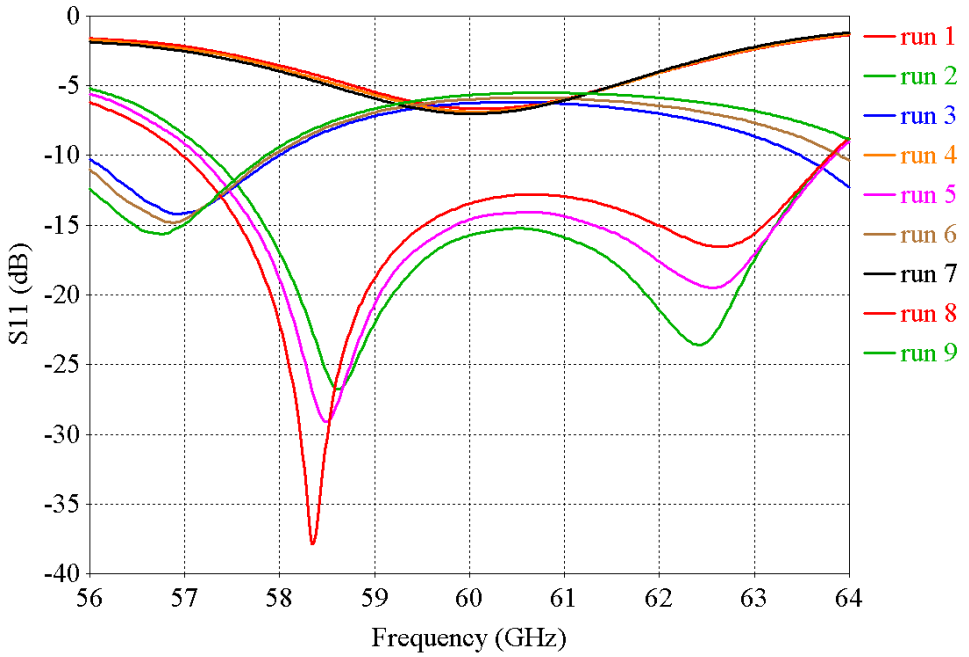

Fig. 5.23 Frequency responses of the reflection coefficient for 0.1 mm variance around the center value

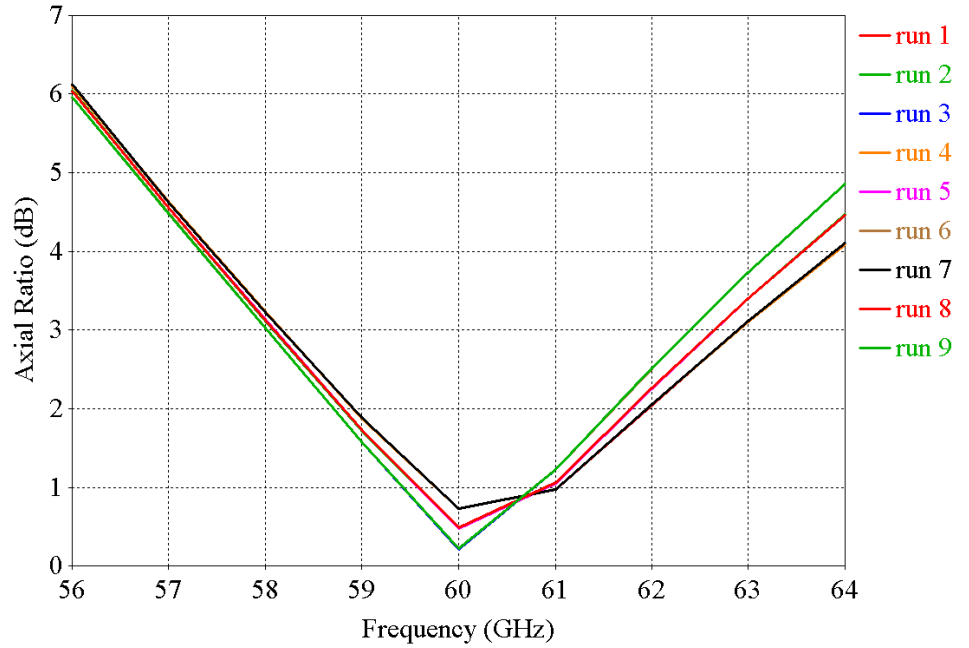

Fig. 5.24 Frequency responses of the axial ratio for 0.1 mm variance around the center value

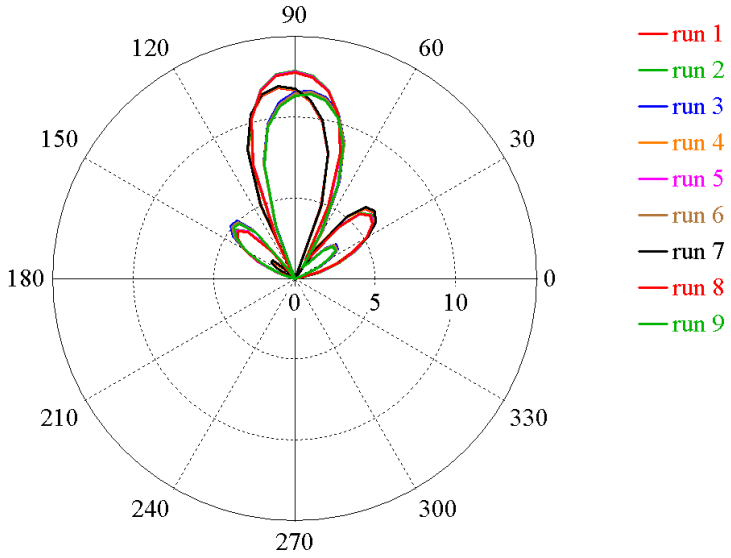

Fig. 5.25 Radiation patterns in XY plane for 0.1 mm variance around the center value

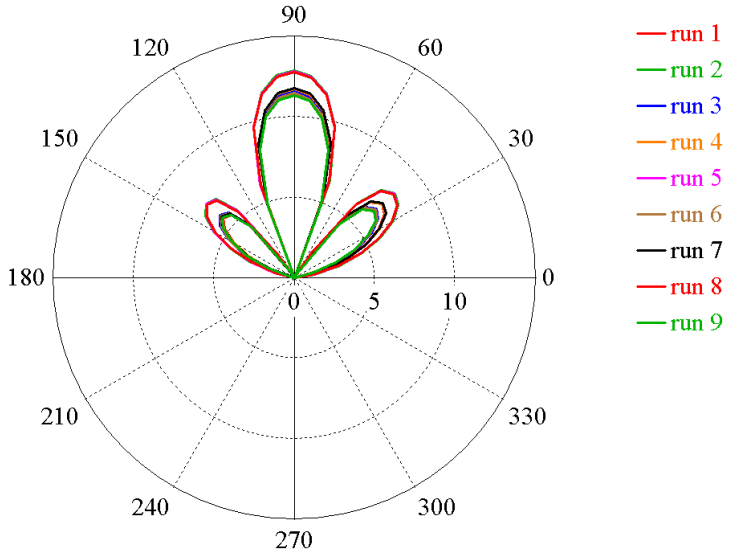

Fig. 5.26 Radiation patterns in YZ plane for 0.1 mm variance around the center value

As can be seen in Fig. 5.23 – 5.26, by varying the position of the slot between the layers, the reflection coefficient is influenced whose magnitude has significantly risen. As a result, also the gain decreased as indicated in the radiation patterns. Therefore, precise alignment is identified as critical for the performance of the antenna array.

5.5.5 Position of the shorting pin of the power divider

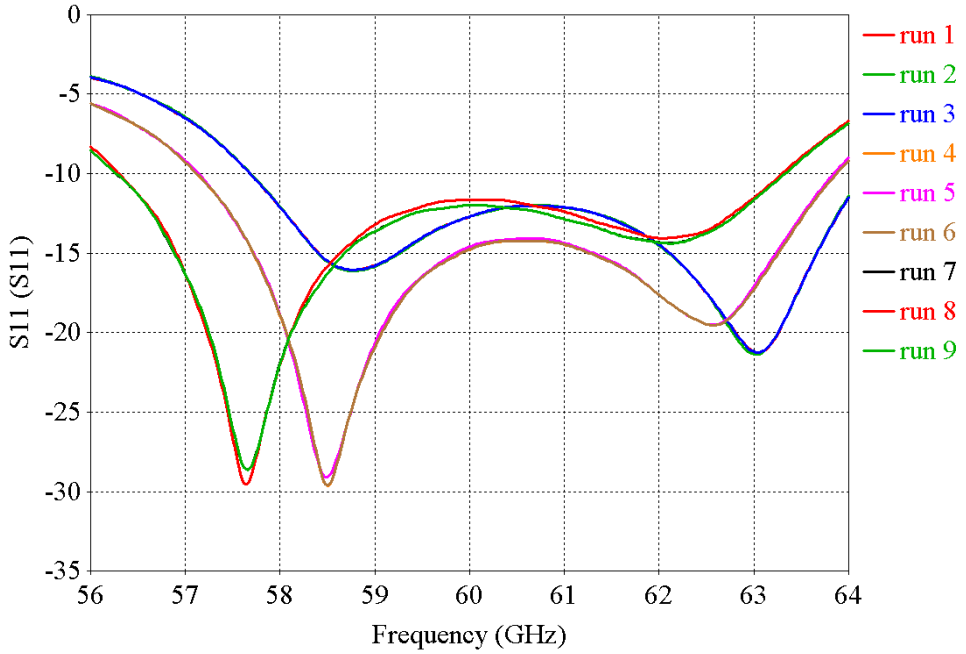

Fig. 5.27 Frequency responses of the reflection coefficient for 0.1 mm variance around the center value

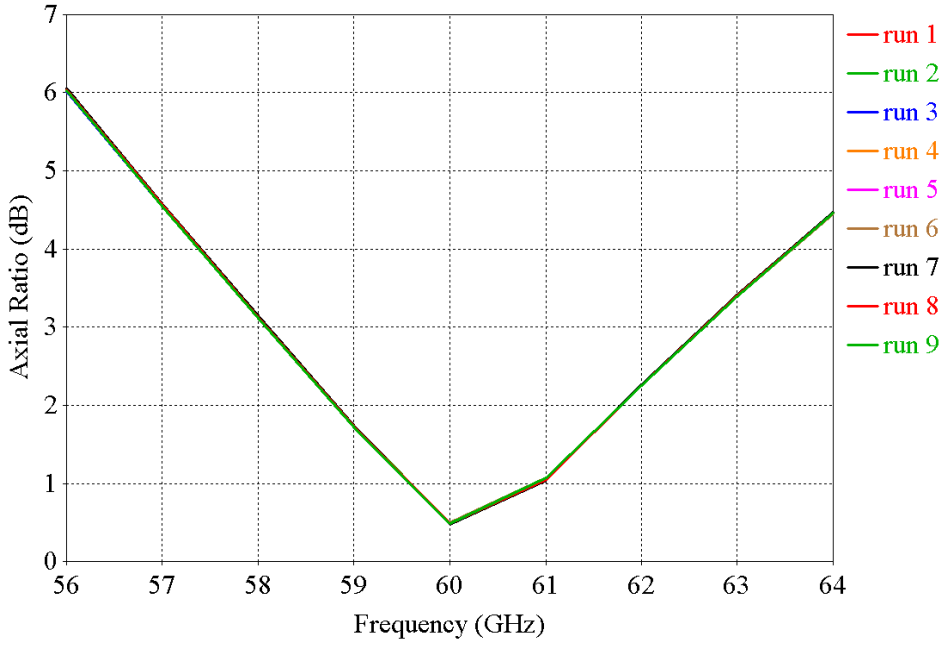

Fig. 5.28 Frequency responses of the axial ratio for 0.1 mm variance around the center value

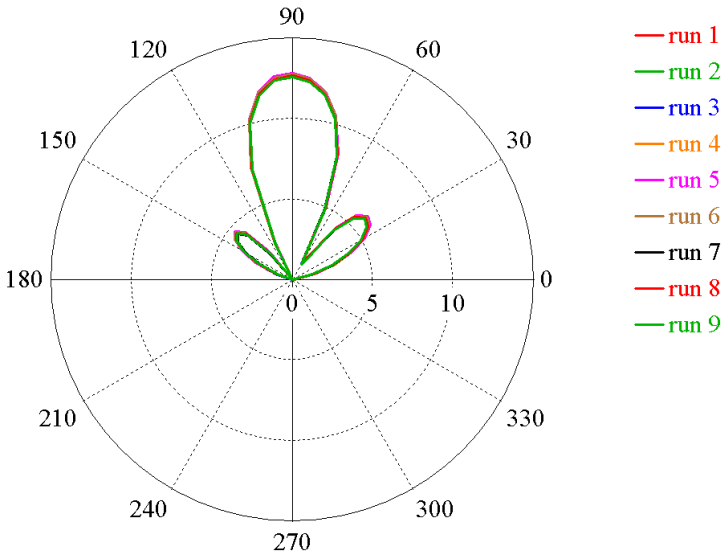

Fig. 5.29 Radiation patterns in XY plane for 0.1 mm variance around the center value

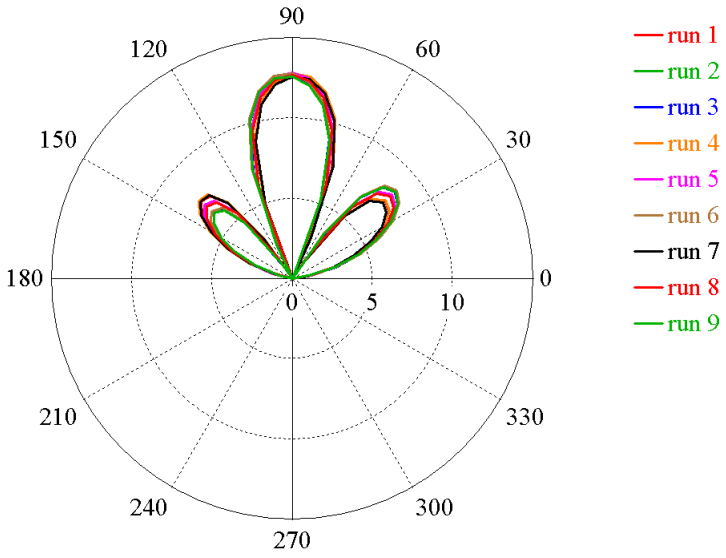

Fig. 5.30 Radiation patterns in YZ plane for 0.1 mm variance around the center value

As can be seen in Fig. 5.27 – 5.30, by varying the position of the shortening pin of the power divider mainly the reflection coefficient is influenced, whose magnitude has risen, and the characteristics are shifted. Therefore, correct position of the pin is critical for meeting the bandwidth requirements.

5.5.6 Width of the waveguides

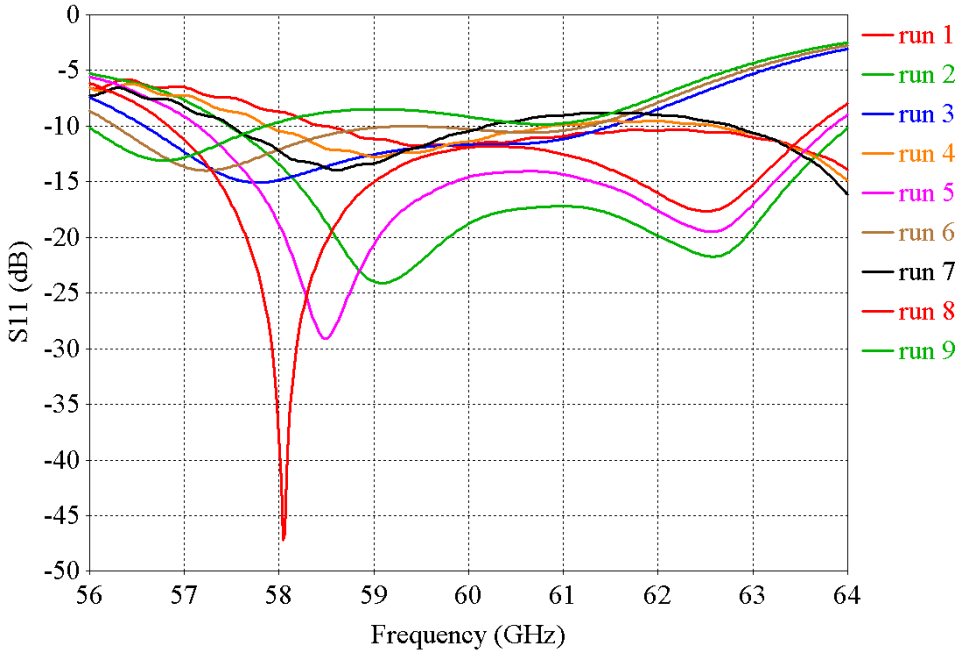

Fig. 5.31 Frequency responses of the reflection coefficient for 0.1 mm variance around the center value

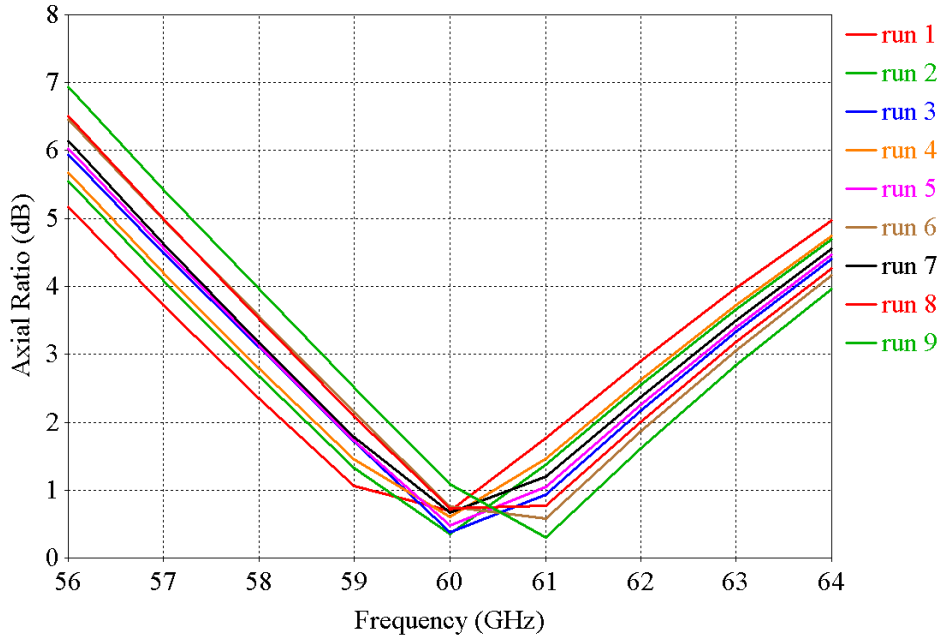

Fig. 5.32 Frequency responses of the axial ratio for 0.1 mm variance around the center value

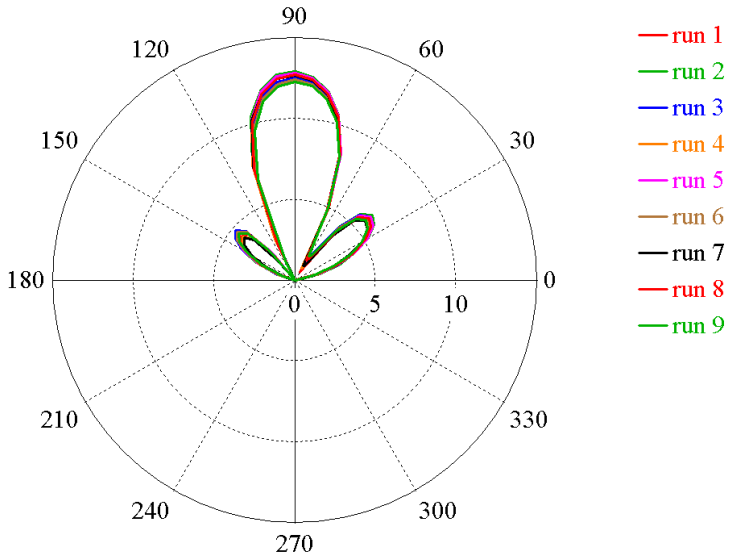

Fig. 5.33 Radiation patterns in XY plane for 0.1 mm variance around the center value

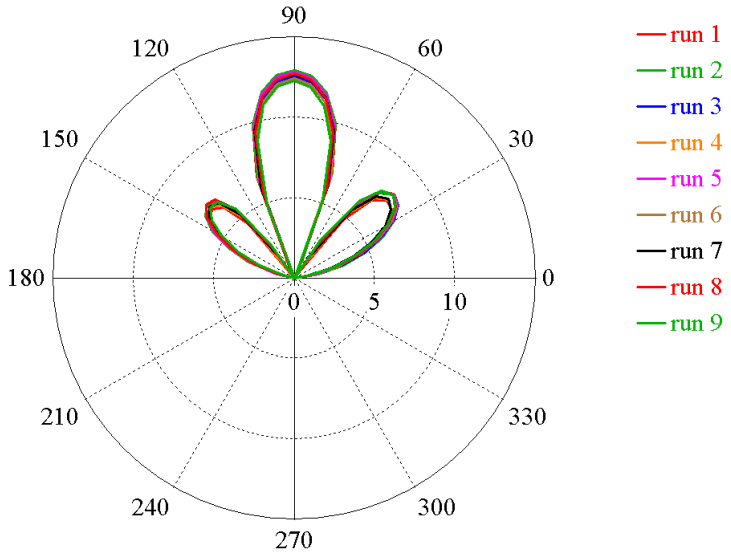

Fig. 5.34 Radiation patterns in YZ plane for 0.1 mm variance around the center value

As can be seen in Fig. 5.31 – 5.34, by varying the widths of the waveguide mainly the reflection coefficient is influenced. The overall magnitude has risen, the characteristics has been shifted due to changes of the guided wavelengths and the bandwidth has been reduced. As a result, precision of this parameter is critical for the performance of the array. Also, the characteristics of the Axial Ratio have been shifted however, the change is not significant in this case.

5.5.7 Dimensions of the patches

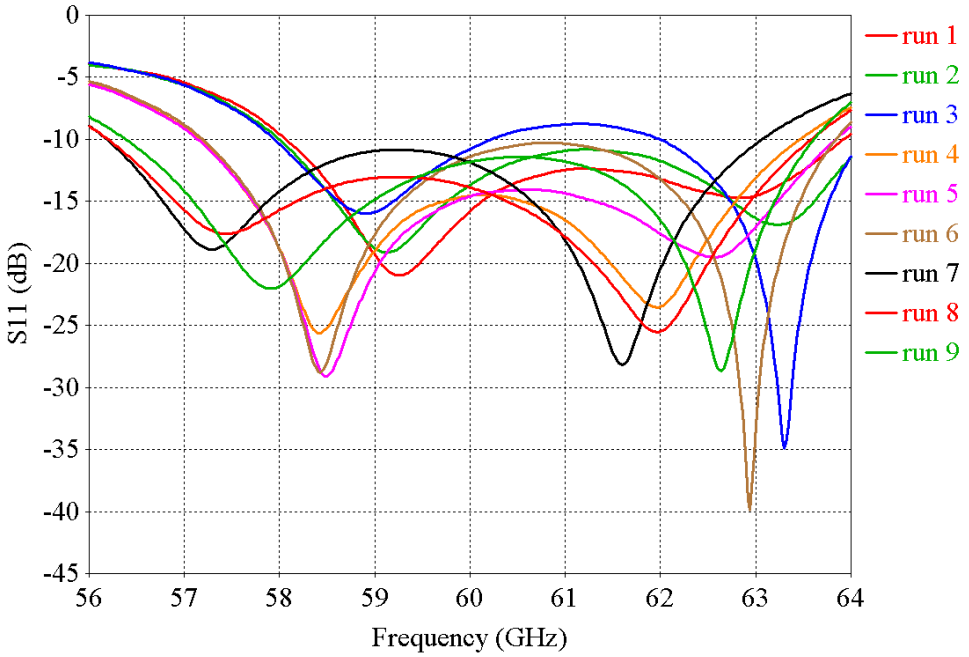

Fig. 5.35 Frequency responses of the reflection coefficient for 0.1 mm variance around the center value

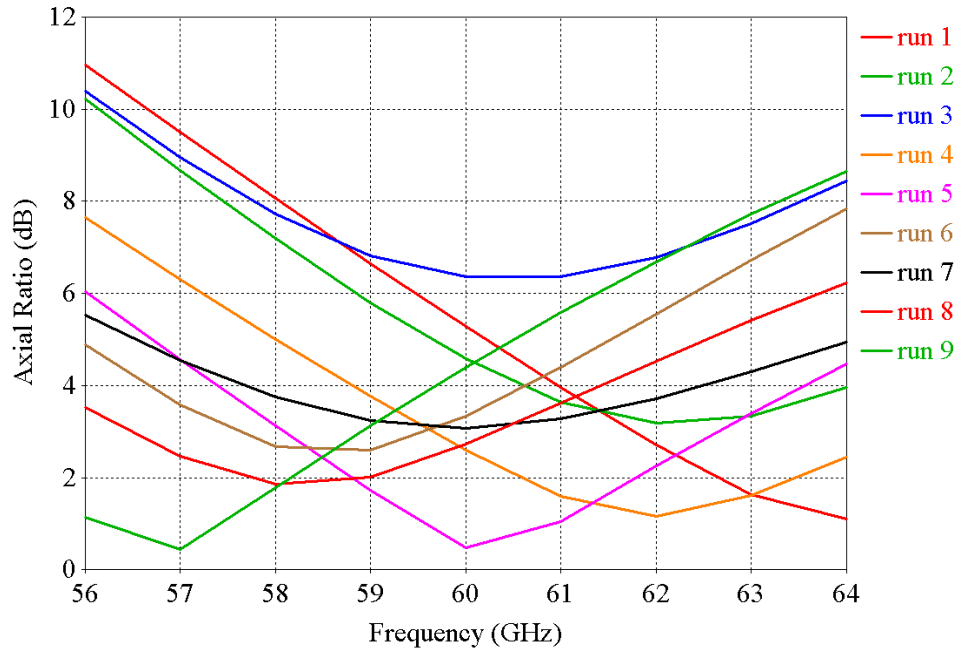

Fig. 5.36 Frequency responses of the axial ratio for 0.1 mm variance around the center value

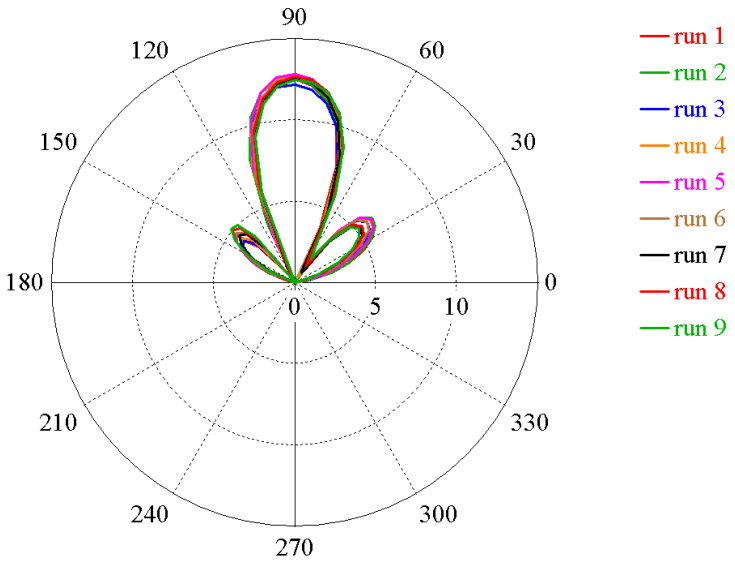

Fig. 5.37 Radiation patterns in XY plane for 0.1 mm variance around the center value

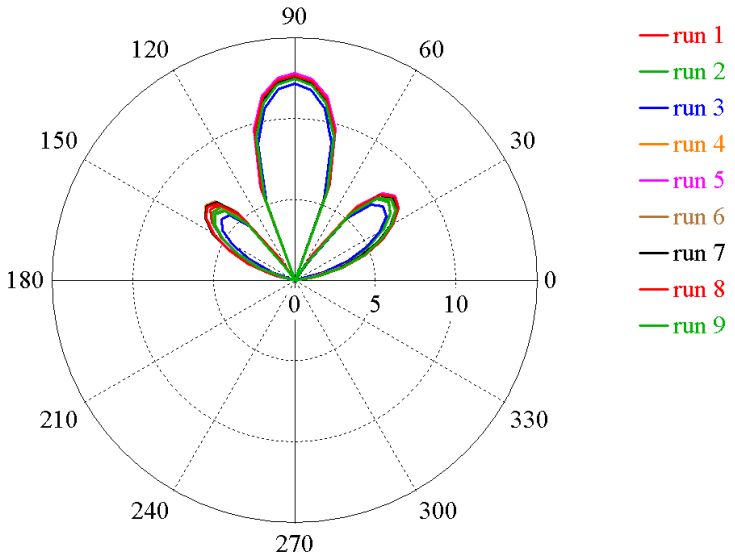

Fig. 5.38 Radiation patterns in YZ plane for 0.1 mm variance around the center value

Fig. 5.35 – 5.38 show that the variation of the dimensions of patches influences the axial ratio mainly. Significant changes of magnitude, center frequency and 3 dB bandwidth can be observed. So, accurate patch dimensions are critical to meet the axial ratio requirements. Also, the reflection coefficient characteristics show significant changes in the magnitude and the center frequency.

5.5.8 Summary

According to the results of the sensitivity, the following parameters were shown to be critical:

- Dimensions of coupling slots between layers
- Position of coupling slots between layers
- Width of waveguides
- Dimensions of patches

The rest of the parameters showed a minor influence on the properties of the array. The results indicate that manufacturing technologies those can offer an overall precision of 0.1 mm around the center value is insufficient for mass production of such a structure. However, such technologies can be used for prototyping and verification of the design.

5.6 MEASURED RESULTS

Manufactured array can be seen in Fig. 5.39.

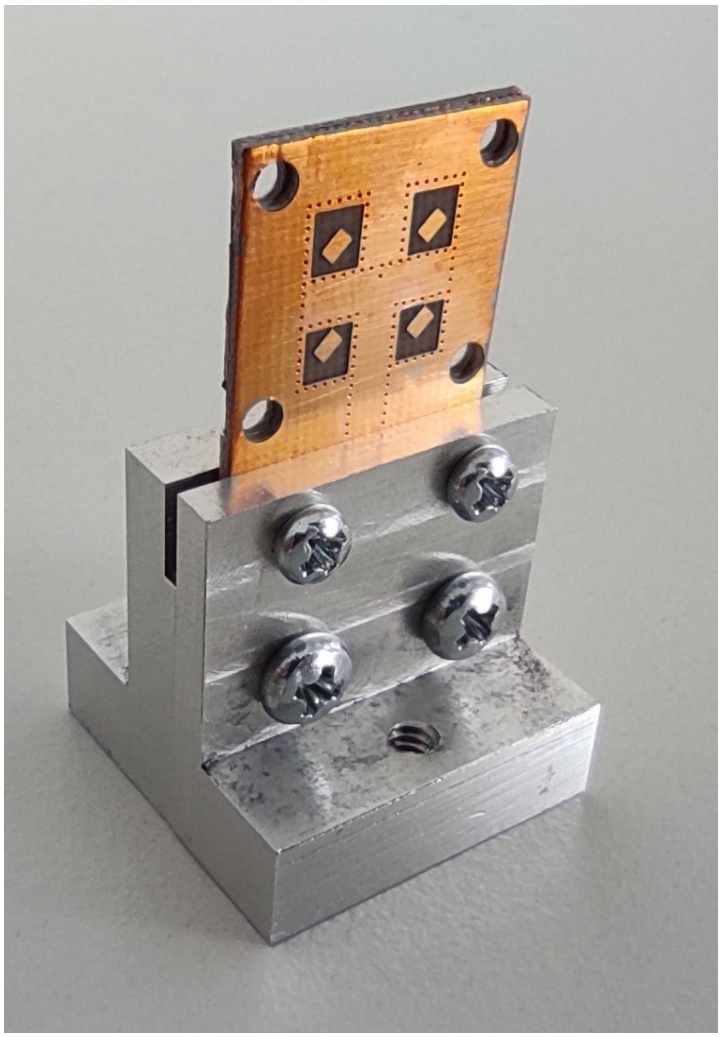

Fig. 5.39 Manufactured array for the center frequency of 60 GHz

Fig. 5.40 shows comparison of the simulated and measured frequency response of the reflection coefficient. As can be seen, impedance bandwidth of the measured array is smaller (59.72 – 62.86 GHz, 5.2% relatively) in comparison to the simulated array (58.9 – 62.4 GHz, 5.8% relatively). In addition, the characteristic is shifted towards higher frequency.

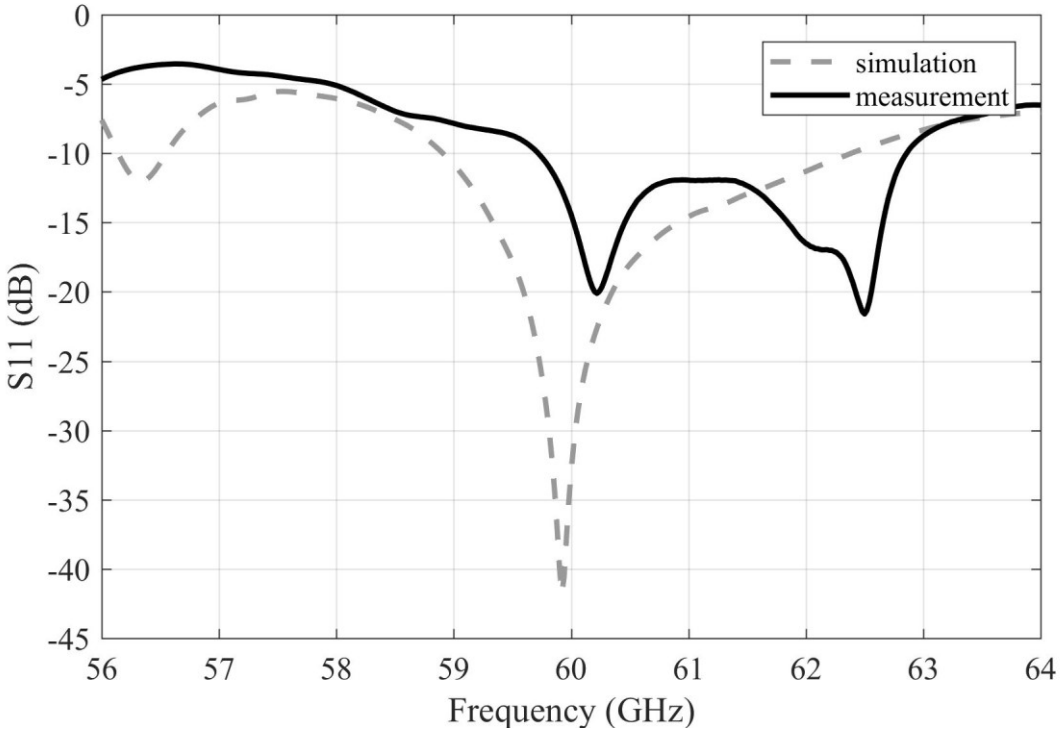

Fig. 5.40 Frequency responses of the magnitude of reflection coefficient for the simulated and measured antenna array.

Fig. 5.41 shows comparison of the simulated and measured frequency response of axial ratio. Only minimal match between the simulated and measured data can be identified between 58 – 59 GHz and between 62 – 63 GHz, where the measured characteristic reaches its minimum magnitude. The $|AR| < 3$ dB bandwidth of the simulated array is from circa 57.5 to 62.5 GHz (8.3% relatively) and the bandwidth of the measured array is only from 58.5 to 58.9 GHz (0.7% relatively) and from 62.3 to 62.5 GHz (0.3 % relatively).

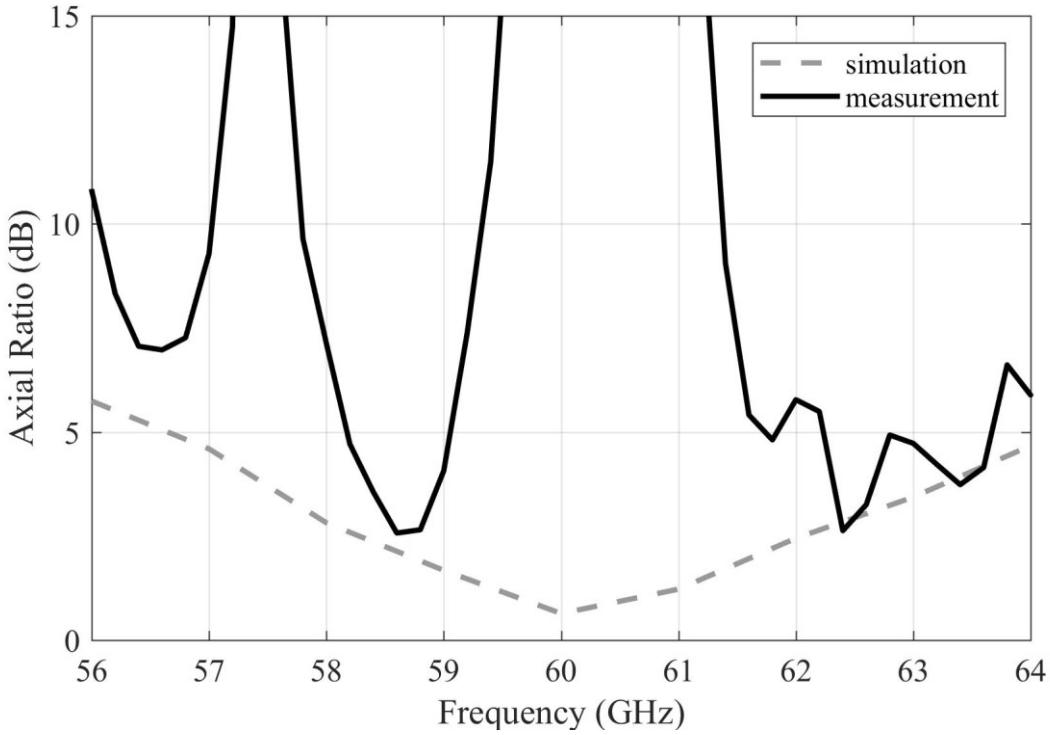

Fig. 5.41 Frequency responses of the magnitude of axial ratio for the simulated and measured antenna array.

Based on the reflection coefficient and axial ratio characteristics it was determined that the array does not function as expected. Manufacturing defects of the vias that form the substrate integrated waveguides were identified as the probable cause since their diameter is relatively small (0.2 mm) and also the ratio between the diameter and the height of the vias was beyond the recommended limit. As a result, it was investigated if the array can utilize vias with a larger diameter that would allow more reliable manufacturing.

5.7 RESULTS OF THE ARRAY WITH THE LARGER VIA DIAMETER

In this array, the diameter of the vias was increased from 0.2 mm to 0.6 mm as illustrated in Fig. 5.42 in order to lower the chance of the defects associated with their manufacturing.

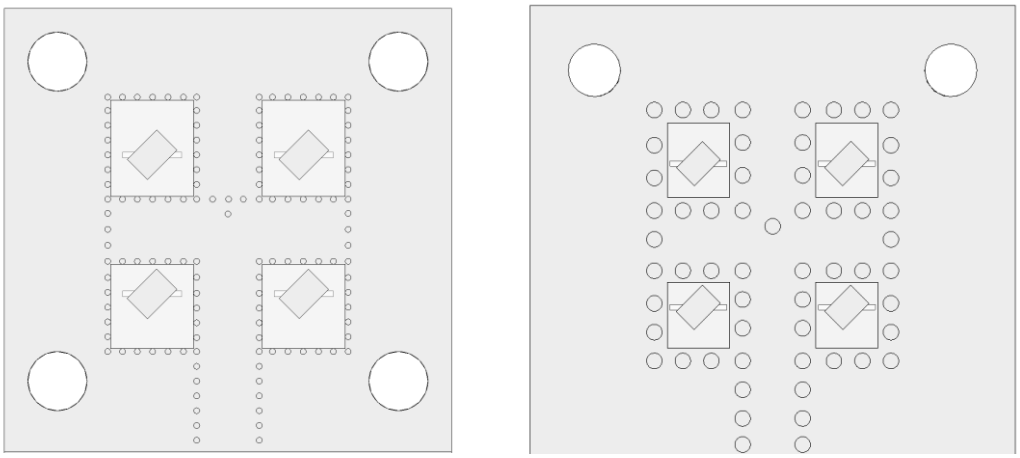

Fig. 5.42 Comparison of the arrays with smaller via diameter (left) and larger via diameter (right).

5.7.1 Comparison between the array with smaller and larger via diameter

Fig. 5.43 shows comparison of the reflection coefficient for the simulated arrays with smaller and larger via diameter. As can be seen, increasing the diameter brought an increase in the impedance bandwidth caused by the lower resonance shift towards the lower frequencies. 58.9 – 62.4 GHz, 5.8% relatively for original array with the smaller via diameter and 57.6 – 62.4 GHz, 8% relatively for the array with the larger via diameter.

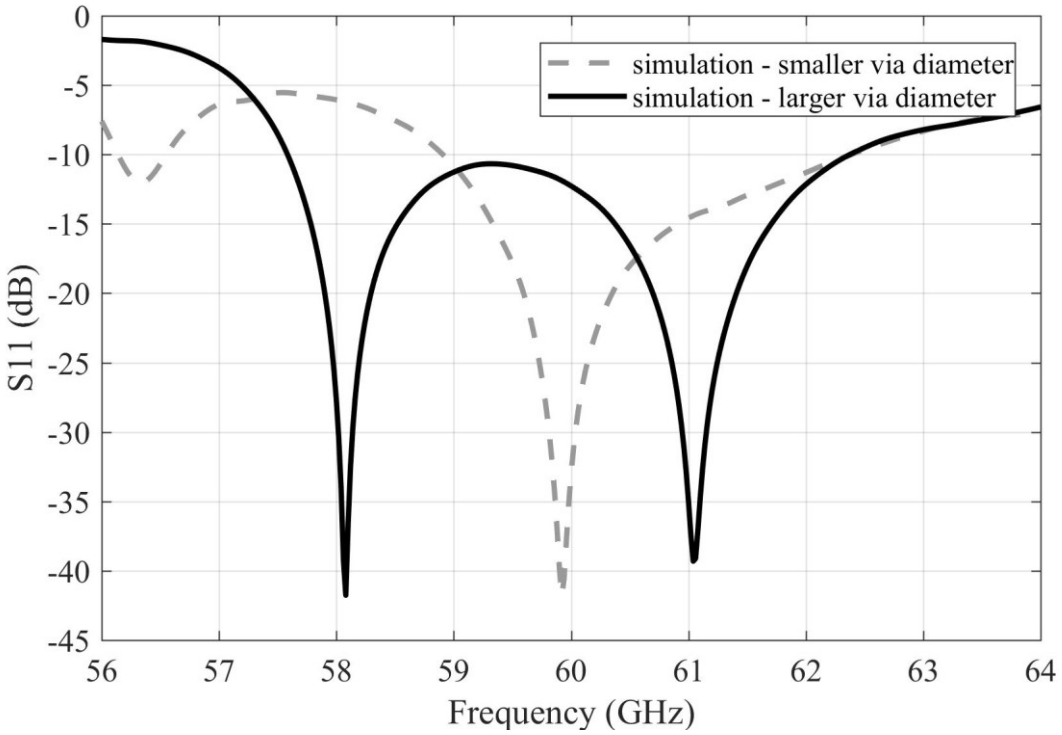

Fig. 5.43 Frequency responses of the magnitude of reflection coefficient for the simulated array with smaller and larger via diameter.

Fig. 5.44 shows comparison of axial ratio for the simulated arrays with smaller and larger via diameter. As can be seen, the $|AR| < 3$ dB bandwidth of the array with larger vias was shifted towards the lower frequencies by approximately 1 GHz. 57.5 to 62.5 GHz (8.3% relatively) for the array with the smaller via diameter, 56.5 to 61.5 GHz (8.3% relatively) for the array with the larger via diameter.

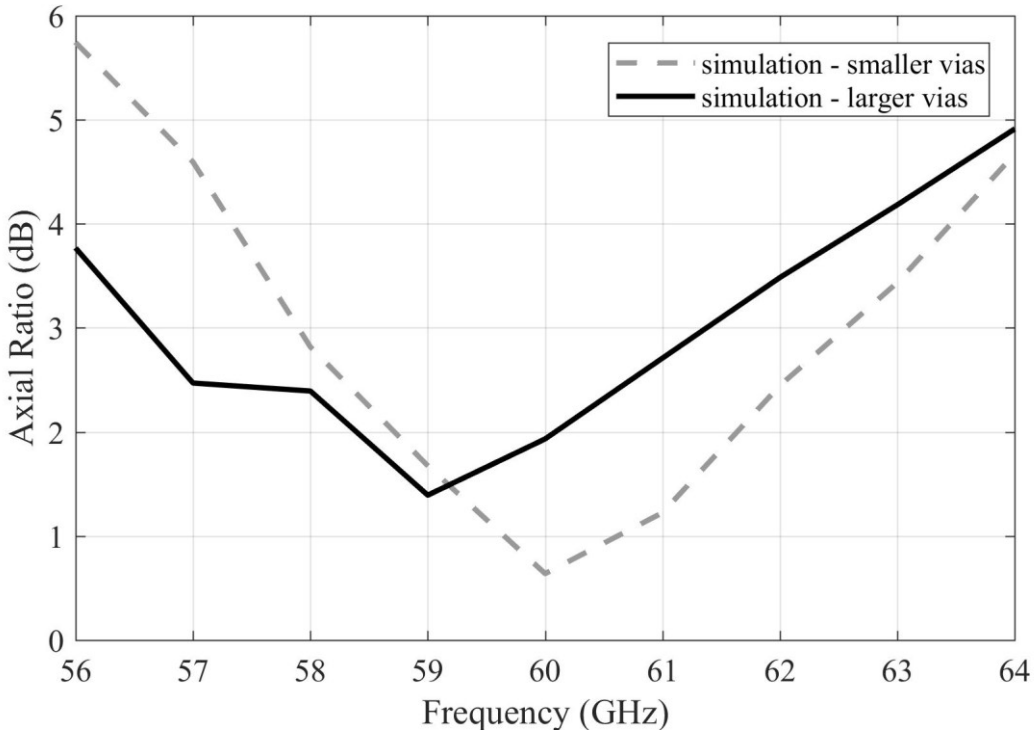

Fig. 5.44 Frequency responses of the magnitude of axial ratio for the simulated array with smaller and larger via diameter.

Fig. 5.45 shows comparison of the radiation patterns for the simulated arrays with smaller and larger via diameter in *xy* (up) and *yz* (down) planes. As can be seen, the array with the larger via diameter shows a higher realized gain (13.3 vs. 12.2 dB in the main lobe direction) and a more uniform pattern in the *yz* plane. Beam width is reduced in both planes in case of the array with the larger via diameter. 30.9° vs. 22° in the *xy* plane and 28.8° vs. 23° in the *yz* plane.

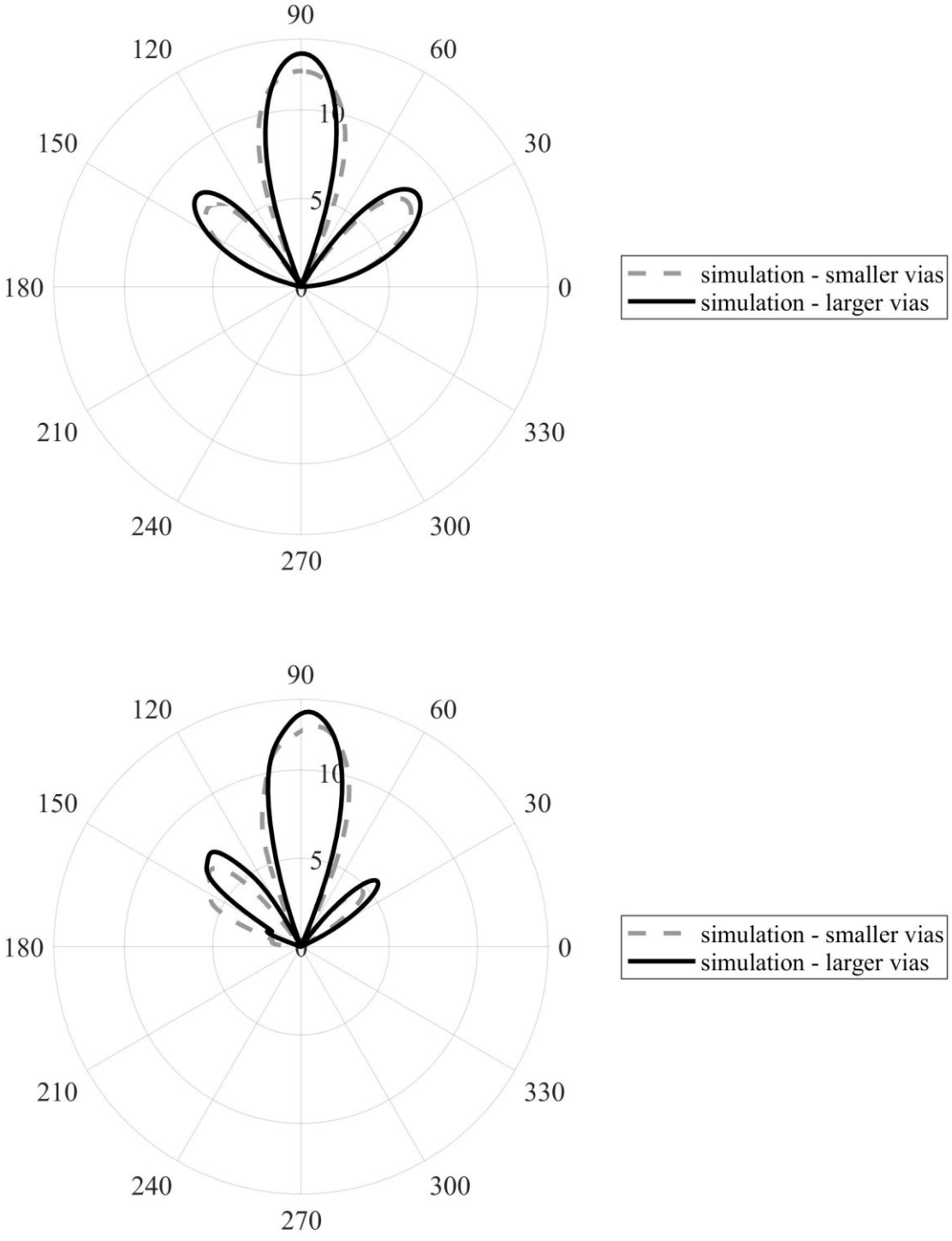

Fig. 5.45 Comparison of the radiation patters of the arrays with smaller and larger via diameter in *xy* (up) and *yz* (down) planes. Shown in realized gain (dB).

Based on the comparisons, the changes in properties of the array were evaluated as acceptable and the array was manufactured.

5.7.2 Measured results of the array with the larger via diameter

Manufactured array with the larger via diameter can be seen in Fig. 5.47. The same WR15 to SIW transition as in case of the array with smaller via diameter was utilized. As an improvement, 3D printed elements (black) were designed and manufactured to better align and fix the two substrate layers, from which the array comprises, as a convenient custom-made solution.

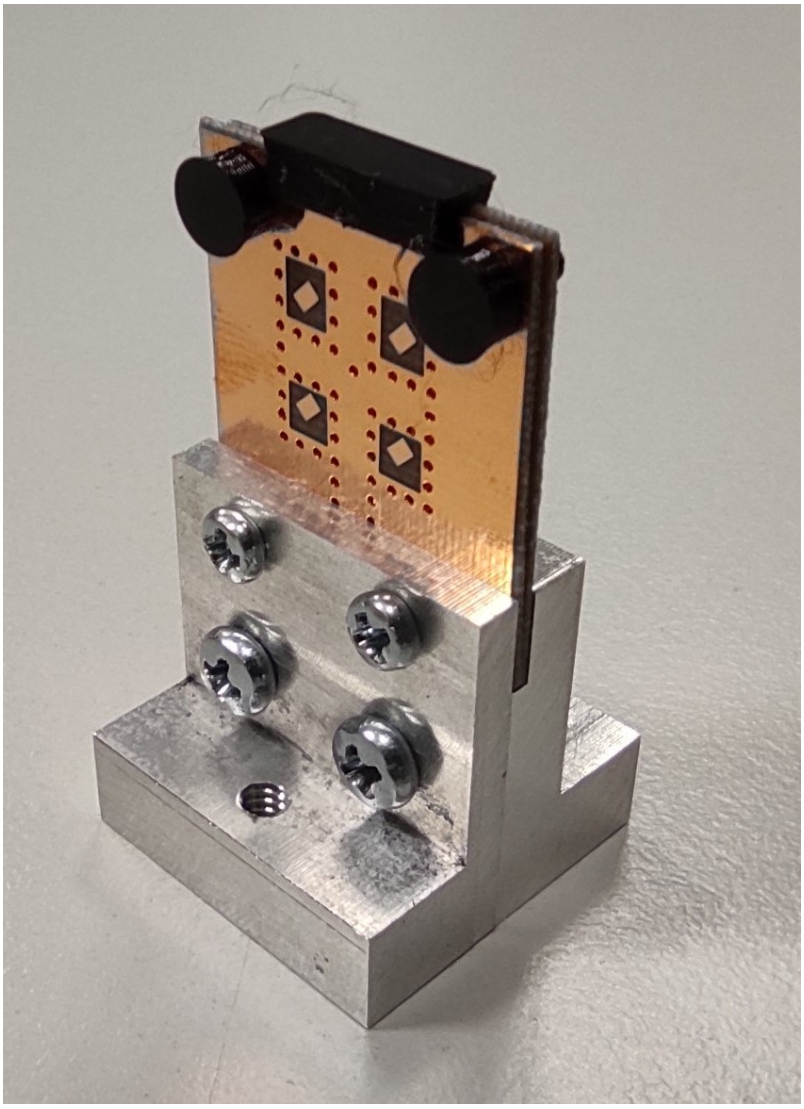

Fig. 5.46 Manufactured array with the larger via diameter

Fig. 5.47 shows comparison of the simulated and measured frequency responses of the reflection coefficient for the simulated and manufactured array. As can be seen, a better match with the simulations was obtained, compared to the array with the smaller via diameter. By using the data obtained by the sensitivity analysis (Chapter 5.5), it was identified, that deviations from the ideal dimensions of the coupling slots between the substrate layers and/or misalignment of the substrate layers in the manufactured array are likely responsible for the differences (Chapter 5.5.3). The characteristic is

consistent with the situation where the length of the coupling slot is increased by 0.05 mm and the width of the slot is decreased by 0.075 mm. The impedance bandwidth of the simulated array is 57.6 – 62.4 GHz, 8% relatively. The impedance bandwidth of the measured array is 58.9 – 64 GHz, 8.5% relatively.

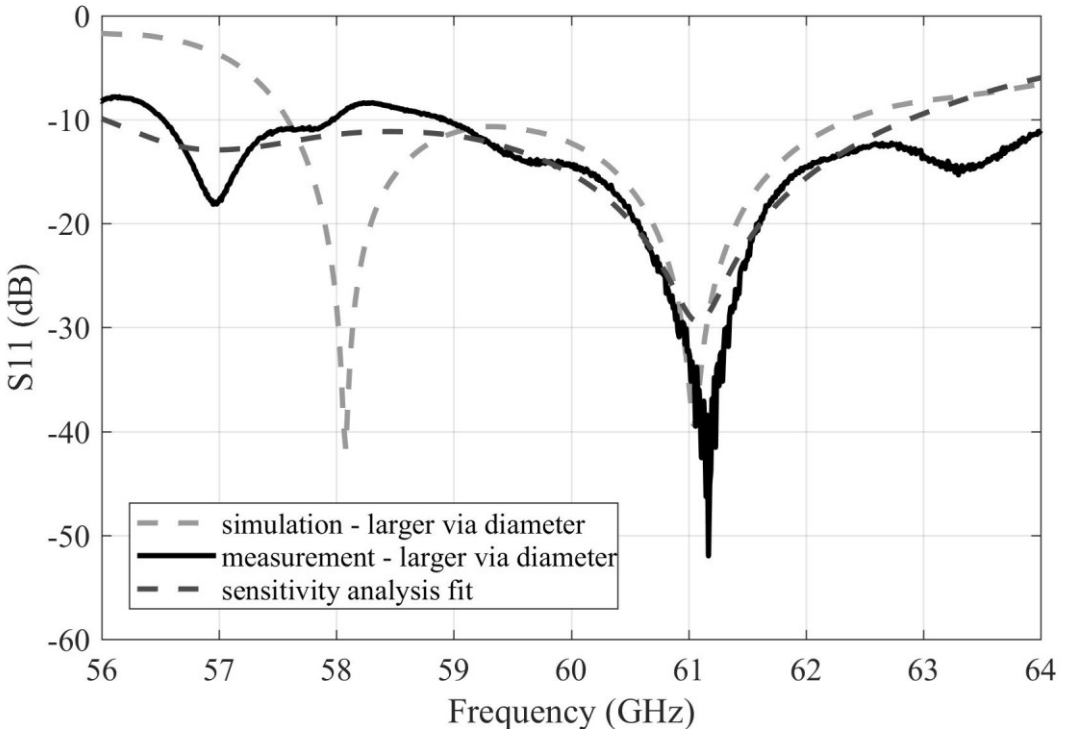

Fig. 5.47 Frequency responses of the magnitude of reflection coefficient for the simulated and measured array with the larger via diameter.

Fig. 5.48 details comparison of the simulated and measured frequency responses of axial ratio for the simulated and manufactured array. As can be seen, a better match with the simulations was obtained also in this case. Since the dimensions of the coupling slots between the substrate layers do not influence the axial ratio characteristics (see Fig. 5.20), the observed differences cannot be accounted to those manufacturing imperfections. As the sensitivity analysis showed that the dimensions of the patches are the only parameters that effectively influence the axial ratio characteristics, a fit was searched by varying these dimensions (see Chapter 5.5.7). The closest fit was obtained for the situation where the width of the patch is increased by 0.1 mm, while the length of the patch remains the same. The resulting curve still has only limited match with the measured data. It is probable that the rest of the differences is accounted to imperfect via manufacturing where not all of the vias were correctly created despite the enlarged diameter. Unfortunately, it is not feasible to simulate these effects due to the number of combinations of via manufacturing errors that could possibly occur. The axial ratio bandwidth of the simulated array is from 56.5

to 61.5 GHz (8.3% relatively). The axial ratio bandwidth of the measured array is from 57.6 to 59.3 GHz (2.8% relatively).

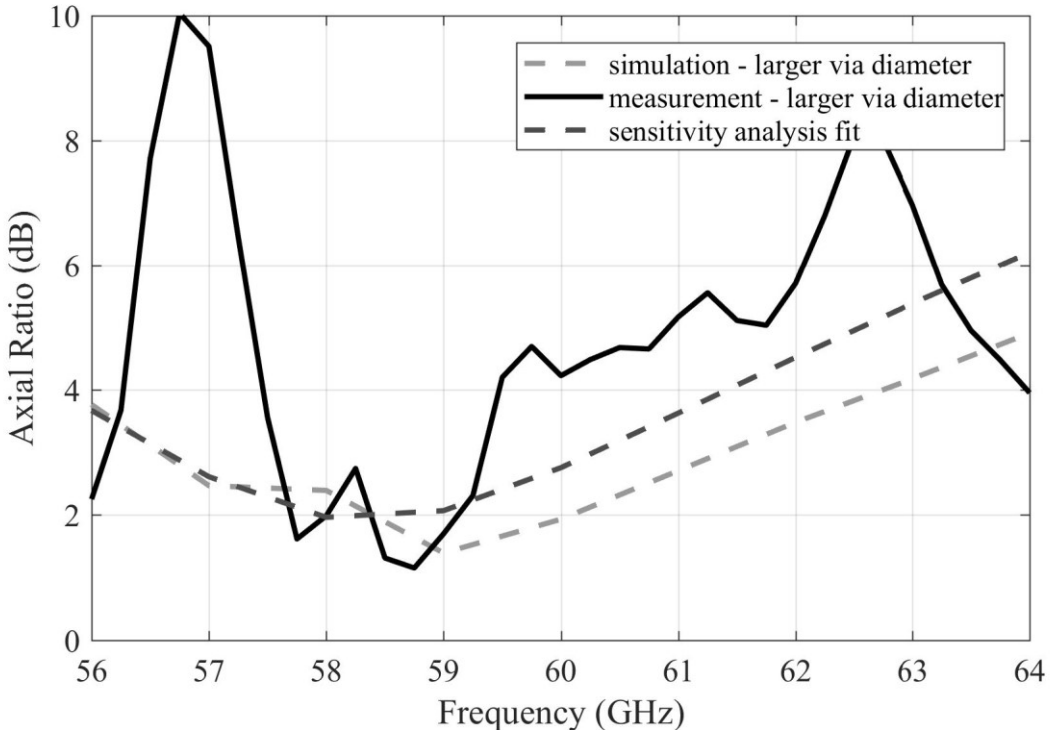

Fig. 5.48 Frequency responses of the magnitude of axial ratio for the simulated array with smaller and larger via diameter.

Fig. 5.49 shows comparison of the radiation patterns for the simulated and manufactured arrays with the larger via diameter in *xy* (up) and *yz* (down) planes. A good match with the simulated and measured characteristics was obtained for both planes. Beam width of the simulated array is 22° in the *xy* plane vs. 20° in case of the measured array. Beam width of the simulated array is 23° in the *yz* plane vs. 18°in case of the measured array. Minor deviation of the main lobe direction is observed in both *xy* and *yz* plane characteristics for the measured array.

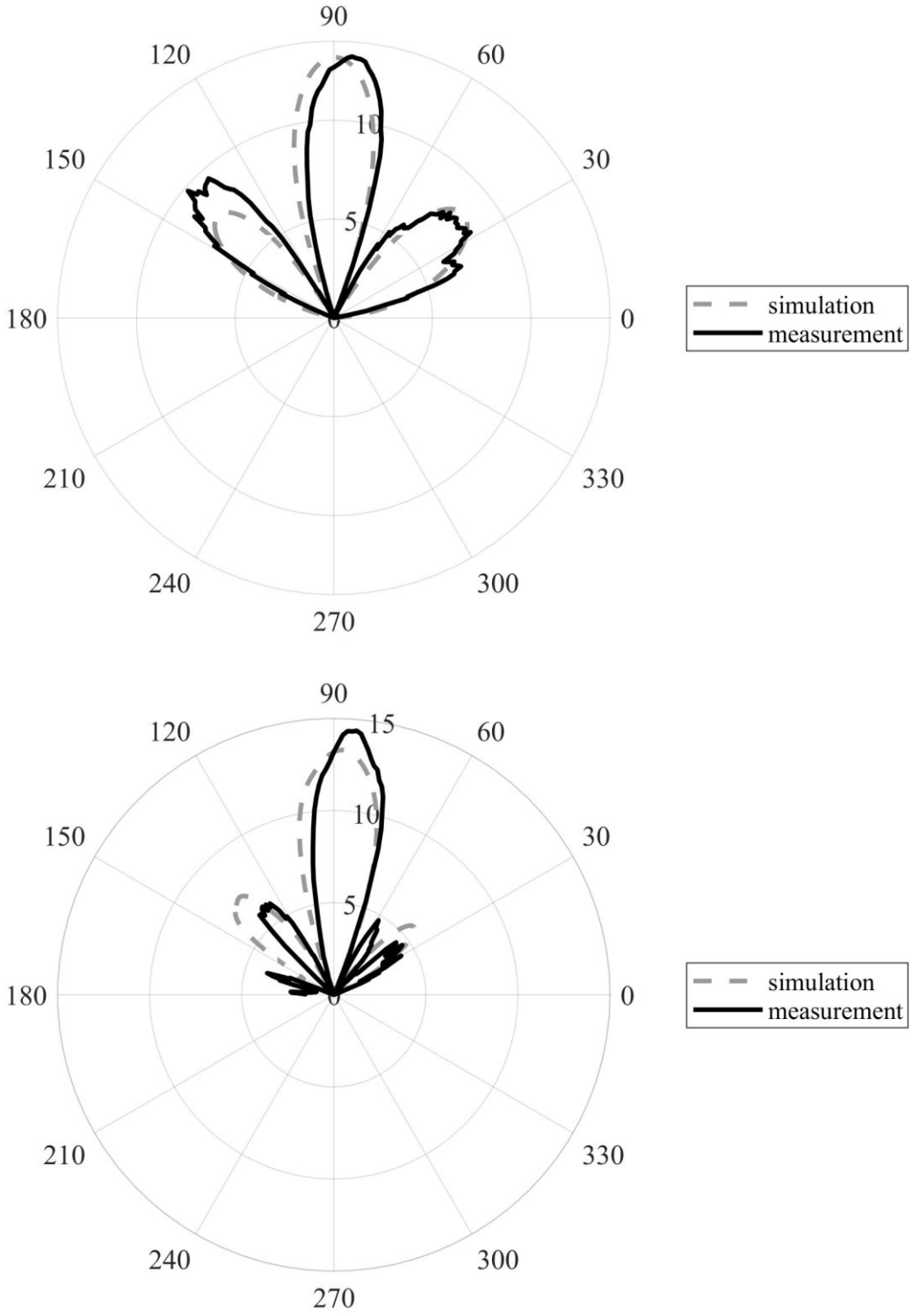

Fig. 5.49 Comparison of the radiation patters of the simulated and measured array with the larger via diameter in *xy* (up) and *yz* (down) planes. Shown in realized gain (dB).

Final dimensions of the array with the larger via diameter are summarized in Table III. Refer to Fig 4.2 and Fig 4.3 to see how each parameter corresponds to the design of the array. Parameters that relate to the transition between the GCPW and SMA connector (L_5, L_6, W_6, W_7, W_8, W_9, D_7) are ignored in this case since this section is replaced with a SIW in the design for the center frequency of 60 GHz. Unless denoted otherwise in the figures, all dimensions related to the SIWs are referenced to the centers of the vias.

Table III Final dimensions of the array for the center frequency of 60 GHz (the larger via diameter).

parameter	***dimension (mm)***	***parameter***	***dimension (mm)***
L	21.000	W_4	1.428
L_1	9.600	W_5	2.316
L_2	2.175	D_1	2.316
L_3	2.200	D_2	4.000
L_4	0.984	D_3	1.950
L_7	3.850	D_4	2.550
L_8	3.450	D_5	0.016
W	18.732	D_6	0.300
W_1	3.408	D_v	0.600
W_2	0.200	D_S	1.150
W_3	0.200	R	45°

5.8 CONCLUSION

In the chapter, conversion of the original design from the center frequency of 17 GHz to the center frequency of 60 GHz is described. A good match of the simulations with the measurements was achieved. Conversion to the higher center frequency is challenging mainly from the manufacturing point of view. The following findings were derived:

- The attainable precision of the manufacturing method needs to be thoroughly considered and assessed. Sensitivity analysis suggests that a manufacturing method that can offer production precision with less than +/- 0.1 mm variance of the dimensions around the center (ideal) value is needed.

- It needs to be considered that manufacturing of the vias is generally more difficult in case of the microwave substrates like Cuclad 217 LX since drilling leaves residual material in the drilled holes that complicates the metallization processes. This issue becomes more significant with decreasing diameter of the vias. As a result, this diameter needs to be carefully chosen so acceptable production quality of the vias with respect to the manufacturing technology could be guaranteed.

- Since the width of the coupling slots between the substrate layers is reduced to 0.2 mm, precise alignment of the substrates is critical. It is desirable to include additional alignment points to the design in order to increase the precision.

The achieved results were presented in the following publications:

[1] J. Spurek, Z. Raida, “Sensitivity analysis of a modular circularly polarized antenna array for 60 GHz band,“ In Proceedings of MIKON 2020. Warsaw, Poland: IEEE, 2020. pp. 45-49. ISBN: 978-83-949421-6-8.

6 EXTENDING AXIAL RATIO BANDWIDTH OF THE ARRAY BY PARASITIC PATCHES

6.1 PRINCIPLE

A matrix of parasitic patches, carried by an air-like substrate, is placed above the original antenna array in a certain distance. Coupling and phase shift between the patches allows to equalize the magnitude of the rotating electric field intensity vector. Parameters of the parasitic patches (dimensions, position in x and y axis and the orientation) are identical to the patches in the original array.

6.2 EXTENSTION OF THE ARRAY BY PARASITIC PATCHES

The array was extended with the parasitic structure as can be seen in Fig. 6.1 and 6.2. Based on the simulation results, the substrate ARLON FoamClad (the height $h = 5.64$ mm = 3 x 1.88 mm, the dielectric constant $\varepsilon_r = 1.25$) was chosen as the carrier. The distance between the antenna array and the array of parasitic elements is $d = 3$ mm (z axis).

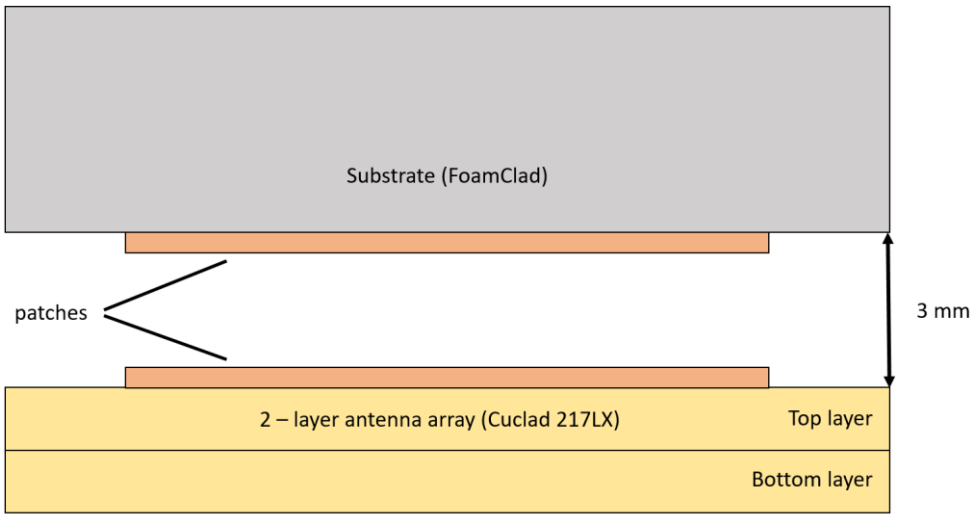

Fig. 6.1 Side view on the geometry of the structure.

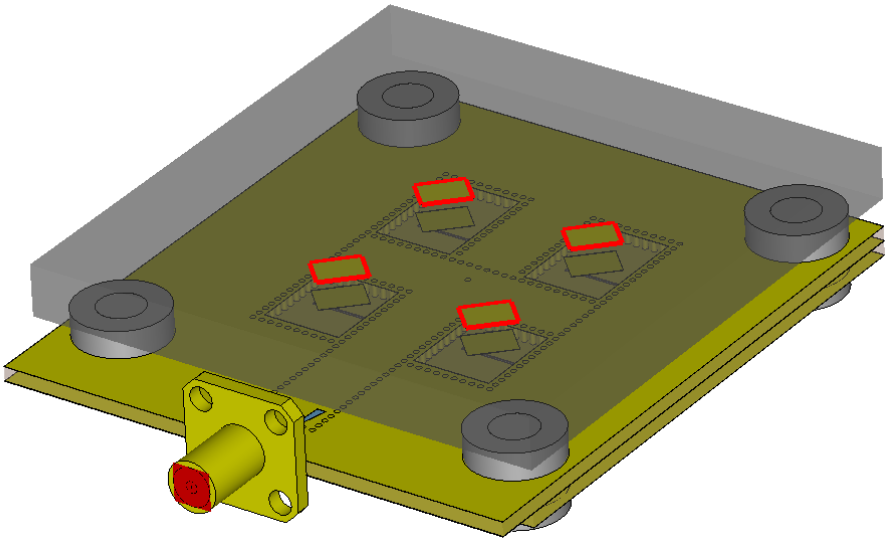

Fig. 6.2 Antenna array with parasitic patches (bounded in red).

The array was simulated for the center frequency of 17 GHz and a fully realistic model of the structure was used as it was in case of the original array (see Fig. 6.2). The parasitic structure was then manufactured and fitted to the already existing antenna array prototype (shown in Chapter 4) to conduct the measurements.

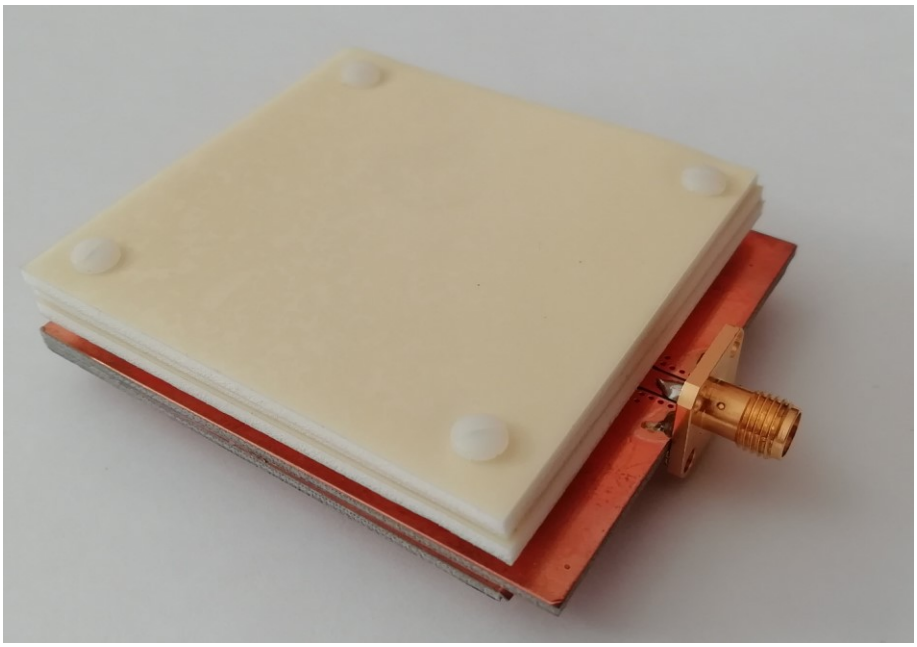

Fig. 6.3 Manufactured antenna array with parasitic patches.

6.2.1 Simulations and measurements

Frequency responses of axial ratio were computed for the main lobe direction, which is perpendicular to the antenna array.

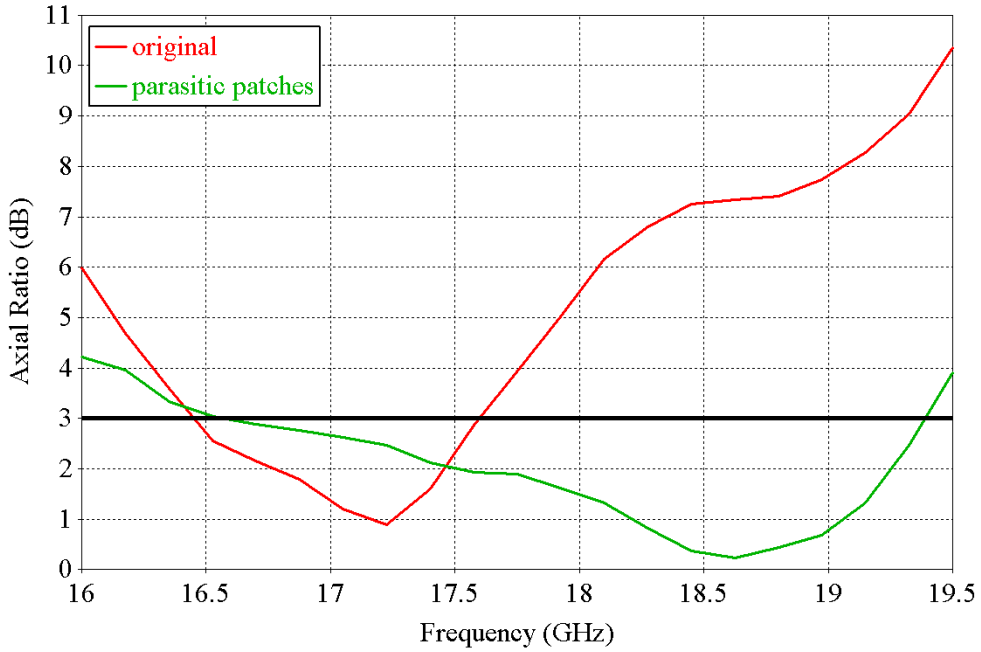

Fig. 6.4 Frequency response of the axial ratio in the main lobe direction of the simulated antenna array without parasitic patches (red) and with parasitic patches (green). Frequency of operation: 17 GHz.

Fig. 6.4 shows that the axial ratio bandwidth (the condition |AR| < 3 dB) is 16.45 GHz to 17.59 GHz (1.14 GHz, i.e. 6.7 % relatively) for the original array, and 16.56 GHz to 19.40 GHz (2.84 GHz, i.e. 16.7 % relatively) for the array with parasitic patches.

Model refinement

Prior manufacture, the numerical model was extended with elements needed to physically attach the parasitic structure to the reference antenna array (plastic screws, spacer pillars and nuts) and the FoamClad substrate was divided into three standalone layers in order to investigate potential influence on the parameters of the entire system and to match the simulated conditions as close as possible to the real-world conditions (see Fig. 6.5).

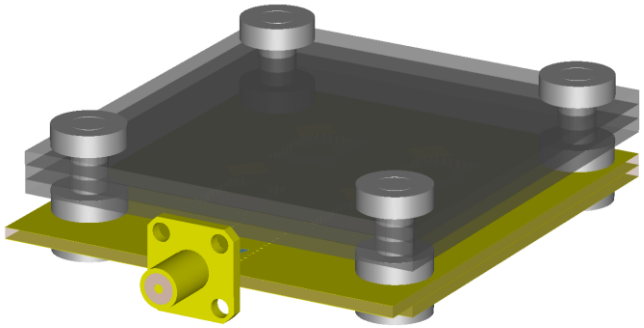

Fig. 6.5 Refined numerical model of the array

In Fig. 6.6 – Fig. 6.8 are shown comparisons of the relevant properties.

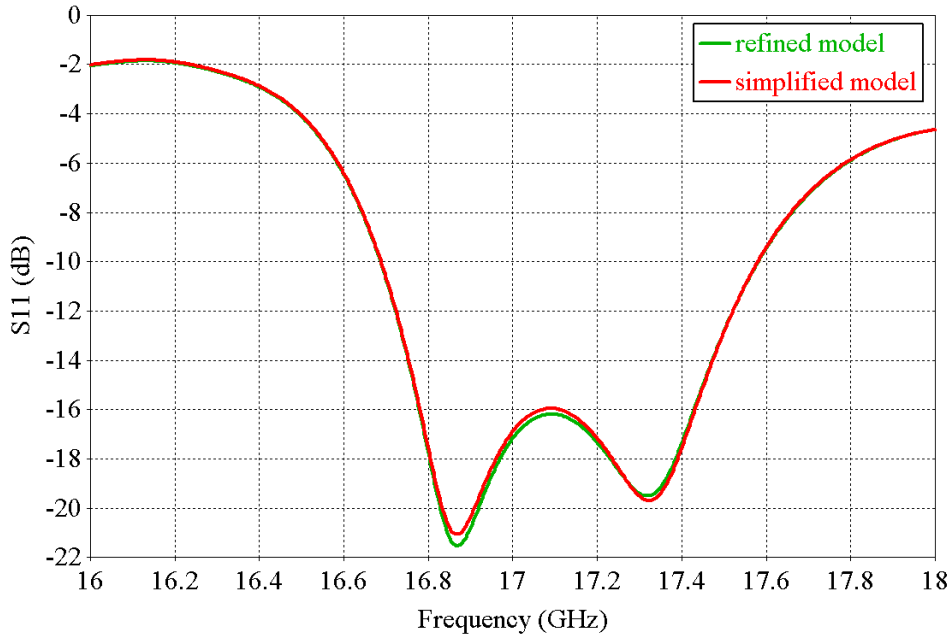

Fig. 6.6 Comparison of the frequency responses of the reflection coefficient.

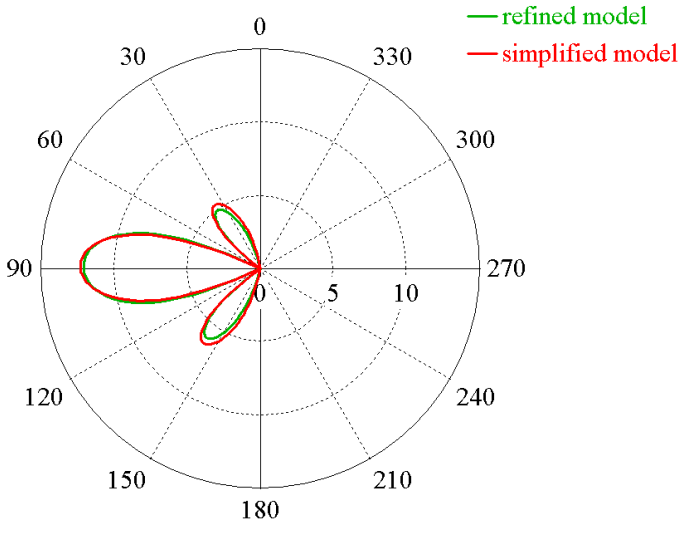

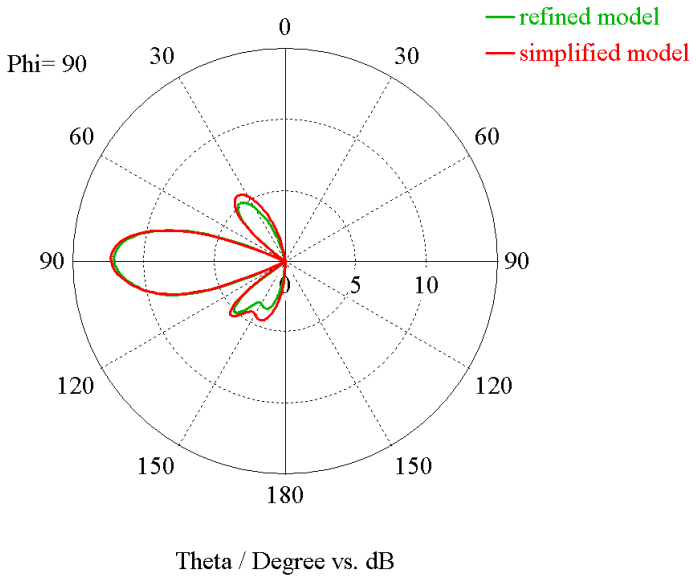

Fig. 6.7 Comparison of the radiation patterns in YZ (top) and XY (bottom) planes. Realized gain, magnitude in dB.

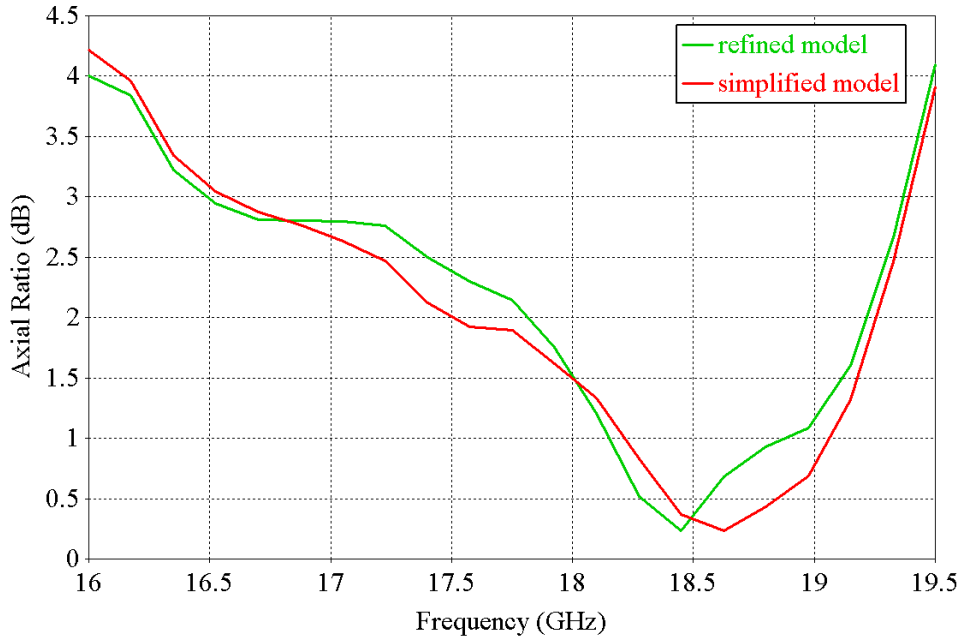

Fig. 6.8 Comparison of the frequency responses of the axial ratio.

As seen in the figures, there are only minor differences in the simulated properties. Therefore, influence of the additional elements was found as negligible.

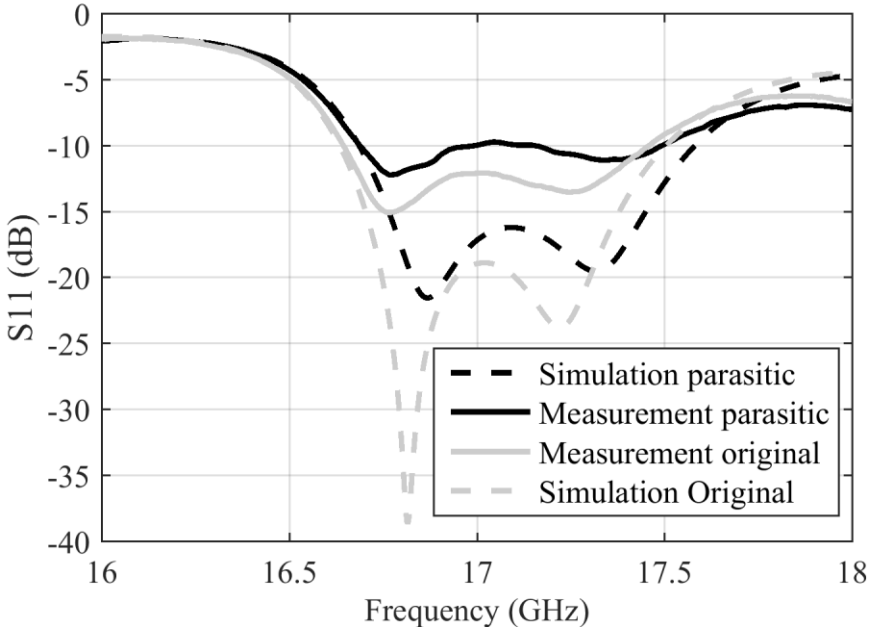

Fig. 6.9. Frequency responses of the reflection coefficient of the simulated (dotted line) and measured (solid line) antenna array with and without parasitic patches.

Fig. 6.9 shows frequency responses of the reflection coefficient of the simulated and manufactured array fitted with the parasitic structure compared to the original array. The results are in agreement and consistent with the data obtained earlier with the original array. Impedance bandwidth of the simulated array is from 16.69 GHz to 17.49 GHz (4.7 % relatively). The low frequency limit of the measured array appears at 16.69 GHz, and the upper one is at 17.58 GHz. The results indicate that addition of the parasitic structure does not significantly influence the impedance bandwidth of the array. The overall magnitude has risen by approximately 3 dB in comparison to the original array. The rise of the measured curve above the -10 dB limit near the center frequency is neglected due to re-usage of the prototype from Chapter 4. The same rise in the magnitude, caused by inaccurate SMA connector mounting, can be observed for both variants as a result.

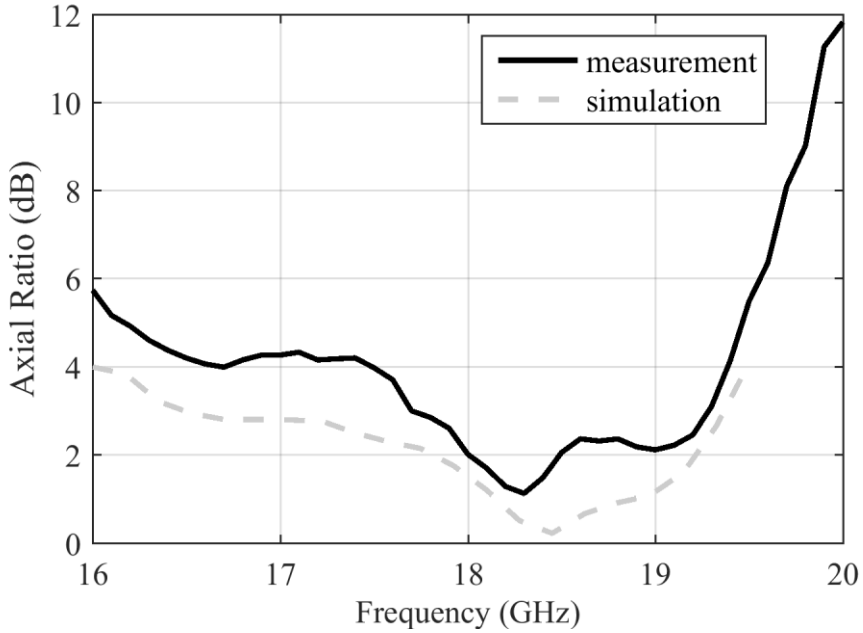

Fig. 6.10 Frequency responses of the axial ratio of the simulated (red line) and measured (blue line) antenna array with parasitic patches.

Fig. 6.10 depicts comparison of the simulated and measured frequency responses of the axial ratio of the array with parasitic patches. The results show good match though there is a constant offset added to the measured line. This degradation is caused by manufacturing imperfections which are mostly accounted to the structural limits of the used Foamclad substrate, which is very prone to deformation. As a result, airgaps have been created between the three stacked layers of the substrate and also the distance between the parasitic and original structure isn't constant – a parameter that is identified as critical for the performance of the system (see Fig. 6.11). With a more precise manufacturing method, better results can be achieved.

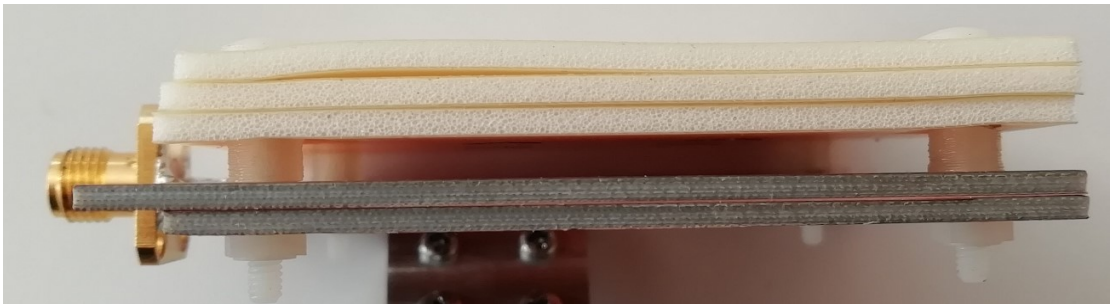

Fig. 6.11 Manufacturing imperfections – airgaps between the substrate layers and non-constant spacing between the original and parasitic structure.

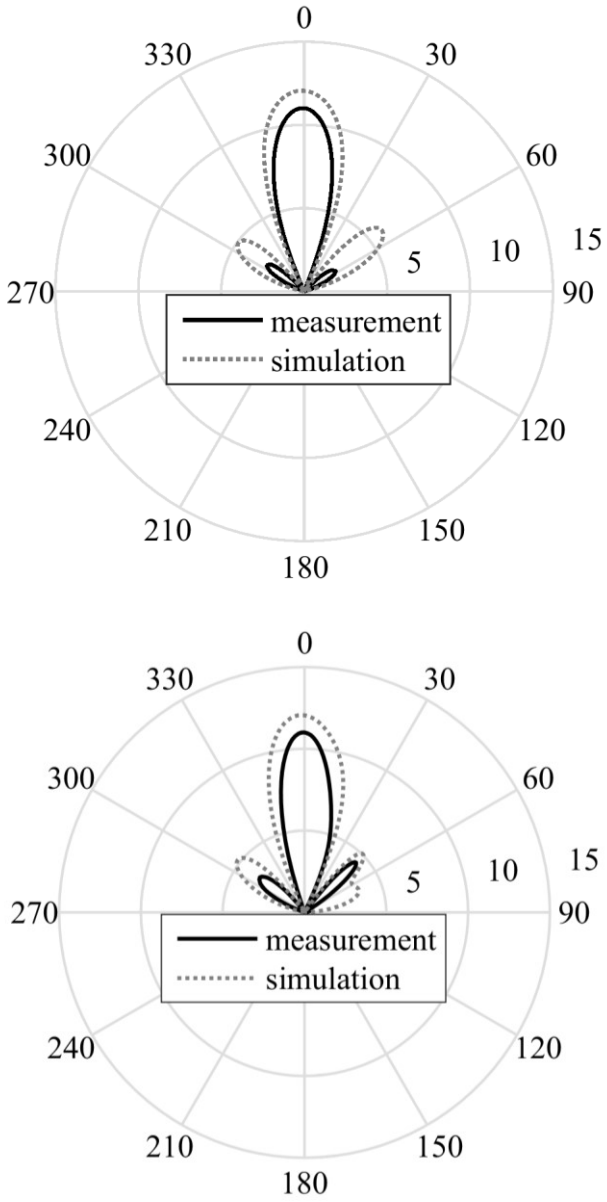

Fig. 6.12 Comparison of the simulated and measured radiation patterns of the array with parasitic patches (LHCP, realized gain). Top XY plane, down YZ plane.

Fig. 6.12 shows the comparison of the simulated and measured radiation patterns of the array with parasitic patches in YZ and XY plane. The results are in agreement. The measured array exhibits lower gain than the simulated due to higher measured reflection that was discussed earlier (see Fig. 6.9).

6.3 ADAPTATION OF THE ARRAY TO 60 GHZ

At 60 GHz, the model was simplified to reduce simulation time requirements:

- Vias, forming the SIW distribution network, were replaced by solid side walls.
- The SMA connector and the grounded coplanar waveguide to SIW transition were removed.
- Conductive materials were represented by perfect electric conductor.

In order to convert the antenna to the higher frequency, height of the FoamClad carrier substrate was reduced to $h = 1.88$ mm, and the distance between the antenna and the parasitic layer was changed to $d = 0.8$ mm.
In the 60 GHz model, adaptive mesh refinement was used to guarantee accuracy of the results. In the realistic model at 17 GHz, accuracy requirements are safely met thanks to the requirements for meshing of the vias, which form the SIW feeding network.

6.3.1 Simulations and measurements

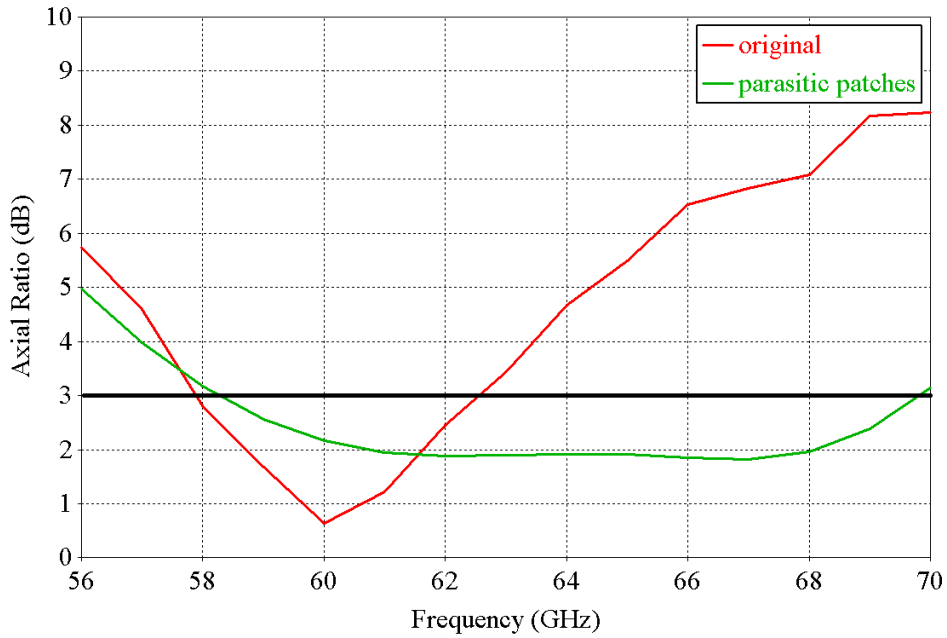

Fig. 6.13 Frequency response of the axial ratio in the main lobe direction of the antenna array without parasitic patches (red) and with parasitic patches (green). Frequency of operation: 60 GHz.

Fig. 6.13 shows that the axial ratio bandwidth (the condition |AR| < 3 dB) is 57.88 GHz to 62.49 GHz (4.61 GHz, i.e. 7.6 % relatively) for the original array, and 58.31 GHz to 69.78 GHz (11.47 GHz, i.e. 19.1 % relatively) for the array with parasitic patches.

Obviously, there is agreement between results at 17 GHz and 60 GHz (see Chapter

6.2). For the center frequency of 60 GHz, parameters of the array were swept to demonstrate the influence of the distance *d* between the original structure and the array of parasitic patches, to the properties of the studied structure (see Fig. 6.14).

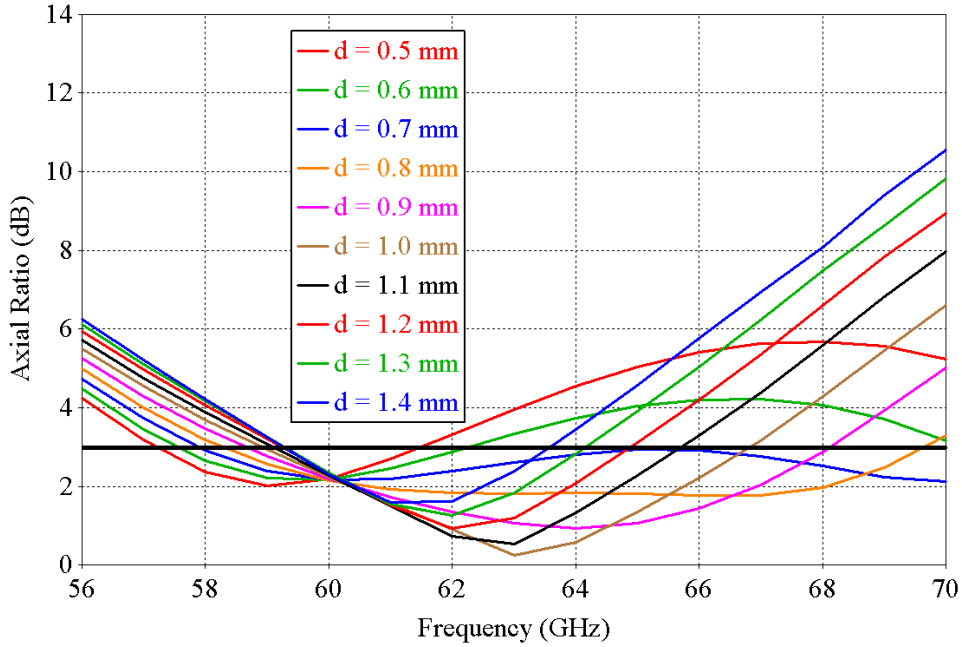

Fig. 6.14 Parametric sweep – variation of the distance between the array and the parasitic structure at 60 GHz.

Measured results

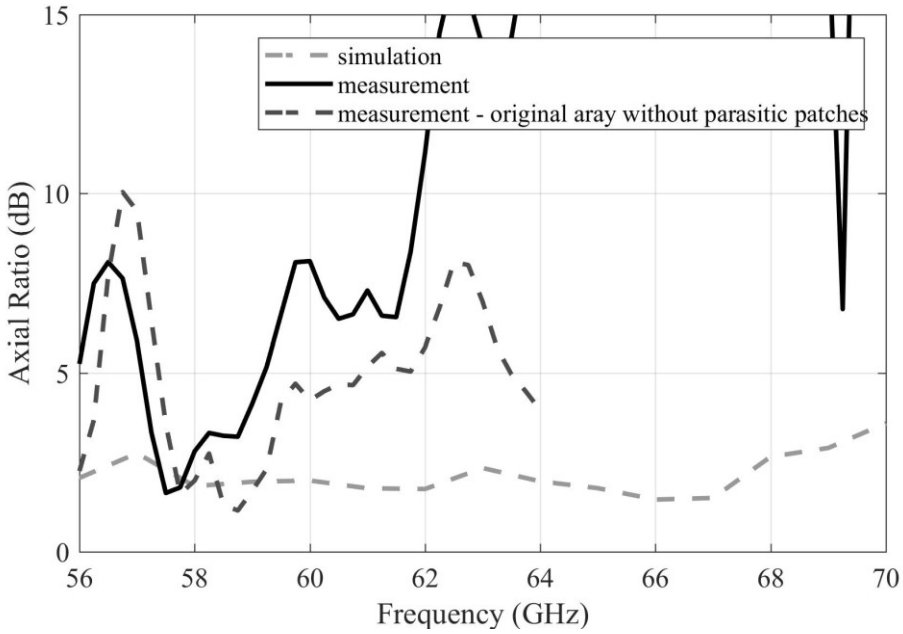

Fig. 6.15 Frequency response of the axial ratio of the simulated and measured array extended with the parasitic patches.

Fig. 6.15 depicts comparison of the simulated and measured frequency responses of axial ratio of the array equipped with the parasitic patches. As can be seen, the

measured characteristic is not in agreement with the simulation. This is caused by the imperfect axial ratio properties of the original array described in Chapter 5.5 (added to the figure for convenience), which was used for the experiment and extended with the parasitic structure. Its inherent sub-optimal axial ratio properties are superimposed to the result, not allowing the parasitic structure to make any visible effect on the characteristic.

6.4 CONCLUSION

In the chapter, the concept of parasitic patches, placed above the radiating elements at defined distance, as means of extending axial ratio bandwidth is presented. The analysis and verification were performed on the original antenna array described in sections 4 and 5, which was extended by the parasitic structure. Two frequency setpoints were investigated – 17 and 60 GHz.

The results for 17 GHz show a good match between the simulations and the measurements, confirming validity of the concept. The measured results for 60 GHz differ from the simulations due to the inherited imperfections of the antenna array used for the experiment, concluding that obtaining optimal properties of the base antenna array is critical to achieve a good performance of the parasitic structure. Requirements for manufacturing precision are therefore increased.

The achieved results were presented in the following publications:

[1] J. Spurek, Z. Raida, “Extending axial ratio bandwidth of antenna array by parasitic patches,“ In 2018 22nd International Microwave and Radar Conference (MIKON). Poznan: IEEE, 2018.pp. 357-359. ISBN: 978-83-949421-1-3.

[2] J. Spurek, Z. Raida, “Realization of circularly polarized antenna array with parasitic patches,“ In 2019 IEEE-APS Topical Conference on Antennas and Propagation in Wireless Communications (APWC). Granada, Spain: IEEE, 2019. pp. 239-242. ISBN: 978-1-7281-0566-6.

7 SUMMARY

The dissertation thesis presents, characterizes and derives the methodology for a new concept of circularly polarized patch antenna arrays based on the substrate integrated waveguide technology. The concept focuses on modularity and usability of the array as a base building block for creation of larger arrays. The design of the base building block also serves as a template for extension. The array was simulated and experimentally verified at the center frequencies of 17 GHz and 60 GHz. The results show good agreement between the simulations and measurements and between the frequency setpoints.

Together with the new concept, also a new technique of extending axial ratio bandwidth of the array by utilizing parasitic patches, placed above the original radiating elements at defined distance, was presented, and studied at the same center frequencies of 17 and 60 GHz. The obtained results are in agreement for the center frequency of 17 GHz, the results for the center frequency of 60 GHz show only limited match, indicating that limitations of the available manufacturing technology do not allow production with the required precision.

Subsequent research in this area could focus on the following areas:

- Techniques to reduce the requirements put on manufacturing precision
- Possibility to integrate additional optional elements into the SIW power delivery network that would add new levels of modularity and enhance the capabilities of the system (beamforming, side lobe level suppression etc.)

REFERENCES

[1] DESLANDES, D. a K. WU. Integrated microstrip and rectangular waveguide in planar form. IEEE Microwave and Wireless Components Letters. 2001, 11(2), 68-70. DOI: 10.1109/7260.914305. ISSN 1531-1309.

[2] DESLANDES, Dominic a Ke WU. Design Consideration and Performance Analysis of Substrate Integrated Waveguide Components. In: *32nd European Microwave Conference, 2002*. IEEE, 2002, 2002, pp. 1-4. DOI: 10.1109/EUMA.2002.339426.

[3] CHEN, Xiao-Ping a Ke WU. Low-loss ultra-wideband transition between conductor-backed coplanar waveguide and substrate integrated waveguide. In: 2009 IEEE MTT-S International Microwave Symposium Digest. IEEE, 2009, 2009, pp. 349-352. DOI: 10.1109/MWSYM.2009.5165705. ISBN 978-1-4244-2803-8.

[4] KARIMABADI, Sara Sadat a Amir Reza ATTARI. Broadband substrate integrated waveguide four-way power divider. In: 6th International Symposium on Telecommunications (IST). IEEE, 2012, 2012, pp. 80-83. DOI: 10.1109/ISTEL.2012.6482959. ISBN 978-1-4673-2073-3.

[5] MOHAMMADI, Pejman a Simsek DEMIR. Two layers substrate integrated waveguide power divider. In: 2011 XXXth URSI General Assembly and Scientific Symposium. IEEE, 2011, 2011, pp. 1-4. DOI: 10.1109/URSIGASS.2011.6050563. ISBN 978-1-4244-5117-3.

[6] ZHARGCHENG HAO, WEI HONG, HAO LI, HUA ZHANG a KE WU. Multiway broadband substrate integrated waveguide (SIW) power divider. In: 2005 IEEE Antennas and Propagation Society International Symposium. IEEE, 2005, pp. 639-642 . DOI: 10.1109/APS.2005.1551401. ISBN 0-7803-8883-6.

[7] WANG, Liyuan, Chuanfang ZHANG, Mengjia LUO, Chunchun MA a Cheng JIN. W-band substrate integrated waveguide filter with cross-coupling. In: 2015 Asia-Pacific Microwave Conference (APMC). IEEE, 2015, 2015, pp. 1-3. DOI: 10.1109/APMC.2015.7413089. ISBN 978-1-4799-8765-8.

[8] NASRI, Abdelkhalek, Hassen ZAIRI a Ali GHARSALLAH. A compact bandpass substrate integrated waveguide filter. In: 2014 International Conference on Electrical Sciences and Technologies in Maghreb (CISTEM). IEEE, 2014, 2014, pp. 1-4. DOI: 10.1109/CISTEM.2014.7076931. ISBN 978-1-4799-7300-2.

[9] BHATTACHARJEE, A.K., A.K. MUKHOPADHYAY, J. KUNDU, B. MONDAL a S. MOITRA. Substrate integrated waveguide (SIW) filter using stepped-inductive posts for KU-Band applications. In: Third International Conference on Computational Intelligence and Information Technology (CIIT

2013). Institution of Engineering and Technology, 2013, 2013, pp. 398-401. DOI: 10.1049/cp.2013.2619. ISBN 978-1-84919-859-2.

[10] BEN CHAIEB, Tahar, Abdelkhalek NASRI a Hassen ZAIRI. Low loss substrate integrated waveguide slot antenna. In: 2017 International Conference on Advanced Systems and Electric Technologies (IC_ASET). IEEE, 2017, 2017, pp. 25-29. DOI: 10.1109/ASET.2017.7983661. ISBN 978-1-5090-6634-6.

[11] TAN, Ke-jun a Xiu-zhen LUAN. Millimeter wave circularly polarized substrate integrated waveguide antenna. In: 2008 International Conference on Microwave and Millimeter Wave Technology. IEEE, 2008, 2008, pp. 1058-1061. DOI: 10.1109/ICMMT.2008.4540604. ISBN 978-1-4244-1879-4.

[12] ZHIJUN CHEN, WEI HONG, ZHENQI KUAI, JIXIN CHEN a KE WU. Circularly polarized slot array antenna based on substrate integrated waveguide. In: 2008 International Conference on Microwave and Millimeter Wave Technology. IEEE, 2008, 2008, pp. 1066-1069. DOI: 10.1109/ICMMT.2008.4540606. ISBN 978-1-4244-1879-4.

[13] LEMBERG, K. V., O. A. NAZAROV, V. S. PANKO a Y. P. SALOMATOV. X-band substrate integrated waveguide (SIW) slot antenna array. In: 2013 International Siberian Conference on Control and Communications (SIBCON). IEEE, 2013, 2013, pp. 1-2. DOI: 10.1109/SIBCON.2013.6693589. ISBN 978-1-4799-1062-5.

[14] HAO WANG, Y. ZHENG, L. QIAN, J. XI, S. JI. Low Side-Lobe Substrate Integrated Cavity Antenna Array Using Unequal Microstrip-Ridge Gap Waveguide Feeding Network at 94 GHz. In: Applied Computational Electromagnetics Society Symposium (ACES), 2017. IEEE, 2017. ISBN: 978-0-9960-0785-6

[15] LIU, Hao, Anyong QING, Ziqiang XU a Zhao YANG. Low-Cost and High-Gain W-Band Circularly Polarized SIW Slot Antenna. In: 2019 IEEE International Symposium on Antennas and Propagation and USNC-URSI Radio Science Meeting. IEEE, 2019, 2019, s. 661-662. ISBN 978-1-7281-0692-2. doi:10.1109/APUSNCURSINRSM.2019.8888551

[16] WU, Yi-Wen, Zhang-Cheng HAO a Zhuo-Wei MIAO. A Planar W -Band Large-Scale High-Gain Substrate-Integrated Waveguide Slot Array. IEEE Transactions on Antennas and Propagation. 2020, 68(8), 6429-6434. ISSN 0018-926X. doi:10.1109/TAP.2020.2969999

[17] KE WU, D. DESIANDES a Y. CASSIVI. The substrate integrated circuits - a new concept for high-frequency electronics and optoelectronics. In: 6th International Conference on Telecommunications in Modern Satellite, Cable and Broadcasting Service, 2003. TELSIKS 2003. IEEE, 2003, P-III-P-X. DOI: 10.1109/TELSKS.2003.1246173. ISBN 0-7803-7963-2.

[18] BALANIS, Constantine A. Antenna theory: analysis and design. 3rd ed. Hoboken, NJ: John Wiley, c2005. ISBN 9780471667827.

[19] RAPHAEL, Reshma a T. SUDHA. Single-fed circularly polarized patch antenna for 60 GHz wireless applications. In: 2016 International Conference on Emerging Technological Trends (ICETT). IEEE, 2016, 2016, pp. 1-6. DOI: 10.1109/ICETT.2016.7873695. ISBN 978-1-5090-3751-3.

[20] JANG, Tae Hwan, Young Hun HAN, Joonhyung KIM a Chul Soon PARK. 60 GHz Wideband Low-Profile Circularly Polarized Patch Antenna With an Asymmetric Inset. IEEE Antennas and Wireless Propagation Letters. 2020, 19(1), 44-48. ISSN 1536-1225. doi:10.1109/LAWP.2019.2952405

[21] BHATTACHARYYA, A., Y.M.M. ANTAR a A. ITTIPIBOON. Aperture-coupled patch antenna-theoretical and experimental investigations. In: Antennas and Propagation Society Symposium 1991 Digest . IEEE, 1991, pp. 1090-1093. DOI: 10.1109/APS.1991.175036. ISBN 0-7803-0144-7.

[22] ROSSELLO, Joaquim, Fermin MIRA, Ana COLLADO a Apostolos GEORGIADIS. Substrate integrated waveguide aperture coupled patch antenna array for 24 GHz wireless backhaul and radar applications. In: 2014 IEEE Conference on Antenna Measurements & Applications (CAMA). IEEE, 2014, 2014, pp. 1-2. DOI: 10.1109/CAMA.2014.7003408. ISBN 978-1-4799-3678-6.

[23] ALAM, Syah, Indra SURJATI a Yuli Kurnia NINGSIH. Patch modification and slot arrangement of microstrip antenna for improving the axial ratio. In: 2017 International Conference on Broadband Communication, Wireless Sensors and Powering (BCWSP). IEEE, 2017, 2017, pp. 1-5. DOI: 10.1109/BCWSP.2017.8272553. ISBN 978-1-5386-2833-1.

[24] Yue Li, Zhi Ning Chen, Xianming Qing, Zhijun Zhang, Junfeng Xu and Zhenghe Feng, “Axial ratio bandwidth enhancement of 60-GHz substrate integrated waveguide-fed circularly polarized LTCC antenna array,” IEEE Trans. Antennas Propag., vol. 60, no. 10, pp. 4619-4626, 2012.

[25] WU, Qiong-Sen, Xiao ZHANG a Lei ZHU. A Wideband Circularly Polarized Patch Antenna With Enhanced Axial Ratio Bandwidth via Co-Design of Feeding Network. IEEE Transactions on Antennas and Propagation. 2018, 66(10), 4996-5003. ISSN 0018-926X. doi:10.1109/TAP.2018.2851616

[26] LIU, Neng-Wu, Lei ZHU, Zhong-Xun LIU, Guang FU a Ying LIU. Design Approach of a Single Circularly Polarized Patch Antenna With Enhanced AR-Bandwidth Under Triple-Mode Resonance. IEEE Transactions on Antennas and Propagation. 2020, 68(8), 5827-5834. ISSN 0018-926X. doi:10.1109/TAP.2020.2995303

[27] Y. Cai, Z. Qian, W. Cao, Y. Zhang, J. Jin, L. Yang, and N. Jing, “Compact wideband SIW horn antenna fed by elevated-CPW structure,” IEEE Trans. Antennas Propag., vol. 63, no. 10, pp. 4551-4557, 2015.

[28] D. M. Pozar, Microwave Engineering, 4th ed. Hoboken, NJ: J. Wiley & Sons, 2012.

[29] J. Spurek, J. Velim, M. Cupal, Z. Raida, J. Prasek, and J. Hubalek, “Slot loop antennas printed on 3D textile substrate,” in Proc. MIKON, Krakow, Poland, 2016.

[30] Yue Li, Zhi Ning Chen, Xianming Qing, Zhijun Zhang, Junfeng Xu and Zhenghe Feng, “Axial ratio bandwidth enhancement of 60-GHz substrate integrated waveguide-fed circularly polarized LTCC antenna array,” IEEE Trans. Antennas Propag., vol. 60, no. 10, pp. 4619-4626, 2012.

LIST OF FIGURES

Fig. 3.1 Proposed antenna array 13
Fig. 3.2 Proposed antenna array with parasitic patches 14
Fig. 4.1 Power flow within the array structure 16
Fig. 4.2 Layout of the bottom layer 17
Fig. 4.3 Layout of the top layer 17
Fig. 4.4 Example of a 4x4 array assembled from four 2x2 base building blocks 19
Fig. 4.5 Manufactured array 19
Fig. 4.6 Frequency response of the magnitude of reflection coefficient at the input of the antenna array: measured (solid), simulated (dotted). 20
Fig. 4.7 Frequency response of the axial ratio in the main lobe direction of the antenna array: measured (solid), simulated (dotted). 21
Fig. 4.8 Radiation patterns of the array in YZ and XY plane: measured (solid), simulated (dotted). 22
Fig. 5.1 WR15 to SIW transition 25
Fig. 5.2 Simulated frequency response of the reflection coefficient (S11) and the transmission coefficient (S21) of the designed WR15-SIW transition. 26
Fig. 5.3 Manufactured WR15 to SIW transition (1). 26
Fig. 5.4 Manufactured WR15 to SIW transition (2). 27
Fig. 5.5 Final model for 60 GHz 28
Fig. 5.6 Frequency response of the reflection coefficient of the simulated array at 60 GHz. 28
Fig. 5.7 Frequency response of axial ratio of the simulated array at 60 GHz 29
Fig. 5.8 Radiation patterns of the simulated array in YZ (down) and XY (up) plane (LHCP, realized gain). 30
Fig. 5.9 Illustration of the swept dimensions – top and bottom layer. 31
Fig. 5.10 Simplified model of the array with solid side walls. 32
Fig. 5.11 Frequency responses of the reflection coefficient for 0.1 mm variance around the center value 33
Fig. 5.12 Frequency responses of the axial ratio for 0.1 mm variance around the center value 33
Fig. 5.13 Radiation patterns in XY plane for 0.1 mm variance around the center value 34
Fig. 5.14 Radiation patterns in YZ plane for 0.1 mm variance around the center value 34
Fig. 5.15 Frequency responses of the reflection coefficient for 0.1 mm variance around the center value 35
Fig. 5.16 Frequency responses of the axial ratio for 0.1 mm variance around the center value 35

Fig. 5.17 Radiation patterns in XY plane for 0.1 mm variance around the center value 36
Fig. 5.18 Radiation patterns in YZ plane for 0.1 mm variance around the center value 36
Fig. 5.19 Frequency responses of the reflection coefficient for 0.1 mm variance around the center value 37
Fig. 5.20 Frequency responses of the axial ratio for 0.1 mm variance around the center value 37
Fig. 5.21 Radiation patterns in XY plane for 0.1 mm variance around the center value 38
Fig. 5.22 Radiation patterns in YZ plane for 0.1 mm variance around the center value 38
Fig. 5.23 Frequency responses of the reflection coefficient for 0.1 mm variance around the center value 39
Fig. 5.24 Frequency responses of the axial ratio for 0.1 mm variance around the center value 39
Fig. 5.25 Radiation patterns in XY plane for 0.1 mm variance around the center value 40
Fig. 5.26 Radiation patterns in YZ plane for 0.1 mm variance around the center value 40
Fig. 5.27 Frequency responses of the reflection coefficient for 0.1 mm variance around the center value 41
Fig. 5.28 Frequency responses of the axial ratio for 0.1 mm variance around the center value 41
Fig. 5.29 Radiation patterns in XY plane for 0.1 mm variance around the center value 42
Fig. 5.30 Radiation patterns in YZ plane for 0.1 mm variance around the center value 42
Fig. 5.31 Frequency responses of the reflection coefficient for 0.1 mm variance around the center value 43
Fig. 5.32 Frequency responses of the axial ratio for 0.1 mm variance around the center value 43
Fig. 5.33 Radiation patterns in XY plane for 0.1 mm variance around the center value 44
Fig. 5.34 Radiation patterns in YZ plane for 0.1 mm variance around the center value 44
Fig. 5.35 Frequency responses of the reflection coefficient for 0.1 mm variance around the center value 45
Fig. 5.36 Frequency responses of the axial ratio for 0.1 mm variance around the center value 45
Fig. 5.37 Radiation patterns in XY plane for 0.1 mm variance around the center value 46

Fig. 5.38 Radiation patterns in YZ plane for 0.1 mm variance around the center value 46
Fig. 5.39 Manufactured array for the center frequency of 60 GHz..... 47
Fig. 5.40 Frequency responses of the magnitude of reflection coefficient for the simulated and measured antenna array. 48
Fig. 5.41 Frequency responses of the magnitude of axial ratio for the simulated and measured antenna array. 49
Fig. 5.42 Comparison of the arrays with smaller via diameter (left) and larger via diameter (right). 50
Fig. 5.43 Frequency responses of the magnitude of reflection coefficient for the simulated array with smaller and larger via diameter. 51
Fig. 5.44 Frequency responses of the magnitude of axial ratio for the simulated array with smaller and larger via diameter. 52
Fig. 5.45 Comparison of the radiation patters of the arrays with smaller and larger via diameter in *xy* (up) and *yz* (down) planes. Shown in realized gain (dB). 53
Fig. 5.46 Manufactured array with the larger via diameter..... 54
Fig. 5.47 Frequency responses of the magnitude of reflection coefficient for the simulated and measured array with the larger via diameter. 55
Fig. 5.48 Frequency responses of the magnitude of axial ratio for the simulated array with smaller and larger via diameter. 56
Fig. 5.49 Comparison of the radiation patters of the simulated and measured array with the larger via diameter in *xy* (up) and *yz* (down) planes. Shown in realized gain (dB). 57
Fig. 6.1 Side view on the geometry of the structure. 60
Fig. 6.2 Antenna array with parasitic patches (bounded in red). 61
Fig. 6.3 Manufactured antenna array with parasitic patches..... 61
Fig. 6.4 Frequency response of the axial ratio in the main lobe direction of the simulated antenna array without parasitic patches (red) and with parasitic patches (green). Frequency of operation: 17 GHz. 62
Fig. 6.5 Refined numerical model of the array 63
Fig. 6.6 Comparison of the frequency responses of the reflection coefficient. 63
Fig. 6.7 Comparison of the radiation patterns in YZ (top) and XY (bottom) planes. Realized gain, magnitude in dB. 64
Fig. 6.8 Comparison of the frequency responses of the axial ratio. 64
Fig. 6.9. Frequency responses of the reflection coefficient of the simulated (dotted line) and measured (solid line) antenna array with and without parasitic patches. 65
Fig. 6.10 Frequency responses of the axial ratio of the simulated (red line) and measured (blue line) antenna array with parasitic patches. 66
Fig. 6.11 Manufacturing imperfections – airgaps between the substrate layers and non-constant spacing between the original and parasitic structure. 66
Fig. 6.12 Comparison of the simulated and measured radiation patterns of the array with parasitic patches (LHCP, realized gain). Top XY plane, down YZ plane..... 67

Fig. 6.13 Frequency response of the axial ratio in the main lobe direction of the antenna array without parasitic patches (red) and with parasitic patches (green). Frequency of operation: 60 GHz. 68
Fig. 6.14 Parametric sweep – variation of the distance between the array and the parasitic structure at 60 GHz. 69
Fig. 6.15 Frequency response of the axial ratio of the simulated and measured array extended with the parasitic patches. 69

LIST OF TABLES

Table I Dimensions of the array for the center frequency of 17 GHz..... 18
Table II Mapping of the simulation runs to the parameter changes..... 32
Table III Final dimensions of the array for the center frequency of 60 GHz (the larger via diameter). 58

CURRICULIM VITAE

Jan Špůrek

Sladské 1685
756 61
Rožnov p.R.
Czech Republic

e-mail: janspurek@gmail.com
phone: +420 724 310 546

Education

2016 to present	Brno University of Technology, Brno, Czech Republic Ph.D., Electronics and Communication Research topic: SIW-based circularly polarized antenna arrays
2014 – 2016	Brno University of Technology, Brno, Czech Republic MSc., Electronics and Communication Diploma thesis: Textile slot antenna
2011 – 2013	Brno University of Technology, Brno, Czech Republic BSc., Electronics and Communication Bachelor thesis: Antenna for in-car UWB communications

Work experience

2016 to present	NXP Semiconductors s.r.o. Systems engineer
2016 to present	Sewio Networks s.r.o. Antenna designer

Language

English	FCE, level B2

Software skills

CST Microwave studio
MATLAB/Octave
ANSYS Electromagnetic Desktop
Sketchup

LIST OF AUTHOR'S PUBLICATIONS

[1] J.Spurek, Z. Raida, "Circularly polarized modular patch antenna array fed by substrate integrated waveguide," Microwave and Optical Technology Letters, 2018, vol. 60, no. 6, pp. 1398-1403. ISSN: 1098-2760.

[2] J. Spurek, Z. Raida, "Sensitivity analysis of a modular circularly polarized antenna array for 60 GHz band," In Proceedings of MIKON 2020. Warsaw, Poland: IEEE, 2020. pp. 45-49. ISBN: 978-83-949421-6-8.

[3] J. Spurek, Z. Raida, "Extending axial ratio bandwidth of antenna array by parasitic patches," In 2018 22nd International Microwave and Radar Conference (MIKON). Poznan: IEEE, 2018.pp. 357-359. ISBN: 978-83-949421-1-3.

[4] J. Spurek, Z. Raida, "Realization of circularly polarized antenna array with parasitic patches," In 2019 IEEE-APS Topical Conference on Antennas and Propagation in Wireless Communications (APWC). Granada, Spain: IEEE, 2019. pp. 239-242. ISBN: 978-1-7281-0566-6.